Service Life Assessment of Internal Replacement Pipe: External Load Testing of I-Main™

Final Report 1.0

Prepared for:

DOE/ARPA-E

Insituform Technologies Inc.

Prepared by:

REPAIR Testing & Analysis Team

Center for Infrastructure, Energy, and Space Testing
University of Colorado Boulder

Geotechnical Lifelines Large-Scale Testing Facility
Cornell University

December 2024

Table of Contents

Table of Figures

Table of Tables

Acknowledgements

The authors thank DOE/ARPA-E for financially supporting this research and for guiding our progress throughout its execution, in particularly, we thank Dr. Jack Lewnard, Dr. Sade Ruffin, and Matthew Hackworth for their leadership of the Rapid Encapsulation of Pipelines Avoiding Intensive Replacement (REPAIR) program. The team extends its gratitude to the Technical & Testing Specifications Pannel (TTSP), who provided valuable practical feedback and industry guidance through the project. We thank the staff and students at the University of Colorado at Boulder, University of Southern Queensland, and Cornell University for their many contributions to the REPAIR project as well as the work presented herein. We appreciate greatly Insituform Technology's donation of test specimens and support through technical discussions, especially with Dr. Amber Wagner and Dr. Omar Abdulkareem.

The information, data, or work presented herein was funded in part by the Advanced Research Projects Agency-Energy (ARPA-E), US Department of Energy under Award No. DE-AR0001327. The views and opinions of authors expressed herein do not necessarily state or reflect those of the United States Government or any agency thereof.

1 Introduction & Background

Compared to the open trench method, trenchless technology (TT) for water, wastewater, oil and gas pipelines are used increasingly to replace incident-prone legacy pipes. TT results in less environmental damage, the minimization of excavation activities, and lower costs compared to open cut methods (Allouche et al., 2014; Lu et al., 2020; Najafi, 2005; Vladeanu & Matthews, 2018). There has been much effort to develop internal replacement pipe (IRP) technologies as well as the formal standards and documents concerning these technologies (Pipeline Infrastructure Committee 2021; ASME PCC-2 Article 403 2018; ASTM F1216 2016a; ASTM F3182 2016b; ASTM F1743 2017; ASTM D5813 2018; ASTM F2207 2019a; AWWA Committee 2019). Nevertheless, there are some outstanding questions about IRP technologies, including long-term suitability and performance, practical considerations for external loads, and the role of adhesion in the structural capacity and response. Legacy host pipes undergo various failure modes depending on the type of loading. Moreover, studies are lacking for the long-term response of deteriorated host pipes to internal and external loads (Dixon et al., 2023b; Fu et al., 2020).

This report addresses external loads affecting IRP technologies. It presents lab-based methods for evaluating IRP over a 50-year service-life with repaired pipe specimens. The specimens studied featured the cured-in-place pipe (CIPP) material I-Main™, graciously provided by Insituform Technologies, LLC, which is considered a “known” material that has a successful track record in both laboratory and field applications. The external loads are traffic loading, ground movement due to adjacent excavations, and thermally-induced axial deformation of the repaired system. This report is a logical extension of earlier work performed at Cornell University (Jeon et al., 2004; Stewart et al., 2015), which developed an evaluation framework for cured-in-place liners (CIPLs) under external loads. The framework developed at Cornell University assumed negligible mechanical contribution (stiffness) of liner to the pipeline response. This assumption was conservative and appropriate, considering the type of materials that were evaluated by Cornell researchers at the time. The current team has altered this aspect in their framework, now accounting for the stiffness of a repair pipe in the estimation of field deformations. The numerical and analytical methods to estimate field deformations of an I-Main™ IRP are outlined briefly in this report. Detailed test methods and major results are presented. Important observations and aspects of the testing are discussed.

2 Methodology of Mechanical Aging Tests

The following section describes the test methodology to simulate major aspects of the external loading of an internal REPAIR pipe over a 50-year service-life in the field. The approach applies laboratory loading to mimic deformations applied by traffic loading, adjacent excavations, and seasonal temperature fluctuation.

2.1 Lateral Loading

2.1.1 Model Description

A "beam-on-springs" finite element (FE) model was developed in OpenSees for a buried cast iron pipeline subjected to traffic loading and soil displacements representative of adjacent excavation activity. The pipeline elements were represented by 3 in. (75 mm) long, 1D Euler-Bernoulli beam elements. A circumferential gap opening (also referred to as crack) was modeled by removing host pipe elements. For the cases in which an IRP repair was combined with the host pipe, the missing element or gap was replaced with a beam element with properties of the IRP material and length equal to the width of the gap opening. CI joints were modeled using rotational, shear, and axial springs. Soil was represented using soil springs with a hyperbolic force-displacement.

2.1.2 Traffic Loading

As described in detail by Klingaman et al., (2022), traffic loading was derived from an HS-20 design truck and was conservatively increased to 30 kips (130 kN). The resulting traffic load was assumed to be applied at the ground surface according to the Boussinesq stress distribution for a point load on a semi-infinite elastic medium. The stress calculated at a depth of 30 in. (762 mm) was multiplied by the vertically projected area of the pipe (diameter times element size) and discreetly applied to each pipeline node in the FE model (Figure 1). Resulting pipe deformations (e.g., relative rotations) were recorded so that they could be applied in the lab.

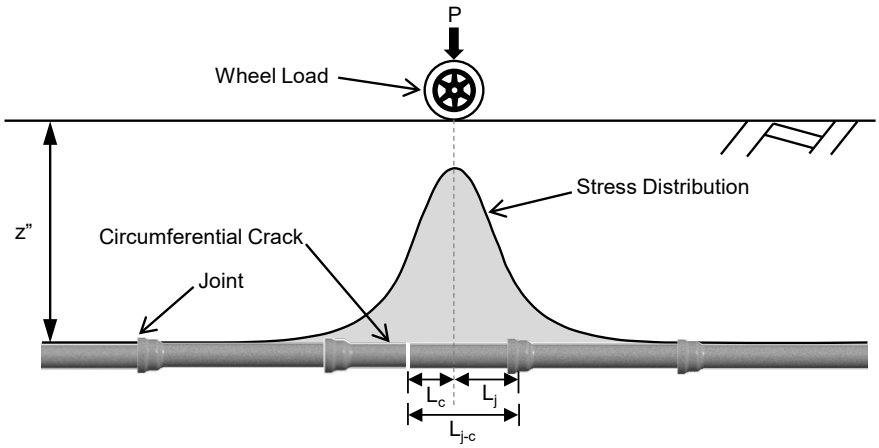

Figure 1. Schematic of traffic loading scenario

2.1.3 Adjacent Excavation (AE)

As described by Klingaman et al. (2024), soil displacement profiles were developed using a functional form proposed by Roboski & Finno (2006), which requires 3 inputs: excavation depth, H_e, maximum soil displacement, d_{max}, and the length over which d_{max} is developed, L. The adjacent excavation (AE) depth was assumed to be 20 ft. (6 m), various values of d_{max} were considered, ranging from 2.5-10 in. (63.5-254 mm), and L was assumed to be 50 ft. (15.2 m) (Figure 2). The soil displacements were applied to each soil node in the FE model and resulting rotations were recorded so that they could be applied in the lab. During this study, the smaller and larger parallel (adjacent) excavation events, typically referred to as PE1 and PE2 for each specimen, were associated with d_{max} of 2.5 in. (63.5 mm) and 5 in. (127 mm), respectively.

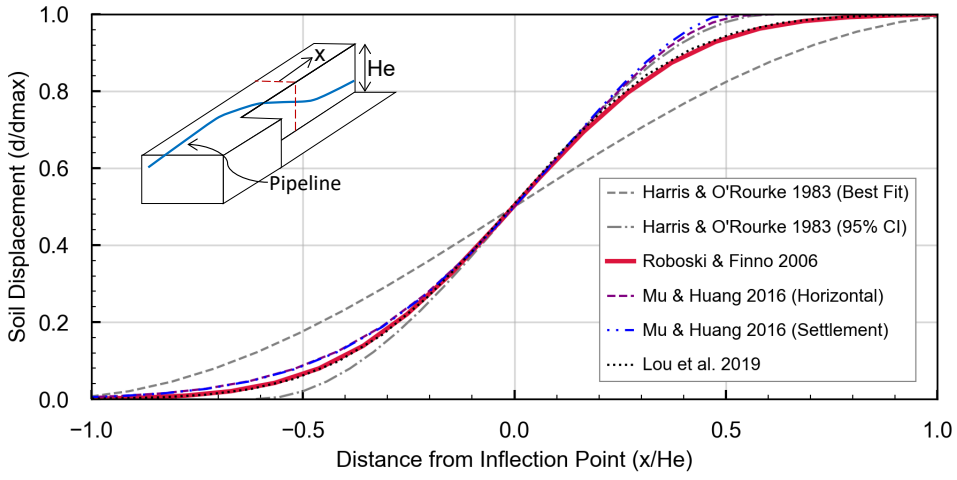

Figure 2. Soil displacement profiles parallel (adjacent) to an excavation from previous studies

2.2 Thermal Loading

Temperature fluctuations in soil will give rise to axial deformation and/or induced axial load in repaired systems from thermal expansion. Previous work used 40°F (22.2°C) as the annual soil temperature variation in New York state (Stewart et al., 2015). This work includes temperature variations of 40°F (22.2°C) and 50°F (27.8°C) and considers granular soil as the backfill material in contact with the host pipe. Additionally, this work considers the stress-free state of the system to be the highest temperature (T_{max}), such that all temperature variation is negative. To understand the problem, a mechanics based analytical approach has been developed as shown in Figure 3 (Dixon et al., 2023a).

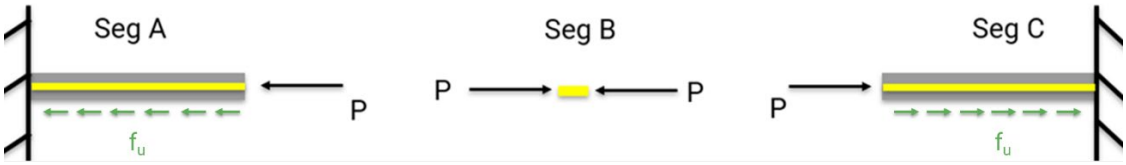

Figure 3. Fully bonded approach schematic with friction from pipe-soil interaction

The specimen is divided into three regions/segments: Segment A refers to combined host and REPAIR section, and Segment B refers to the exposed REPAIR pipe region (Segment C would refer to the other combined host and REPAIR section but symmetry allows the use of only Segment A and B). The host and repair pipe are treated as fully bonded in Segment A. Simple analytical expressions for the fully unbonded case are straightforward, and it is noted as the gap width (length of Segment B) approaches the system length, induced loads calculated with a fully-bonded assumption approach those for the unbonded case. Furthermore, even in "unbonded" systems some level of intimate mechanical contact is necessary for successful installation, and so the initial assumption will be fully bonded (if results from initial assessments with small levels of axial displacement demonstrate a fully unbonded system then the unbonded approach will be used). In this approach Segment A acts as a single unit, i.e., combined section properties and thermo-mechanical response with no differential displacement between the repair and host within the segment. Soil friction, f_u, is accounted for in the approach. Compatibility between the segments is used to solve for the induced load, which then can be used to determine the elongation of Segment B, i.e., the crack/gap opening displacement (COD). The forementioned assumptions are intended to produce the largest expected deformation at the crack, and therefore establish a conservative estimate of thermally induced displacement.

Additionally, details of load transfer across the interface and the soil-structure interaction are simplified. However, this approach is leveraged with previous work, finite element models, and knowledge about I-Main™ to obtain target displacements for axial loading (e.g., Ahmadi et al., 2024) that are

conservative in magnitude (i.e., displacements greater than those that more detailed methods) and hence a safety factor on target displacements was taken as 1.0.

3 Test Specimens and Material

The specimens consisted of steel host pipes of 12 in. (305 mm) nominal diameter, repaired with Insituform's I-Main™. Each specimen consisted of two segments of host pipe, arranged such that, when repaired, full circumferential (ring) gaps of exposed I-Main™ are present near the center of the specimen. This condition is intended to represent a worst-case scenario which the fully structural PIP would need to accommodate during its service life. The nominal gap widths were either 0.5 in. (12.7 mm) or 6 in. (152.4 mm). The former dimension reflects a partially displaced (pulled-out) joint in a legacy cast-iron gas distribution system, which is still functional (determined from utility input), and the latter dimension corresponds to a region of extreme deterioration of host pipe post-repair. The Testing & Analysis (T&A) Team notes these circumferential cracks are fairly severe, requiring the load to be carried entirely by the repair pipe over a section while simultaneously capturing interactions between host and repair pipe that potentially could give rise to stress concentrations and failures, which would not be observed in the host pipe alone.

I-Main™ is cured-in-place pipe system, with proven competence in water contexts. The structural component of I-Main™ is a thermoset resin and felt/fiber composite system utilizing a tube consisting of one or more layers of flexible needled polyester felt and fiber reinforcements capable of carrying resin. The tube is vacuum impregnated with resin, installed in an existing sewer or water main pipes, and heat cured. The composite construction of the polyester felt, fiber reinforcements and resin can be designed to carry varying internal pressures and external loads as required.

The felt fiber composite tube is manufactured at Insituform's manufacturing plant in Batesville, MS, USA. The outermost layer of all of the tubes is a needled felt with a layer of Polypropylene (PP) or Polyurethane (PU) extruded onto the surface. Tube construction is identical to that covered under current NSF-61 Listing. The typical tube construction variants are shown in Figure 4.

After the felt fiber composite tube is manufactured, it is impregnated with Thermosetting Resin/Curing Agent mixture Epoxy Resin Systems. After the impregnation, the tube is refrigerated, transported, and installed into a host pipe and expanded tight to the inside of the host pipe using water or air pressure. The lining system is then cured with 180 F water or steam. During the installation process, the PP/PU coated surface of the tube becomes the innermost surface of the new lining system and therefore becomes the wetted surface.

Two of the four specimens included the installation of a pre-liner prior to installation of the structural liner. The preliner is used in some field applications to help protect the liner from host pipe abrasion when it is installed using the inversion method (typically not used for pull-in-place installation method) and it also serves as a barrier to keep the resin within the host pipe and directing any excess resin

toward either end of the installation. Miller WEKO-SEALs[1] were installed at either end of the test specimens to promote sealing between the host pipe and IRP.

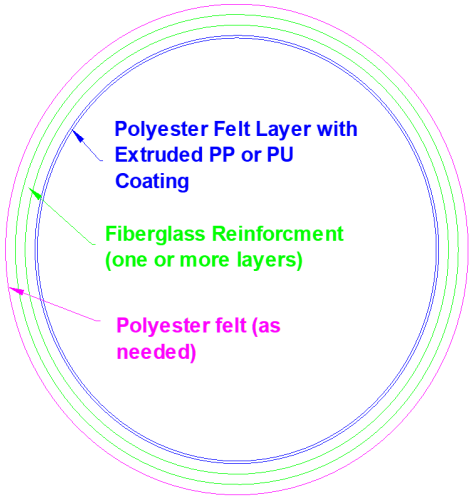

Figure 4. Cross-sectional drawing of the lining system in the installed state.

Full-scale test specimens and flat plate samples were prepared by Insituform at their facilities (Figure 5). Host pipes were shipped in specially designed crates to the manufacturer, and the specimens were prepared following typical installation procedures and then shipped back to the respective testing laboratories.

The internal surfaces of the steel host pipe segments were unprotected. No treatment was applied to them prior to lining. As mentioned, I-Main is a CIPP system that is widely used in water contexts, and its installation is consistent with standard field applications.

[1] https://wekoseal.com/wp-content/uploads/2017/08/WEKO_2016-1.pdf

Figure 5. Installation setup of Insituform test specimen

3.1 Material Characterization

Tensile coupon and burn out tests were performed at the University of Southern Queensland. The purpose of these tests is to determine the tensile properties and fiber mass fraction of Insituform material. A total of six specimens were prepared from panels prepared by the manufacturer during the specimen preparation process. All tensile coupons were subjected to testing until capacity. Their corresponding load, deflection, and strain values were recorded to establish the material properties. Burn out test results are included in

3.1.1 Tensile Coupon Set-up

The tensile testing of Insituform materials was carried out in accordance with ASTM D638 (ASTM, 2014) (another appropriate test method option for composites is ASTM D3039/D3039M (ASTM, 2017a)]. The tensile test setup is depicted in Figure 5. Loading is applied in the hoop direction of the installed liner. The specimens were subjected to a tensile load at a rate of 1.3 mm/min using a 100 kN MTS machine. An extensometer was affixed to the middle of the specimen until an extension of at least 0.15 mm was reached. From this test, the maximum load, modulus of elasticity, ultimate tensile strength and failure strain were determined.

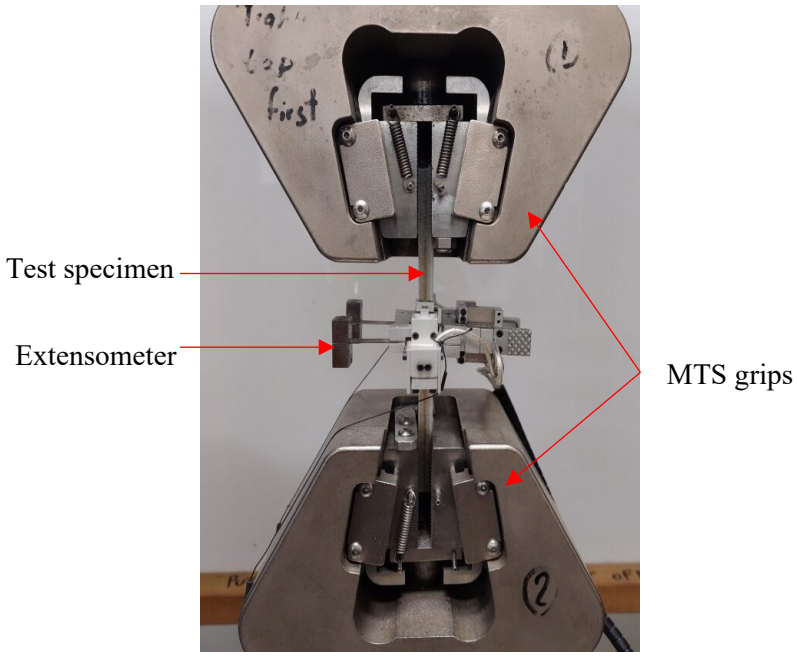

Figure 5. Test set-up for tensile test

3.1.2 Coupon Test Results

Figure 6a and b show the tensile load vs. displacement and stress vs. strain behavior of Insituform tensile coupons, respectively, in the circumferential direction. Table 1 provides a summary of the results, including ultimate tensile strength, maximum load, modulus of elasticity, and fiber strain. The modulus of elasticity is determined by taking the average of the initial stiffnesses of all tested coupons.

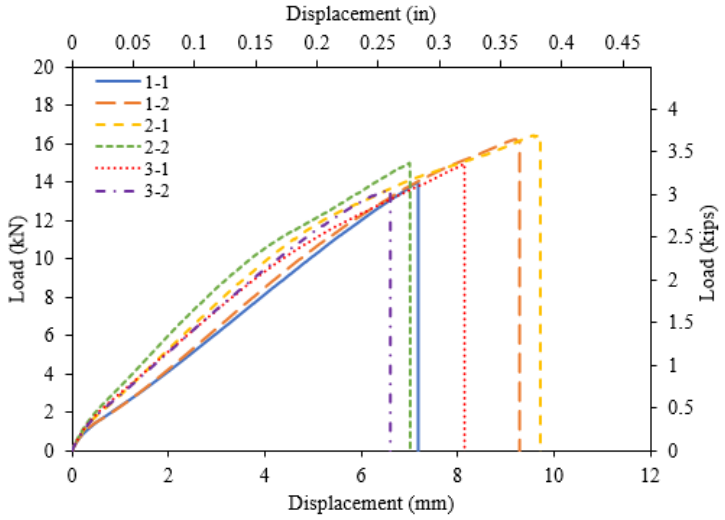

(a)

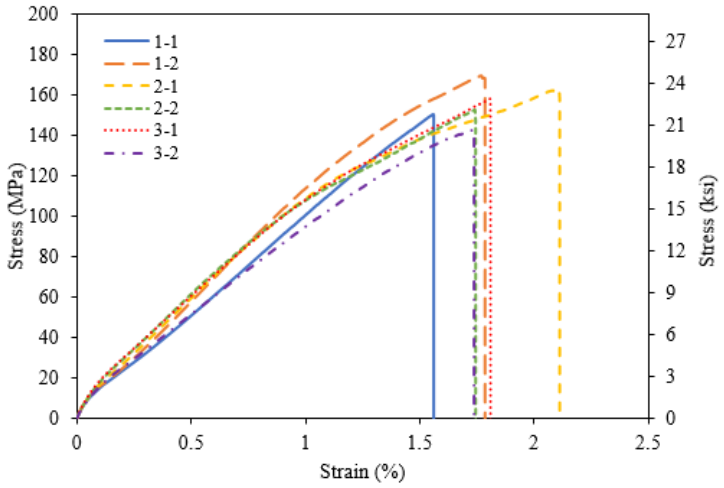

(b)

Figure 6. Tensile test results including (a) load vs. deflection and (b) stress vs. strain behavior (circumferential)

Table 1. Tensile test results of coupons (circumferential direction)

Specimen no.	Ultimate tensile strength		Maximum load		Modulus of elasticity		Failure strain
	(MPa)	(ksi)	(kN)	(ksi)	(GPa)	(ksi)	(%)
1-1	150.3	21.80	13.99	3.15	10.11	1465	1.56
1-2	169.3	24.55	16.22	3.65	11.60	1682	1.77
2-1	162.3	23.54	16.45	3.70	12.11	1756	2.11
2-2	152.5	22.11	14.99	3.37	12.27	1779	1.74
3-1	158.0	22.91	14.94	3.36	12.14	1761	1.81
3-2	142.4	20.65	13.61	3.06	10.07	1460	1.73
Maximum	169.3	24.55	16.45	3.70	12.27	1779	2.11
Minimum	142.4	20.65	13.61	3.06	10.07	1460	1.56
Average	**155.8**	**22.59**	**15.03**	**3.38**	**11.38**	**1651**	**1.79**
Standard Deviation (SD)	9.5	1.38	1.14	0.26	1.03	149	0.18

Insituform tensile dog bone coupons exhibited initial elastic behavior followed by an immediate failure due to fiber fracture. Figure 7 and Figure 8 show the failure of the Insituform tensile dog bone coupons. Figure 7 shows photos of each specimen in the loading apparatus at the end of testing. Fracture of the resin and fibers as well as delamination of resin from the fibers is presented. Figure 8 provides a collective view of the failed specimens.

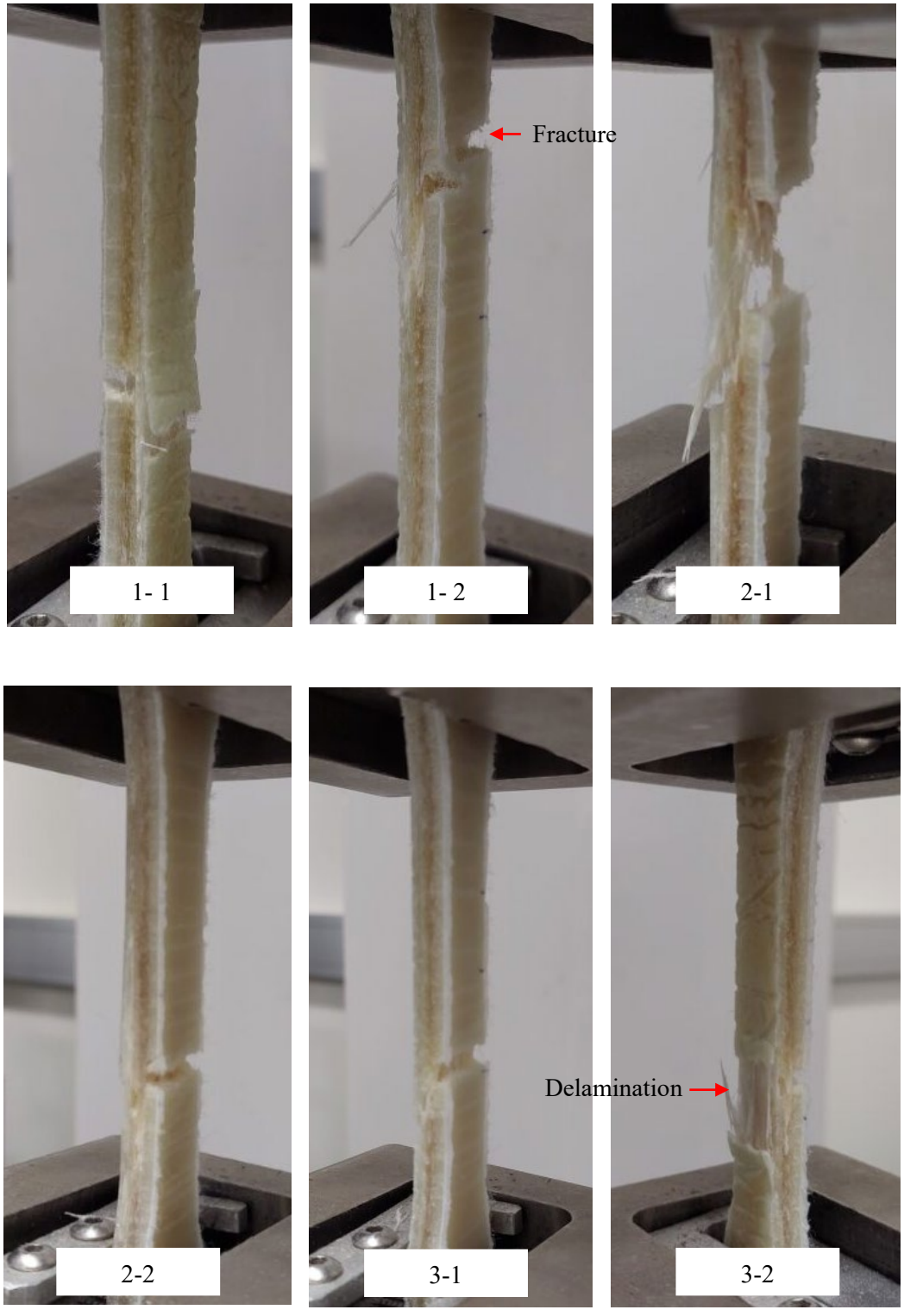

Figure 7. Failure of tensile coupons

Figure 8. Tested tensile coupons

4 Experimental Methods

This section describes the procedures performed on the test specimens. The section is divided into bending and axial sections, and these sections are further broken down by the specific specimen. All CU Boulder specimens were tested using the Structural Testing System (STS) at CIEST. General methods were similar among the specimens, but differences in exact instrumentation and methods warrant such a breakdown. Four specimens were investigated. Their general constructions are as described above. The four specimens were as follows: ISES01 - steel host pipe with a nominal 0.5 in. (12.7 mm) gap width installed with a pre-liner; ISES02 - steel host pipe with a nominal 6 in. (152 mm) gap width installed with a pre-liner; ISES03 - steel host pipe with a nominal 0.5 in. (12.7 mm) gap width installed without a pre-liner; and ISES04 - steel host pipe with a nominal 0.5 in. (12.7 mm) gap width installed without a pre-liner. Specimen details are given in Table 2.

Table 2. I-Main™ test specimen overview

Specimen Label	Host Pipe Material: OD (in. [mm])*	Nominal Crack Width (in. [mm])	Specimen Length (in. [mm])	Pre-liner installed?	Dates under Test
ISES01	Steel: 12.75 [324]	0.5 [12.7]	127 [3226]	Yes	1/25/2024-7/1/2024
ISES02	Steel: 12.75 [324]	6.0 [152.4]	133 [3378]	Yes	5/16/2024-8/22/2024
ISES03	Steel: 12.75 [324]	0.5 [12.7]	127 [3226]	No	7/12/2024-10/7/2024
ISES04 (Cornell)	Steel: 12.75 [324]	0.5 [12.7]	127 [3226]	No	5/1/2024-8/21/2024

Each specimen consisted of two 60 in. (1524 mm) long steel host pipe segments, one of which was intact and the other which featured several holes with diameters ranging from 0.25 in. (6.4 mm) to 1.5 in. (38.1 mm). Figure 9 shows drawings of these specimen dimensions.

4.1 Transverse Loading

All CU Boulder specimens were tested in four-point bending with a 22-kip (100 kN) actuator. The Cornell specimen (ISES04) was tested with a 55-kip (250 kN) actuator. Testing made use of saddles at load and supports points to avoid localized loading effects. Strain gauges (SGs), string pots (SPs), and linear variable differential transducers (LVDTs) were applied to all specimens to record strains and displacement. A schematic showing this deformation measure is given in Figure 10. A schematic of the test arrangement featuring the measurement devices and their positions are shown in Figure 11. The spacing of the sensors and clamps in Figure 11 are listed in detail for each specimen in tables in the following sections.

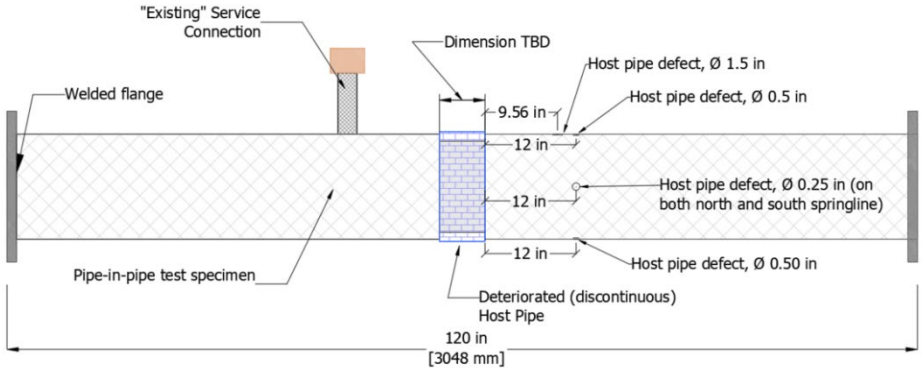

Figure 9. Dimensioned drawings of specimens including locations of defects and service connection

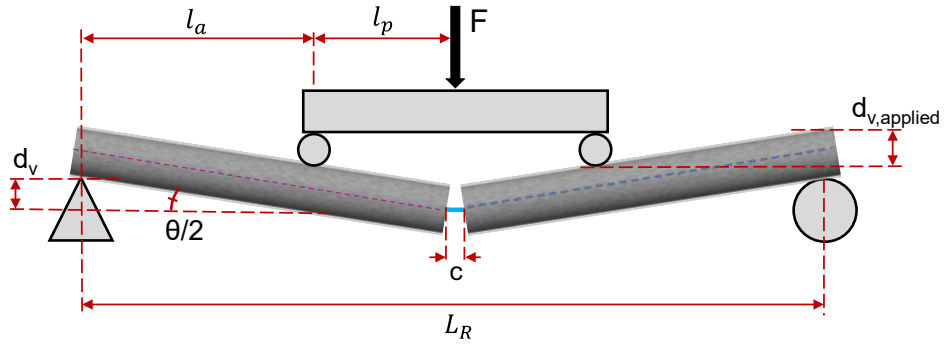

Figure 10. Schematic of 4-pt bending test and rotation angle, θ_t (adapted from Klingaman et al. 2022).

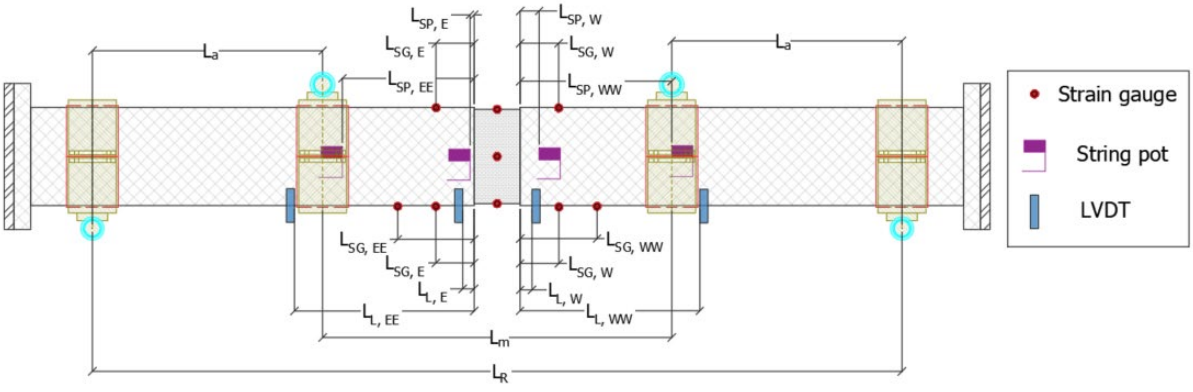

Figure 11. Test instrumentation schematic and dimension

A characteristic of four-point bending is constant moment ($M_{central}$), across the central section of the specimen that separates the two load points [i.e., 2* L_L = 40 in. (1016 mm)]. The moment increases from zero to $M_{central}$ along the specimen between the load and support points [e.g., L_s= 25 in. (625 mm)]. The moment applied to the central portion of the specimen, $M_{central}$, was calculated as

$$M_{central} = \frac{P(L_s)}{2} \quad (1)$$

in which P is the load applied by the actuator to the load beam plus the vertical force of the load beam [e.g., 0.23 kips (1.02 kN)].

Global rotation, also referred to as rotation, is reported herein to characterized specimen deformation and is taken as the relative rotation at the pipeline center between straight line projections of the pipes either side of the gap. The LVDTs between the load points (notation: E & W) were used with distance from the support points for global rotation calculations, such that:

$$\theta_t \text{ (degrees)} = 2 * tan^{-1}\left[\frac{average(d_{v,E}, d_{v,W})}{(L_L + L_s - 0.5c - average(L_{L,E}, L_{L,W})}\right] \quad (2)$$

for which $d_{v,E}$ and $d_{v,W}$ are the relative vertical displacements between the support points and the nearest displacement device (typically LVDT) positioned on either side of the gap. The distances L_L , L_s, and c are depicted in Figure 10 and reported in subsequent sections. As shown in Figure 11, $L_{L,E}$ and $L_{L,W}$ are the LVDT distance from the gap edge and are reported for each test in the tables of subsequent sections.

All setups featured saddles fitted to the pipe and cages about saddle rollers at both the loading and support points of the specimens. The saddle and cage system allowed the pipeline to return to its initial position without being lifted off its support points, thus simulating deflection in the field wherein the pipeline in soil returns to its original position after rolling traffic loads move across the pipe. To duplicate this condition some tensile force is mobilized through the saddles to counterbalance the dead weight of the pipeline. For some operations, these cages were loosened, but for most testing, the cages were secured (exceptions clearly noted). Between tests, specimens were supported by jacks to avoid specimen sag under self-weight. The crossbeam used to distribute load was also lifted away from the specimen and supported by restraining chains between each test.

Traffic loading cycles were performed in block sets to allow for setup, sensor adjustments, and ease of general lab use. To begin a new traffic cycle set, the actuator was first powered on so the restraining chains supporting the crossbeam weight could be removed. The crossbeam was then lowered to contact the specimen so that cages could be secured around the loading saddles. Once secured to the actuator, the

position of the actuator was noted, and the supporting jacks were removed. Specimens were then pressurized to the desired internal pressure prior to beginning cycles. After cycles were concluded for the day, the actuator was returned to its initial position before putting the supporting jacks under the specimen. Cages were removed and the actuator was lifted away from the pipe. This process was repeated for every test performed. Most testing was performed at a nominal pressure of 65 psi (450 kPa) with water.

4.1.1 ISES01 (CUB)

The specimen for ISES01 is composed of a steel host pipe with nominal initial gap opening of 0.5 in. (12.2 mm) and rehabilitated with I-Main CIPP installed with a pre-liner. The geometry of the specimen was set up in a 4-point bending configuration, with distances between supports and load points being 30 in. – 40 in. – 30 in. (762 mm – 1016 mm - 762 mm), centered about the crack opening.

The instrumentation used for ISES01 during lateral testing is outlined in Table 3. The instrumentation consisted of strain gauges on the crown and invert over the middle 40 in. (1000 mm) (maximum moment) span in the vicinity of the crack. Linear variable differential transducers (LVDTs) and string potentiometers (SPs) were vertically arranged to measure pipe deflection at various locations on the beam. LVDTs were mounted on stands on the ground and the rods were connected to the pipes with brackets or screw sockets. SPs were mounted on the pipe, stands on the grounds, and beams extending from the strong wall (frame support). Additionally, the north facing side of the pipe over and in the vicinity of the gap was painted white and speckled black for digital image correlation (Figure 12) (see Appendix A for further discussion of DIC). Figure 11 provides a schematic of specimen measurements and instrumentation locations and Table 4 gives the values corresponding to the figure used for this specimen.

Table 3. ISES01 bending instrumentation

Instrument Description	Local Instrument Name	Location	Channel No.
East, Crown, 5 in. from crack edge, Circumferential	SG5E_CC	On steel host pipe, crown, east side 5 in. from crack edge	Ch 10
East, Crown, 5 in. from crack edge, Axial	SG5E_CA	On steel host pipe, crown, east side 5 in. from crack edge	Ch 11
East, Invert 5 in. from crack edge, Circumferential	SG5E_IC	On steel host pipe, invert, east side 5 in. from crack edge	Ch. 12
East, Invert, 5 in. from crack edge, Axial	SG5E_IA	On steel host pipe, invert, east side 5 in. from crack edge	Ch. 13
East, Invert 10 in. from crack edge, Circumferential	SG10E_IC	On steel host pipe, invert, east side 10 in. from crack edge	Ch. 8
East, Invert, 10 in. from crack edge, Axial	SG10E_IA	On steel host pipe, invert, east side 10 in. from crack edge	Ch. 9

West, Invert 10 in. from crack edge, Circumferential	SG10W_IC	On steel host pipe, invert, east side 10 in. from crack edge	Ch. 14
West, Invert, 10 in. from crack edge, Axial	SG10W_IA	On steel host pipe, invert, east side 10 in. from crack edge	Ch. 15
West, Crown, 5 in. from crack edge, Circumferential	SG5W_CC	On steel host pipe, crown, west side 5 in. from crack edge	Ch. 16
West, Crown, 5 in. from crack edge, Axial	SG5W_CA	On steel host pipe, crown, west side 5 in. from crack edge	Ch. 17
West, Invert, 5 in. from crack edge, Circumferential	SG5W_IC	On steel host pipe, invert, west side 5 in. from crack edge	Ch. 18
West, Invert 5 in. from crack edge, Axial	SG5W_IA	On steel host pipe, invert, west side 5 in. from crack edge	Ch. 19
VSP: West, South Springline on Saddle (19.75 in. from crack edge)	SP18-10_WW	On west saddle (centered), south springline, 19.75 in. from crack edge	Ch 1.
VSP: West, South Springline on Host Pipe (2.5 in. from crack edge)	SP17-20_W	On steel host pipe, west side, south springline, 2.5 in. from crack edge	Ch. 2
VSP: East South Springline on Host Pipe (0.5 in. from crack edge)	SP15-10_E	On steel host pipe, east side, south springline, 0.5 in. from crack edge	Ch. 3
VSP: East, South Springline on Saddle (19.75 in. from crack edge)	SP19-20_EE	On east saddle (centered), south springline, 19.75 in. from crack edge	Ch. 5
LVDT 1020, West, Invert, 1.5 in from crack edge ($d_{v,W}$)	LVDT06_1020W	On backet on steel, west, invert, 1.5 in. from crack edge	LVDT Ch. 6
LVDT 1021, East Invert, 1.5 in from crack edge ($d_{v,E}$)	LVDT07_1021E	On backet on steel, east, invert, 1.5 in. from crack edge	LVDT Ch. 7
LVDT 1017, West, Invert, 23 in from crack edge ($d_{v,WW}$)	LVDT2_1017WW	On bracket on steel, west, invert, outside east load saddle, 23 in from crack edge	LVDT Ch. 2
LVDT 1008, East, Invert, 23 in from crack edge ($d_{v,EE}$)	LVDT10_1008EE	On bracket on steel, east, invert, outside east load saddle, 23 in from crack edge	LVDT Ch. 10
110-kip Load Cell	Applied Force	MTS Crosshead (Above Specimen)	
MTS Actuator Piston Position		MTS Crosshead (Above Specimen)	
150 psi Pressure Transducer	N/A	N/A	Ch. 21

* VSP: vertical string pot, LVDT: linearly varying differential transducer, SG: foil stain gage

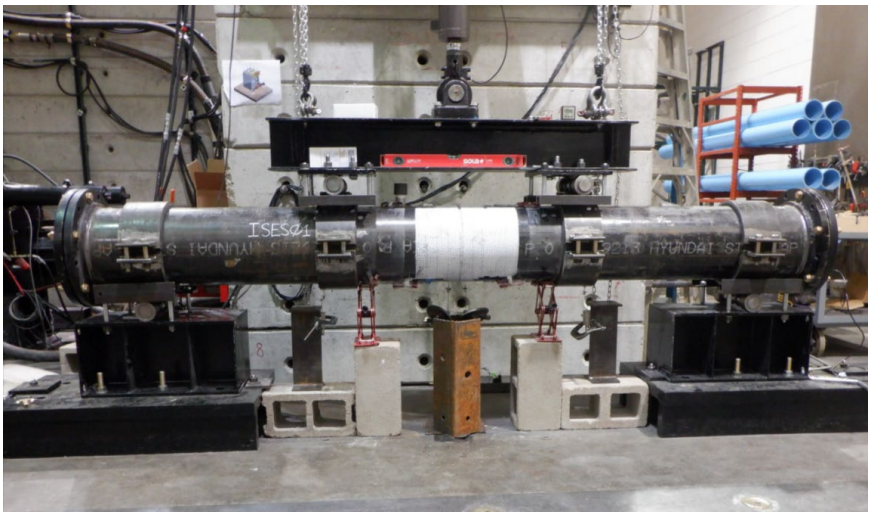

Figure 12. Image of ISES01 bending setup

Table 4. ISES01 instrumentation schematic dimensions

Sensor / Measurement	Symbol	Distance
Strain Gauge (EE)	$L_{SG, EE}$	10 in
Strain Gauge (E)	$L_{SG, E}$	5 in
Strain Gauge (W)	$L_{SG, W}$	5 in
Strain Gauge (WW)	$L_{SG, WW}$	10 in
String Pot (EE)	$L_{SP, EE}$	19.75 in
String Pot (E)	$L_{SP, E}$	0.5 in
String Pot (W)	$L_{SP, W}$	2.5 in
String Pot (WW)	$L_{SP, WW}$	19.75 in
LVDT (EE)	$L_{L, EE}$	23 in
LVDT (E)	$L_{L, E}$	1.5 in
LVDT (W)	$L_{L, W}$	1.5 in
LVDT (WW)	$L_{L, WW}$	23 in
Distance between reaction and applied force	L_a	30 in
Distance between reactions	L_R	100 in
Distance between applied forces	L_m	40 in

Several preliminary lateral tests were performed on ISES01 to check that instrumentation was functioning properly. Data recorded from these preliminary tests was also used to assess the initial lateral stiffness of the specimen. Once target rotations were established, traffic loading cycles were performed at cyclic frequencies of 1 Hz and 2 Hz, associated with sample rates of 64 Hz and 124 Hz, respectively. For ISES01, the targeted rotation was 0.024°, which was determined from the analysis as described in Section

2.1.2 increased to 0.036° with a safety factor of 1.5. All traffic cycles were performed with constant pressure ranging from 10 psi to 65 psi. Results for testing are detailed in later sections.

After 500,000 traffic cycles were performed, two larger lateral displacements were applied, simulating the effects of ground motions caused by adjacent excavation events. These tests were conducted with a constant internal pressure of 65 psi. The cages used to secure the specimen to the actuator were slightly loosened prior to these tests to ensure the freedom of rotation and translation for each support and loading point. The first AE test consisted of an initial target rotation of 0.58°. The actuator was returned to the initial test position before applying the larger of the two AE deformations, which consisted of a target rotation of 1.1°.

After the adjacent excavation testing, the cages were resecured to perform 100,000 subsequent traffic cycles with similar target rotations as the previous traffic cycles. This concluded the bending procedure for ISES01.

4.1.2 ISES02 (CUB)

The specimen for ISES02 is composed of a steel host pipe with nominal initial gap opening of 6.0 in. (150 mm) and rehabilitated with I-MAIN CIPP installed with a pre-liner. The instrumentation used for ISES02 during lateral testing is outlined in Table 5. The instrumentation consisted of strain gauges on the crown and invert over the middle 40 in. (1000 mm) (maximum moment) span in the vicinity of the crack. LVDTs and SP were vertically arranged to measure pipe deflection at various locations on the beam. LVDTs were mounted on stands on the ground and the rods were connected to the pipes with brackets or screw sockets. SPs were mounted on the pipe, stands on the grounds, and beams extending from the strong wall (frame support). Additionally, the north facing side of the pipe over and in the vicinity of the gap was painted white and speckled black for digital image correlation (Figure 13).

Table 5. ISES02 bending instrumentation

Instrument Description	Local Instrument Name	Location	Channel No.
East, Crown, 5 in. from crack edge, Circumferential	SG5E_CC	On steel host pipe, crown, east side 5 in. from crack edge	Ch 0
East, Crown, 5 in. from crack edge, Axial	SG5E_CA	On steel host pipe, crown, east side 5 in. from crack edge	Ch 6
East, Invert 5 in. from crack edge, Circumferential	SG5E_IC	On steel host pipe, invert, east side 5 in. from crack edge	Ch. 3
East, Invert, 5 in. from crack edge, Axial	SG5E_IA	On steel host pipe, invert, east side 5 in. from crack edge	Ch. 9
Center, Crown 0in. from crack edge, Circumferential	SG0 _CC	On liner, crown, center	Ch. 2

East, Invert, 10 in. from crack edge, Axial	SG10E_IA	On steel host pipe, invert, east side 10 in. from crack edge	Ch. 8
Center, Invert 0in. from crack edge, Circumferential	SG0 _IC	On liner, invert, center	Ch. 11
West, Invert, 10 in. from crack edge, Axial	SG10W_IA	On steel host pipe, invert, east side 10 in. from crack edge	Ch. 5
West, Crown, 5 in. from crack edge, Circumferential	SG5W_CC	On steel host pipe, crown, west side 5 in. from crack edge	Ch. 1
West, Crown, 5 in. from crack edge, Axial	SG5W_CA	On steel host pipe, crown, west side 5 in. from crack edge	Ch. 7
West, Invert, 5 in. from crack edge, Circumferential	SG5W_IC	On steel host pipe, invert, west side 5 in. from crack edge	Ch. 4
West, Invert 5 in. from crack edge, Axial	SG5W_IA	On steel host pipe, invert, west side 5 in. from crack edge	Ch. 10
Center, Spring line 0in. from crack edge, Circumferential	SG0 _SC	On liner, spring line, center	Ch. 12
Center, Spring line 0in. from crack edge, Axial	SG0 _SA	On liner, spring line, center	Ch. 13
Center, Crown 0in. from crack edge, Axial	SG0 _CA	On liner, crown, center	Ch. 14
Center, Invert 0in. from crack edge, Axial	SG0 _IA	On liner, invert, center	Ch. 15
Vertical String pot, West, South Springline on Saddle (19.75 in. from crack edge)	SP18-10_WW	On west saddle (centered), south springline, 19.75 in. from crack edge	Ch. 1
Vertical String pot, West, South Springline on Steel Pipe (2.5 in. from crack edge)	SP17-20_W	On steel host pipe, west side, south springline, 2.5 in. from crack edge	Ch. 2
Vertical String pot, East South Springline on Steel Pipe (0.5 in. from crack edge)	SP15-10_E	On steel host pipe, east side, south springline, 0.5 in. from crack edge	Ch. 3
Vertical String pot, East, South Springline on Saddle (19.75 in. from crack edge)	SP19-20_EE	On east saddle (centered), south springline, 19.75 in. from crack edge	Ch. 5
LVDT 1020, West, Invert, 1.5 in from crack edge	LVDT06_1020W	On backet on steel, west, invert, 1.5 in. from crack edge	LVDT Ch. 6
LVDT 1021, East Invert, 1.5 in from crack edge	LVDT07_1021E	On backet on steel, east, invert, 1.5 in. from crack edge	LVDT Ch. 7
LVDT 1017, West, Invert, 23 in from crack edge	LVDT2_1017WW	On bracket on steel, west, invert, outside east load saddle, 23 in from crack edge	LVDT Ch. 2
LVDT 1008, East, Invert, 23 in from crack edge	LVDT10_1008EE	On bracket on steel, east, invert, outside east load saddle, 23 in from crack edge	LVDT Ch. 10
110-kip Load Cell	Applied Force	MTS Crosshead (Above Specimen)	
MTS Actuator Piston Position		MTS Crosshead (Above Specimen)	
150 psi Pressure Transducer	N/A	N/A	Ch. 21

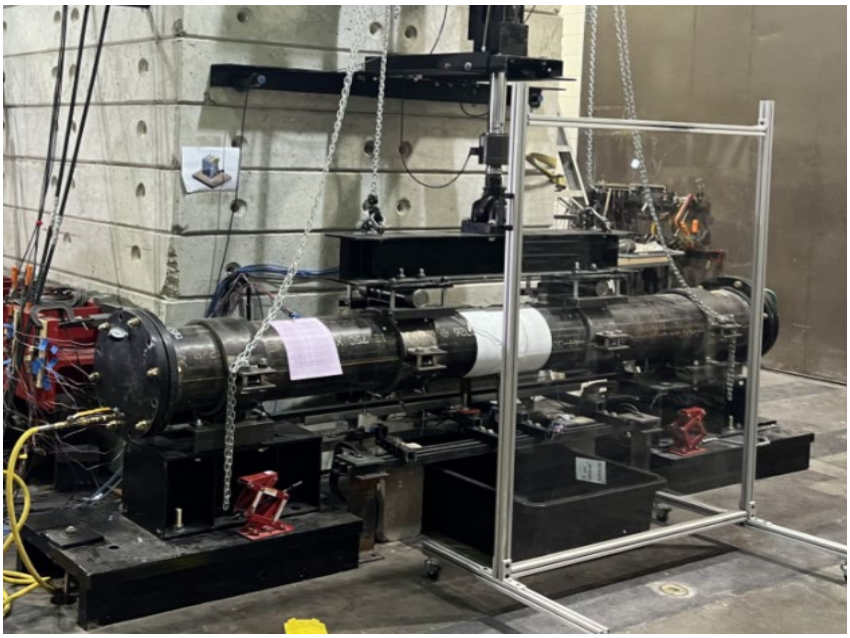

Figure 13. Photo of ISES02 bending setup

Table 6 gives the values corresponding to the dimensions previously shown in Figure 11. The geometry of the specimen was set up in a 4-point bending configuration, with distances between supports and load points being 30 in. – 40 in. – 30 in. (762 mm – 1016 mm - 762 mm), centered about the crack opening.

Several preliminary lateral tests were performed on ISES02 to check that instrumentation was functioning properly. Data recorded from these preliminary tests was also used to assess the initial lateral stiffness of the specimen. Once target rotations were established, traffic loading cycles were performed at cyclic frequencies of 1 Hz and 2 Hz, associated with sample rates of 64 Hz and 124 Hz, respectively. For ISES01, the targeted rotation was 0.024°, which was determined from the analysis as described in Section 2.1.2 increased to 0.036° with a safety factor of 1.5. All traffic cycles were performed with constant pressure ranging from 10 psi to 65 psi. Results for testing are detailed in later sections.

After 500,000 traffic cycles were performed, two larger lateral displacements were applied, simulating the effects of ground motions caused by adjacent excavation events. These tests were conducted with a constant internal pressure of 65 psi. The cages used to secure the specimen to the actuator were slightly loosened prior to these tests to ensure the freedom of rotation and translation for each support and loading point. The first AE test consisted of an initial target rotation of 0.40°. The actuator was returned to

the initial test position before applying the larger of the two AE deformations, which consisted of a target rotation of 0.80°.

After the adjacent excavation testing, the cages were resecured to perform 100,000 subsequent traffic cycles with similar target rotations as the previous traffic cycles. This concluded the bending procedure for ISES02.

Table 6. ISES02 instrumentation schematic dimensions

Sensor / Measurement	Symbol	Distance
Strain Gauge (EE)	$L_{SG, EE}$	10 in
Strain Gauge (E)	$L_{SG, E}$	5 in
Strain Gauge (W)	$L_{SG, W}$	5 in
Strain Gauge (WW)	$L_{SG, WW}$	10 in
String Pot (EE)	$L_{SP, EE}$	19.75 in
String Pot (E)	$L_{SP, E}$	0.5 in
String Pot (W)	$L_{SP, W}$	2.5 in
String Pot (WW)	$L_{SP, WW}$	19.75 in
LVDT (EE)	$L_{L, EE}$	23 in
LVDT (E)	$L_{L, E}$	1.5 in
LVDT (W)	$L_{L, W}$	1.5 in
LVDT (WW)	$L_{L, WW}$	23 in
Distance between reaction and applied force	L_a	30 in
Distance between reactions	L_R	100 in
Distance between applied forces	L_m	40 in

4.1.3 ISES03 (CUB)

The specimen for ISES03 is composed of a steel host pipe with nominal initial gap opening of 0.5 in. (12.7 mm) and rehabilitated with I-Main CIPP installed without a pre-liner. The instrumentation used for ISES03 during lateral testing is outlined in Table 7. The instrumentation consisted of strain gauges on the crown and invert over the middle 40 in. (1000 mm) (maximum moment) span in the vicinity of the crack. LVDTs and SPs were vertically arranged to measure pipe deflection at various locations on the beam. LVDTs were mounted on stands on the ground and the rods were connected to the pipes with brackets or screw sockets. SPs were mounted on the pipe, stands on the grounds, and beams extending from the strong wall (frame support). Additionally, the north facing side of the pipe over and in the vicinity of the gap was painted white and speckled black for digital image correlation (see Figure 14).

Table 7. ISES03 bending instrumentation

Instrument Description	Local Instrument Name	Location	Channel No.
East, Crown, 5 in. from crack edge, Circumferential	SG5E_CC	On steel host pipe, crown, east side 5 in. from crack edge	Ch 0
East, Crown, 5 in. from crack edge, Axial	SG5E_CA	On steel host pipe, crown, east side 5 in. from crack edge	Ch 6
East, Invert 5 in. from crack edge, Circumferential	SG5E_IC	On steel host pipe, invert, east side 5 in. from crack edge	Ch. 3
East, Invert, 5 in. from crack edge, Axial	SG5E_IA	On steel host pipe, invert, east side 5 in. from crack edge	Ch. 9
East, Invert, 10 in. from crack edge, Circumferential	SG10E_IC	On steel host pipe, invert, east side 10 in. from crack edge	Ch. 2 (switched to ch. 12 before test BC08)
East, Invert, 10 in. from crack edge, Axial	SG10E_IA	On steel host pipe, invert, east side 10 in. from crack edge	Ch. 8
West, Invert, 10 in. from crack edge, Circumferential	SG10W_IC	On steel host pipe, invert, east side 10 in. from crack edge	Ch. 11
West, Invert, 10 in. from crack edge, Axial	SG10W_IA	On steel host pipe, invert, east side 10 in. from crack edge	Ch. 5
West, Crown, 5 in. from crack edge, Circumferential	SG5W_CC	On steel host pipe, crown, west side 5 in. from crack edge	Ch. 1
West, Crown, 5 in. from crack edge, Axial	SG5W_CA	On steel host pipe, crown, west side 5 in. from crack edge	Ch. 7
West, Invert, 5 in. from crack edge, Circumferential	SG5W_IC	On steel host pipe, invert, west side 5 in. from crack edge	Ch. 4
West, Invert 5 in. from crack edge, Axial	SG5W_IA	On steel host pipe, invert, west side 5 in. from crack edge	Ch. 10
East, Crown 1 in. from crack edge, Axial	SG1E_CA	On steel host pipe, Crown, East side 1 in. from crack edge	Ch. 12 (switched to ch. 2 before test BC08)
West, Crown 1 in. from crack edge, Axial	SG1W_CA	On steel host pipe, Crown, West side 1 in. from crack edge	Ch. 13
East, Invert 1 in. from crack edge, Axial	SG1E_IA	On steel host pipe, Invert, East side 1 in. from crack edge	Ch. 14
West, Invert 1 in. from crack edge, Axial	SG1W_IA	On steel host pipe, Invert, West side 1 in. from crack edge	Ch. 15
Vertical String pot, West, South Springline on Saddle (20 in. from crack edge)	SP23-38	On west saddle (centered), south springline, 20 in. from crack edge	Ch. 0

Vertical String pot, West, South Springline on Steel Pipe (2.5 in. from crack edge)	SP24-10	On steel host pipe, west side, south springline, 2.5 in. from crack edge	Ch. 1
Vertical String pot, East South Springline on Steel Pipe (2.5 in. from crack edge)	SP29-10	On steel host pipe, east side, south springline, 2.5 in. from crack edge	Ch. 2
Vertical String pot, East, South Springline on Saddle (20 in. from crack edge)	SP21**	On east saddle (centered), south springline, 20 in. from crack edge	Ch. 3
LVDT SN1004, West, Invert, 1.5 in from crack edge	LVDT06_1020W	On backet on steel, west, invert, 1.5 in. from crack edge	LVDT Ch. 3
LVDT SN10011, East Invert, 1.5 in from crack edge	LVDT07_1021E	On backet on steel, east, invert, 1.5 in. from crack edge	LVDT Ch. 1
LVDT SN1003, West, Invert, 23.5 in from crack edge	LVDT2_1017WW	On bracket on steel, west, invert, outside east load saddle, 23.5 in from crack edge	LVDT Ch. 2
LVDT SN1002, East, Invert, 23.5 in from crack edge	LVDT10_1008EE	On bracket on steel, east, invert, outside east load saddle, 23.5 in from crack edge	LVDT Ch. 0
110-kip Load Cell	Applied Force	MTS Crosshead (Above Specimen)	
MTS Actuator Piston Position		MTS Crosshead (Above Specimen)	
150 psi Pressure Transducer	N/A	N/A	Ch. 21

Table 8 provides the values corresponding to the dimensions shown in Figure 11. The geometry of the specimen was set up in a 4-point bending configuration, with distances between supports and load points being 30 in. – 40 in. – 30 in. (762 mm – 1016 mm - 762 mm), centered about the crack opening.

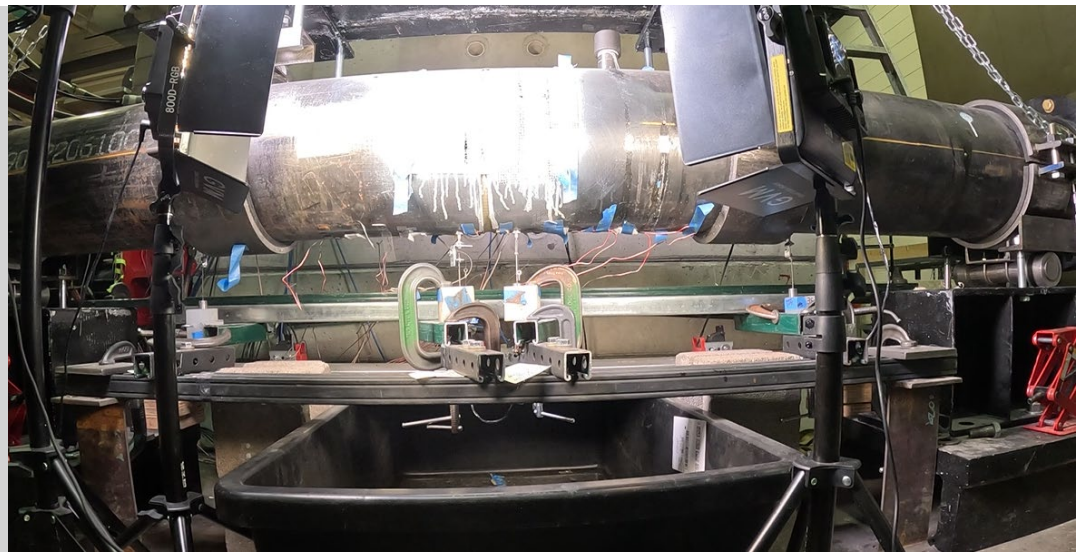

Figure 14. Photo of ISES03 bending setup

Table 8. ISES03 instrumentation schematic dimensions

Sensor / Measurement	Symbol	Distance
Strain Gauge (EE)	$L_{SG, EE}$	10 in
Strain Gauge (E)	$L_{SG, E}$	5 in
Strain Gauge (W)	$L_{SG, W}$	5 in
Strain Gauge (WW)	$L_{SG, WW}$	10 in
Strain Gauge (additional)	$L_{SG, A}$	1 in
String Pot (EE)	$L_{SP, EE}$	20 in
String Pot (E)	$L_{SP, E}$	2.5 in
String Pot (W)	$L_{SP, W}$	2.5 in
String Pot (WW)	$L_{SP, WW}$	20 in
LVDT (EE)	$L_{L, EE}$	23.5 in
LVDT (E)	$L_{L, E}$	1.5 in
LVDT (W)	$L_{L, W}$	1.5 in
LVDT (WW)	$L_{L, WW}$	23.5 in
Distance between reaction and applied force	L_a	30 in
Distance between reactions	L_R	100 in
Distance between applied forces	L_m	40 in

Preliminary bend tests were performed on ISES03 to check that instrumentation was functioning and assess the stiffness. Traffic loading cycles were then performed. These were predominantly performed at cyclic frequencies of 1 Hz and 2 Hz, associated with sample rates of 64 Hz and 128 Hz, respectively. For ISES03, the targeted rotation was 0.044°, which was determined from the analysis as described in Section

2.1.2, and increased with a safety factor of 1.5. The displacement from the LVDTs near the center of the specimen was about 0.017 in. (0.45 mm). All traffic cycles were performed with pressure ranging from 10 psi to 65 psi.

After approximately 500,000 cycles the deformations were applied to simulate parallel excavations. These were performed at an internal pressure of 65 psi. Cages were loosened for this testing. The parallel excavation bend procedure consisted of an initial bend to a rotation of 0.4°, associated with inner LVDT displacements around 0.17 in. (4.3 mm). The actuator was then returned to the initial test position, and the specimen was loaded to a rotation of 0.8°, associated with outer LVDT displacements around 0.34 in. (8.6 mm). These rotations correspond to values from a parallel excavation model considering maximum soil displacements of 2.5 in. and 5 in. (63.5 mm and 127 mm).

After the parallel excavation testing, the cages were retightened. Roughly 100,000 subsequent traffic cycles were then performed. These cycles were performed with the same test set-up parameters (actuator displacement commands) as the previous traffic cycles. This concluded the bending procedure for ISES03.

4.1.4 ISES04 (Cornell)

Table 9 lists the location, instrument type, and local instrument name. The instruments and their locations both north and south of the gap at the center of the specimen are depicted in Figure 15. Vertical displacements along the length of the specimen were measured using LVDTs and VSPs. The LVDTs were mounted on stands on the base frame with their rods positioned against brackets connected to the pipeline. VSPs were mounted next to the LVDTs utilizing the same brackets.

Table 9. ISES04 bending instrumentation

Location	Instrument Description	Local Instrument Name
25 in. North of Centerline	LVDT	LVDT_N25
	String Potentiometer	VSP_N25
14 in. North of Centerline	Invert, Axial Strain	IA_N14
	Invert, Circumferential Strain	IC_N14
	Crown, Axial Strain	*CA_N14
	Crown, Circumferential Strain	*CC_N14
5 in. North of Centerline	Crown, Axial Strain	CA_N5
	Crown, Circumferential Strain	CC_N5
	Invert, Axial Strain	IA_N5
	Invert, Circumferential Strain	IC_N5
1 in. North of Centerline	LVDT	LVDT_N1
	String Potentiometer	VSP_N1

	Crown, Axial Strain	*CA_N1
	Invert, Axial Strain	*IA_N1
1 in. South of Centerline	LVDT	LVDT_S1
	String Potentiometer	VSP_S1
	Crown, Axial Strain	*CA_S1
	Invert, Axial Strain	*IA_S1
5 in. South of Centerline	Crown, Axial Strain	CA_S5
	Crown, Circumferential Strain	CC_S5
	Invert, Axial Strain	IA_S5
	Invert, Circumferential Strain	IC_S5
14 in. South of Centerline	Invert, Axial Strain	IA_S14
	Invert, Circumferential Strain	IC_S14
	Crown, Axial Strain	*CA_S14
	Crown, Circumferential Strain	*CC_S14
25 in. South of Centerline	LVDT	LVDT_S25
	String Potentiometer	VSP_S25
Actuator	MTS Load Xducer (55 kip)	Actuator_Load
	MTS Actuator LVDT (±3 in.)	Actuator_Disp_In
	String Potentiometer	Actuator_Disp_Ex
Pipe South End	Pressure Xducer Pipe	Pressure_Pipe
Wall Valve	Pressure Xducer Wall	Pressure_Deck

*These instruments were added on 17JUL2024, after the initial practice pushes. The purpose of these strain gages was to sense the debonding of the PIP from the host pipe.

A characteristic of four-point bending, for which a schematic is shown in Figure 15, is constant moment ($M_{central}$), across the central 40 in. (1016 mm) that separates the two load points. The moment increases from zero to $M_{central}$ across the 25-in. (625-mm) separation between the load and support points. The moment applied to the central portion of the specimen, $M_{central}$, was calculated as

$$M_{central} = \frac{P\ (25in.)}{2} \quad (1)$$

in which P is the load applied by the actuator to the load beam plus the vertical force of the load beam of 0.23 kips (1.02 kN).

A global rotation was measured, which is the relative rotation at the pipeline center between straight line projections of the pipes either side of the gap. Global rotation in response to traffic loads is shown and discussed by Stewart et al. (2015). In this report global rotation is often referred to as rotation. For the ISES04 results section, rotation was calculated as

$$\theta\ (\text{degrees}) = sin^{-1}\left[\frac{0.80(d_{v1} + d_{v2})}{20in.}\right] \quad (2)$$

for which d_{v1} and d_{v2} are the relative vertical displacements (in.) between the support points and the nearest linear voltage differential transformer (LVDT)/string potentiometer (SP) locations on either side of the gap. The distance 20 in. refers to the separation between the support point and the nearest LVDT/SP location. As shown in Figure 15, load was applied to load and support points through saddles fitted to the pipe. North and south directions for the Cornell specimen are shown by N and S, respectively, in Figure 15 as well as in other test schematics and photographs.

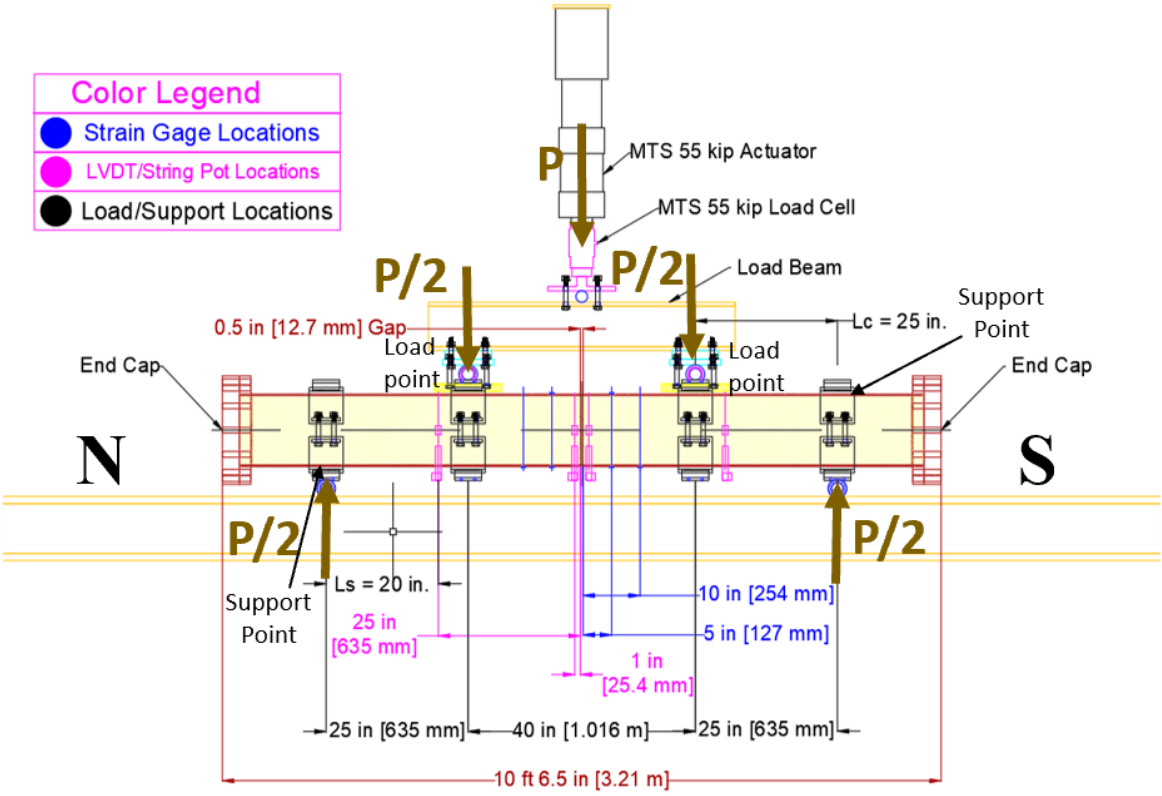

Figure 15. Schematic of four-point bending test for specimen ISES04

The vertical force, P, was applied to the pipeline by a 55-kip (245 kN), 6-in. (152 mm) actuator through a 55-kip (245 kN) load cell. Vertical displacements were measured through LVDTs and SPs located along the pipeline. Strain gauges were also placed at various locations to evaluate the longitudinal and circumferential stress/strain behavior. Four practice loadings were performed on Specimen ISES04 to check that the instrumentation was functioning and to evaluate specimen stiffness. The average water pressure sustained during testing was 10 psi (69 kPa) for the first 100,000 cycles, 30 psi (207 kPa) for the next 300,000 cycles, and 65 psi (448 kPa) for the last 100,000 cycles. A pressure relief valve was connected to

the specimen to maintain constant pressure. All tests were performed with live pressure. The data sampling rate was 32 Hz.

Figure 16 presents a photograph of the test set-up depicted in Figure 15. The test pipeline, MTS actuator, load cell, load beam, load contacts and supports can be seen in the figure. The gap was centered in the load frame. Four-point bending was applied, for which the reaction locations were positioned 25 in. (635 mm) north and south of the loading locations, which were in turn were separated by 40 in. (1016 mm). This arrangement is referred to as a 25 in. – 40 in. – 25 in. configuration.

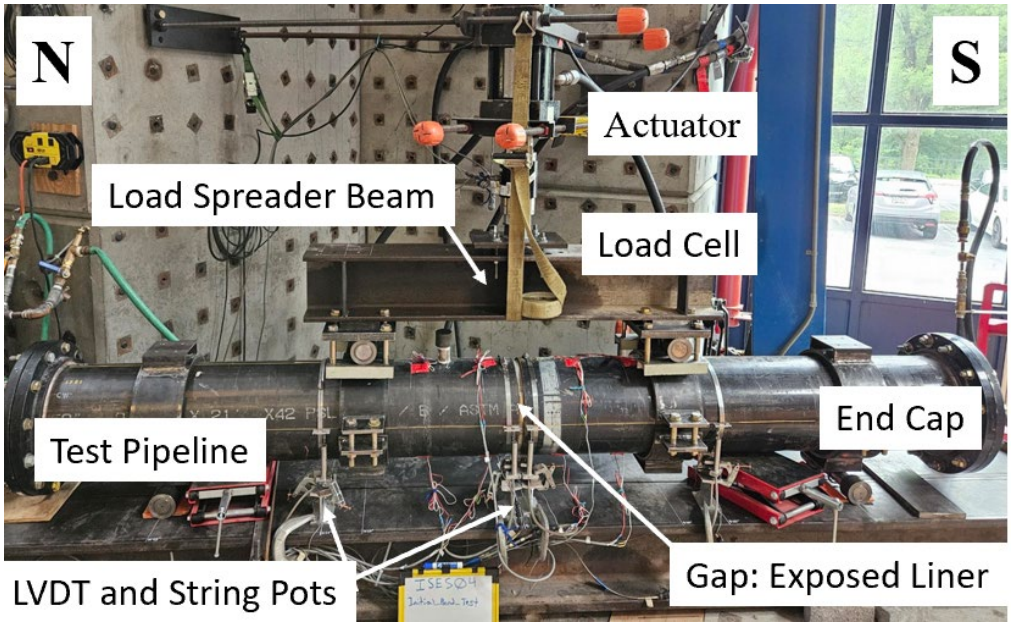

Figure 16. Photograph of ISES04 in bending test frame

4.2 Axial Testing

Axial testing followed the completion of all bending tests. Each specimen was oriented in a horizontal position supported by two supports with low friction Teflon pads between the specimen and the supports to reduce additional unwanted force measurements caused by friction. Specimens were tested with live pressure ranging from 0 psi to 65 psi, with most of the testing using the latter. For thermal cyclic testing, displacements were applied in the tensile direction at a quasi-static strain rate, then returned back to the actuator's initial displacement reading. Load was transferred to the specimens through the flanges with rods.

Target displacements were determined with methods described in Section 2.2. Relatively small initial displacements were applied to each specimen to establish an initial effective crack width, which provided initial target CODs for each specimen. The effective crack width was recalculated after each set of thermal cycles, establishing a new target COD for subsequent cycles. For the first cycle of each set, an initial COD was measured due to pressurization of the specimen. This COD was included in the total COD for each set of tests (i.e., this displacement was considered to contribute to reaching the target crack opening displacement).

After 50 or more thermal cycles were applied to a specimen, ultimate capacity tests were performed. Ultimate capacity tests for each specimen generally included several loading and unloading instances, each with varying pressures or varying load rates. Details on these variations are discussed further in the results section (Section 5). Crack opening displacements were measured with a variety of displacement sensors (details provided for each specimen below).

4.2.1 ISES01 (CUB)

The specimen for ISES01 is composed of a steel host pipe with nominal initial gap opening of 0.5 in. (12.2 mm) and rehabilitated with I-Main CIPP installed with a pre-liner. A 110-kip (500 kN) MTS actuator with an 11 in. (280 mm) stroke mounted in a rigid self-contained loading frame was used to test this specimen. Though strain gauge locations did not change between lateral and axial testing, channels used for recording data did change (see Table 3). SPs and LVDTs were oriented around the crack to record axial deformation, fixed to the host pipe with brackets. Instrumentation details are given in Table 10 while Figure 17 shows the axial test setup of ISES01.

Table 10. ISES01 axial instrumentation

Instrument Description	Local Instrument Name	Location	Channel No.
Horizontal String pot, North Shoulder, over the Crack, fixed to Steel Pipe	SP22-10_NS	North Shoulder, over crack fixed to steel host pipe segments	Ch. 22
Horizontal String pot, South Haunch, over the Crack, fixed to Steel Pipe	SP27-30_SH	South Haunch, over crack fixed to steel host pipe segments	Ch. 04
LVDT 1008, Invert, over crack, fixed to Steel Pipe	LVDT01_1008_I	South shoulder, over crack fixed to steel host pipe segments	LVDT Ch. 1
LVDT 1006, Crown, over crack, fixed to Steel Pipe	LVDT06_1006_C	Crown, over the crack, fixed to steel host pipe segments	LVDT Ch. 6

Figure 17. Image of ISES01 axial test setup

4.2.2 ISES02 (CUB)

The specimen for ISES02 is composed of a steel host pipe with nominal initial gap opening of 6.0 in. (150 mm) and rehabilitated with I-Main CIPP installed with a pre-liner. A 110-kip (500 kN) MTS actuator with

an 11 in. (280 mm) stroke mounted in a rigid self-contained loading frame was used to test this specimen. Though strain gauge locations did not change between lateral and axial testing, channels used for recording data did change (see Table 5). SPs and LVDTs were oriented around the crack to record axial deformation, fixed to the host pipe with brackets. Instrumentation details are given in Table 11. Figure 18 shows the axial test setup of ISES02.

Table 11. ISES02 axial instrumentation

Instrument Description	Local Instrument Name	Location	Channel No.
Horizontal String pot, North Shoulder, over the Crack, fixed to Steel Pipe	SP27-30_NS	North Shoulder, over crack fixed to steel host pipe segments	Ch. 21
Horizontal String pot, South Haunch, over the Crack, fixed to Steel Pipe	SP22-10_SH	South Haunch, over crack fixed to steel host pipe segments	Ch. 22
Horizontal LVDT, Crown, over the Crack, fixed to Steel Pipe	LVDT01_1017_C	Crown, over crack fixed to steel host pipe segments	LVDT Ch. 1
Horizontal LVDT, Invert, over the Crack, fixed to Steel Pipe	LVDT04_1006_I	Invert, over crack fixed to steel host pipe segments	LVDT Ch. 4

Figure 18. Photo of ISES02 axial test setup

4.2.3 ISES03 (CUB)

The specimen for ISES03 is composed of a steel host pipe with nominal initial gap opening of 0.5 in. (12.7 mm) and rehabilitated with I-Main CIPP installed without a pre-liner. A 110-kip (500 kN) MTS actuator with an 11 in. (280 mm) stroke mounted in a rigid self-contained loading frame was used to test this specimen. Though strain gauge locations did not change between lateral and axial testing, channels used for recording data did change (see Table 7). SPs and LVDTs were oriented around the crack to record axial deformation, fixed to the host pipe with brackets. Instrumentation details are provided in Table 12. Figure 19 shows the axial test setup of ISES03.

Table 12. ISES03 axial instrumentation

Instrument Description	Local Instrument Name	Location	Channel No.
Horizontal String pot, North Spring Line, over the Crack, fixed to Steel Pipe	SP27-30_N	North Spring Line, over crack fixed to steel host pipe segments	Ch. 21
Horizontal String pot, South Spring Line, over the Crack, fixed to Steel Pipe	SP18-10_S	South Spring Line, over crack fixed to steel host pipe segments	Ch. 22
Horizontal LVDT, Crown, over the Crack, fixed to Steel Pipe	LVDT01_1017_C	Crown, over crack fixed to steel host pipe segments	LVDT Ch. 1
Horizontal LVDT, Invert, over the Crack, fixed to Steel Pipe	LVDT04_1006_I	Invert, over crack fixed to steel host pipe segments	LVDT Ch. 4

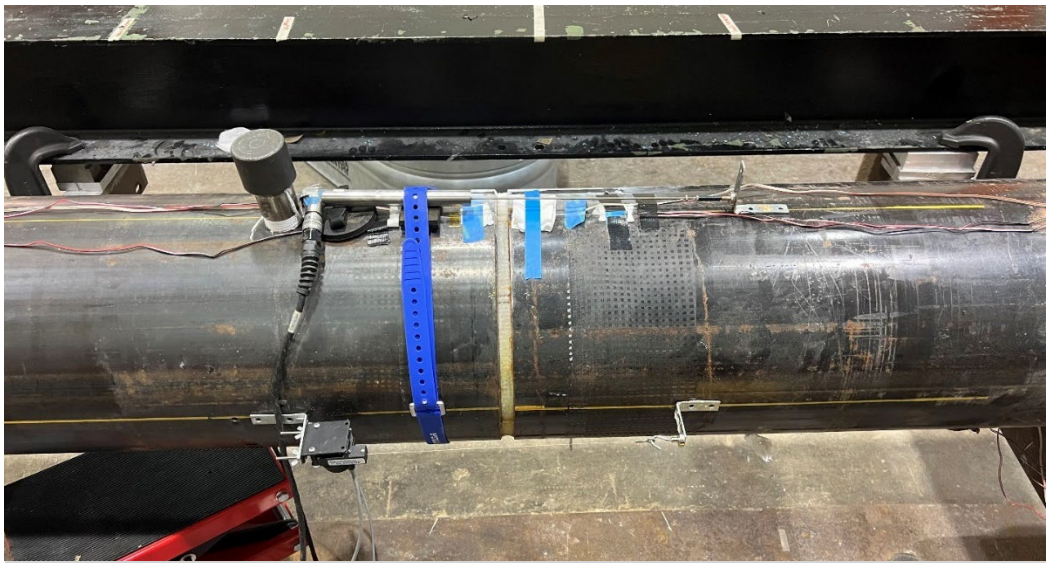

Figure 19. Photo of ISES03 axial test setup

4.2.4 ISES04 (Cornell)

Axial testing was not performed at Cornell due to a fracture occurring in ISES04 during adjacent excavation testing. More details are provided in the subsequent sections of this report.

5 Test Results

The following sections provide the results for traffic cycles, adjacent excavation events, thermal expansion cycles, and ultimate capacity tests for each specimen tested. Variations between test specimens are summarized in Section 4, Table 2.

5.1 ISES01 Results

The specimen for ISES01 is composed of a steel host pipe with nominal initial gap opening of 0.5 in. (12.2 mm) and rehabilitated with I-MAIN CIPP installed with a pre-liner. An overview of the operations performed on ISES01 is provided in Table 13.

Table 13. Major mechanical procedures on ISES01

General Operation	Num. of Cycles	Target Deformations	Test Configuration
Traffic Cycles	500,000	0.036° Rotation	30 in. - 40 in. - 30 in.
Small Adjacent Excavation	1	0.58° Rotation	30 in. - 40 in. - 30 in.
Large Adjacent Excavation	1	1.1° Rotation	30 in. - 40 in. - 30 in.
Traffic Cycles	100,000	0.05° Rotation	30 in. - 40 in. - 30 in.
Thermal Expansion Cycles	50	0.12” – 0.27” COD	Weight supported axial testing
Ultimate Capacity Test	1	Maximum Force	Weight supported axial testing

5.1.1 ISES01 Bending Results

During the first phase of testing, the specimen was subjected to 500,000 traffic cycles at varying pressure levels, as outlined in Table 14. A sinusoidal displacement wave was applied transversely to achieve several different target rotations over the duration of testing. Tests were conducted at a frequency of 1 to 2 Hz throughout. Figure 20 illustrates the moment-rotation response for selected traffic cycles, representative of the overall performance across the testing duration.

Transverse displacements were applied to achieve rotations ranging from 0.030° to 0.038°. The moment required to reach these rotations ranged from 8.0 kip-in. (0.9 kN-m) to 11 kip-in. (1.2 kN-m). In the initial cycles, the apparent stiffness was approximately 330 kip-in./deg. (37.3 kN-m/deg.), while in the later cycles, the apparent stiffness decreased to about 250 kip-in./deg. (28.2 kN-m/deg.), indicating a 24% reduction in stiffness. The variations in the width of the cyclic loops are attributed to the rate of loading effects, which are discussed in greater detail later in this report.

Table 14. Testing details for traffic cycles

Test ID	Approx. Cycle	Internal Pressure [psi]	Loading Rate [Hz.]	Approx. Stiffness [kip-in./deg. (kN-m/deg.)]
BC01	1,000	9	1	330 (37.3)
BC10	100,000	9	2	315 (35.6)
BC14	200,000	26	2	295 (33.3)
BC18	300,000	27	1	270 (30.5)
BC20	400,000	25	1	260 (29.4)
BC23	500,000	53	2	250 (28.2)
BC31	600,000	56	1	235 (26.6)

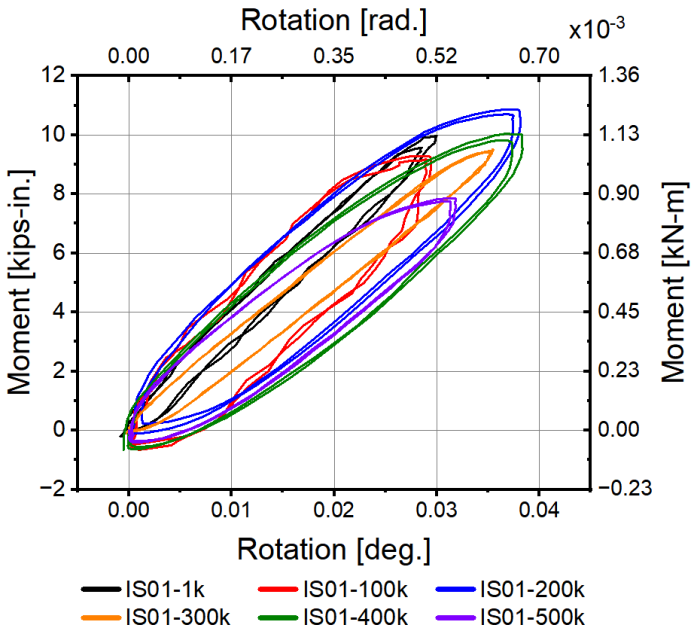

Figure 20. ISES01 moment vs. rotation for selected traffic cycles

Following the application of 500,000 traffic cycles, two larger transverse deformations were applied to the specimen to simulate ground movement caused by adjacent excavation events. Figure 21 presents the actuator displacement and force over time for each lateral deformation applied. Additionally, this figure includes average measurements of the LVDTs positioned 1.5 in. (38 mm) on either side of the crack opening. Based on these measurements, the resultant rotation was calculated and plotted against the corresponding moment applied to the specimen, shown in Figure 22.

The first transverse displacement applied to the specimen simulated a smaller adjacent excavation (AE) event, while the second represented a larger, more significant excavation. During the first test, a maximum rotation of 0.58° was achieved at an applied moment of 70 kip-in. (7.9 kN-m), while the second

test reached a maximum rotation of 1.1° at an applied moment of 120 kip-in. (13.6 kN-m). The apparent stiffness for both AE events was approximately 125 kip-in./deg. (14.1 kN-m/deg.), which is 50% lower than the stiffness measured during the previous traffic cycle (250 kip-in./deg.).

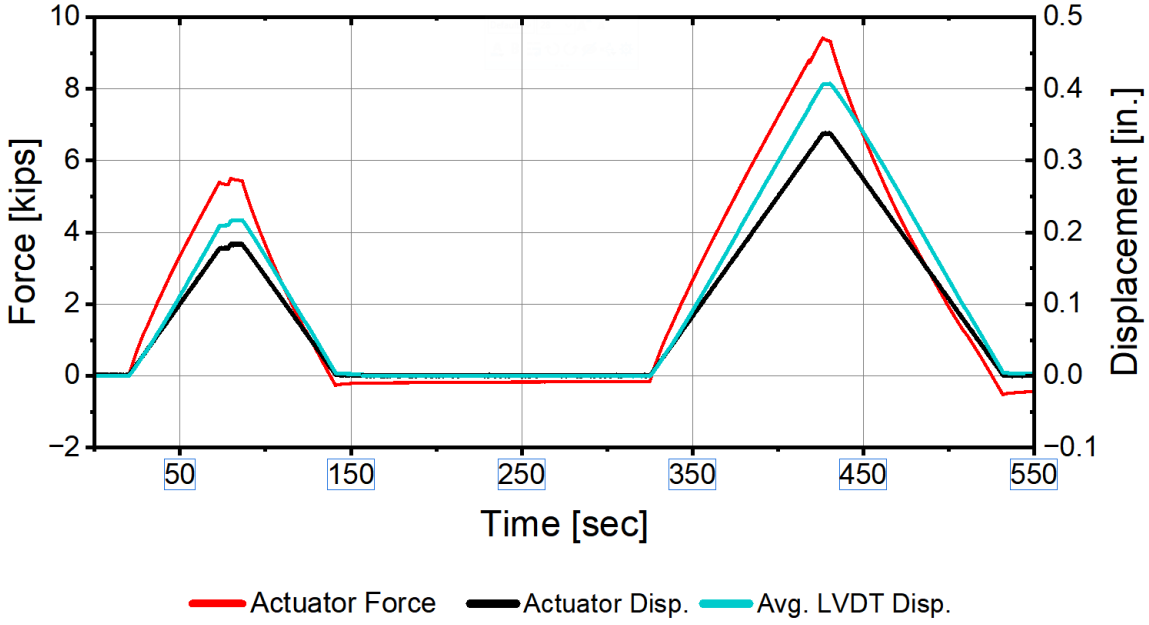

Figure 21. ISES01 actuator displacement, actuator force, average LVDT displacement vs. time for adjacent excavation events

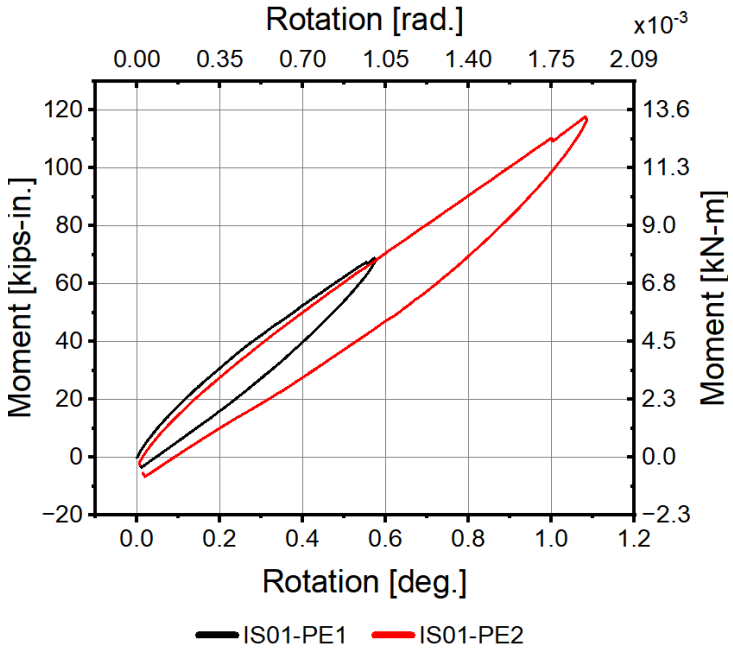

Figure 22. ISES01 moment vs. rotation for adjacent excavation events

To complete transverse testing for this specimen, an additional 100,000 traffic cycles were applied following the larger AE deformations. Figure 23 shows the moment-rotation response of selected cycles. After the AE tests, the traffic cycles were updated to achieve a target rotation of about 0.055°, 83% greater than the target rotation of 0.03° observed during the cycles prior. The applied moment required to reach this target rotation was approximately 11.5 kip-in. (1.2 kN-m), 44% greater than the 8.0 kip-in (0.9 kN-m) applied moment for the cycles prior. Despite these increases, the apparent stiffness for the cycles following the AE events was about 235 kip-in./deg. (26.6 kN-m/deg.), representing a 6% decrease relative to earlier traffic cycles.

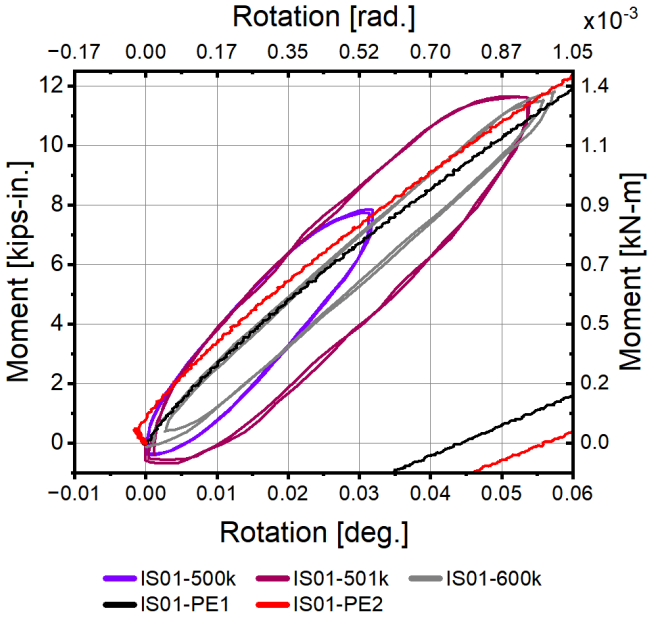

Figure 23. ISES01 moment vs. rotation for traffic cycles pre- and post-AE tests

In summary, the apparent stiffness of the specimen for traffic cycles at the start of testing was approximately 330 kip-in./deg. (37.3 kN-m/deg.), and decreased to 235 kip-in./deg. (26.6 kN-m/deg.), by the end of transverse testing, indicating an overall reduction of 30% after all traffic cycles and AE events were completed.

5.1.2 ISES01 Axial Results

Once transverse testing was completed, the specimen was then moved to the axial testing frame to perform 50 thermal expansion cycles simulating deformations caused by temperature changes over a 50-year design life. To simulate thermal expansion, axial displacements were applied to the specimen at a quasi-static strain rate. Figure 24 presents the applied actuator displacement, actuator force and average LVDT measurements relative to time for each cycle applied. Figure 25 shows the load relative to the applied gap/crack opening displacement (COD) for the selected axial cycles. The COD is the average of the LVDTs located at the crown and invert.

A preliminary cycle with a relatively small target displacement was conducted to measure the specimen's initial stiffness. During this cycle, the actuator applied a displacement that generated approximately 11 kips (49 kN) of tensile force, resulting in a measured COD of 0.09 in. (2.3 mm). From these measurements, an initial stiffness of around 200 kip/in. (35 kN/mm) was calculated. This stiffness was then used to calculate the target COD for the subsequent cycles. As the testing progressed, the target COD increased because the apparent stiffness from each set of cycles was used to adjust the target displacement for the following set. In the early cycles, the average stiffness of the specimen was about 200 kip/in. (35 kN/mm), while during the later cycles, the average stiffness dropped to around 175 kip/in. (30.6 kN/mm), indicating a reduction of about 13%.

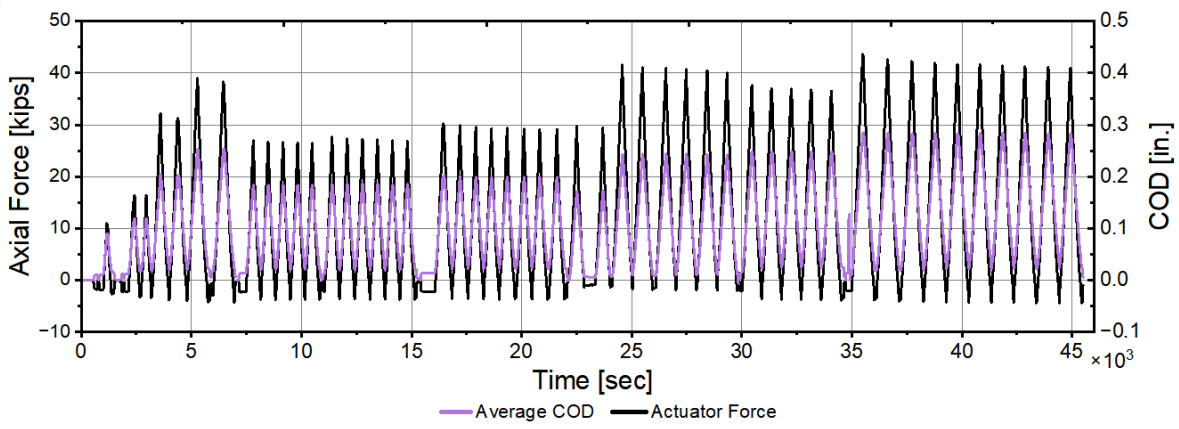

Figure 24. ISES01 actuator force and average LVDT measurements vs. time for thermal expansion cycles

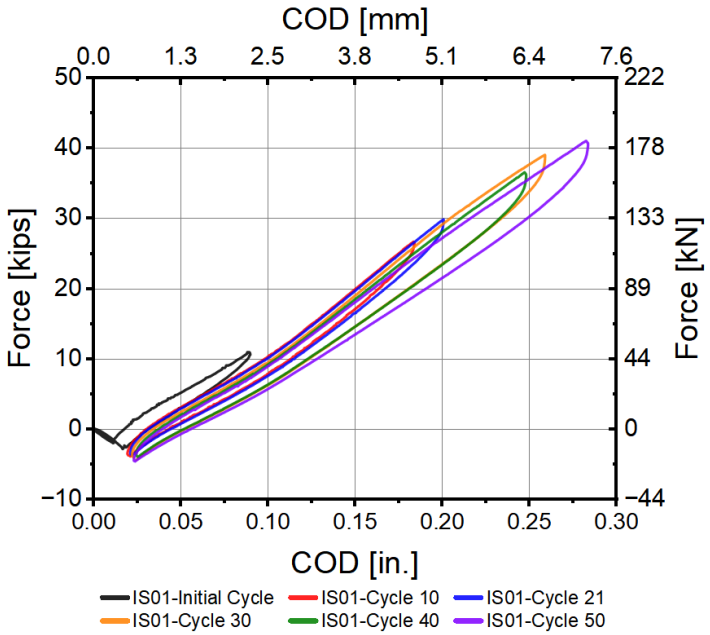

Figure 25. ISES01 actuator load vs. crack opening displacement (COD) for thermal expansion cycles

Once thermal expansion cycles were completed, the specimen was axially loaded to its ultimate capacity. Figure 26 shows the axial force relative to the COD over the duration of this test while Figure 27 provides a sequence of images during the first test sequence. The specimen reached a peak ultimate force capacity of about 61 kips (272 kN) at a COD of about 0.9 in. (23 mm) (Figure 27b). Following this peak, a sudden drop in force occurred, reducing the applied axial tension to around 31 kips (138 kN) and corresponding to some moderate leakage at the gap. As axial displacement continued to be applied, the force built up again until another sudden drop occurred at a local maximum of 58 kips (28 kN) with a COD of about 1.25 in. (31.8 mm). However, this drop in force was less severe, bringing the applied tension to 43 kips (191 kN) before increasing again. This rise and drop in axial force persisted throughout the test, with each successive local maximum and corresponding drop being smaller than the previous one. The first load drop was associated with full detachment of the IRP from the host pipe. Because pressurization plugs were used at either end of the specimen, leakage at the center of the specimen was minimal at detachment, however, it is assumed the specimen would have leaked more if regular end caps had been used. The accumulated force and subsequent drops after the first event are associated with frictional resistance that develops between the IRP and host pipe interface. As the IRP is pulled out of the host pipe, the contact area between the two is reduced, corresponding to a gradual reduction in applied load.

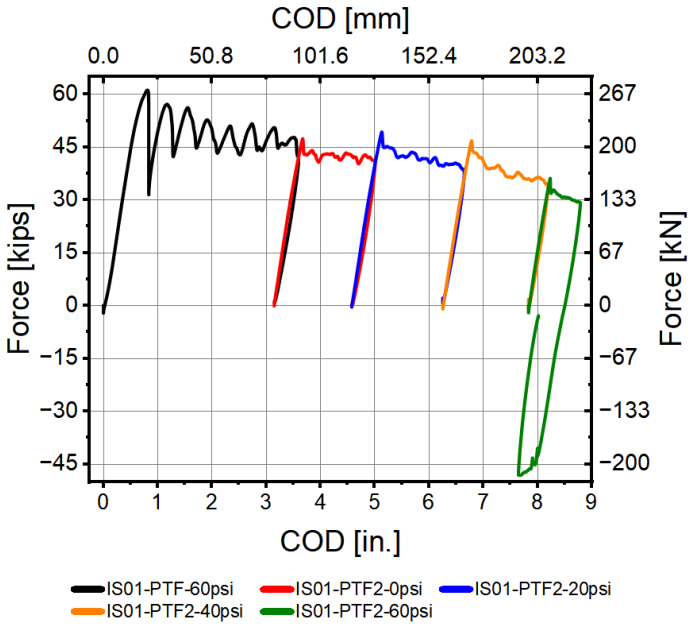

Figure 26. ISES01 axial force vs. crack opening displacement

Following the initial ultimate capacity sequence (shown in black), several additional sequences were performed at varying internal water pressure. Further details about the influence of pressure on the specimen's axial force capacity are discussed in subsequent sections of this report. Overall, the trend showed a gradual decline in force capacity as COD increased. The final maximum tensile force recorded was approximately 30 kips (134 kN) at a COD nearing 10 in. (250 mm). Additionally, one compressive cycle was applied towards the end of the test to compare frictional resistance in the other direction. The axial compressive force reached about 40 kips (178 kN) after 0.5 in. of applied COD before beginning to plateau. The maximum COD change for this compressive test was around 1.0 in. (25 mm), with the highest recorded compressive force being approximately 48 kips (214 kN).

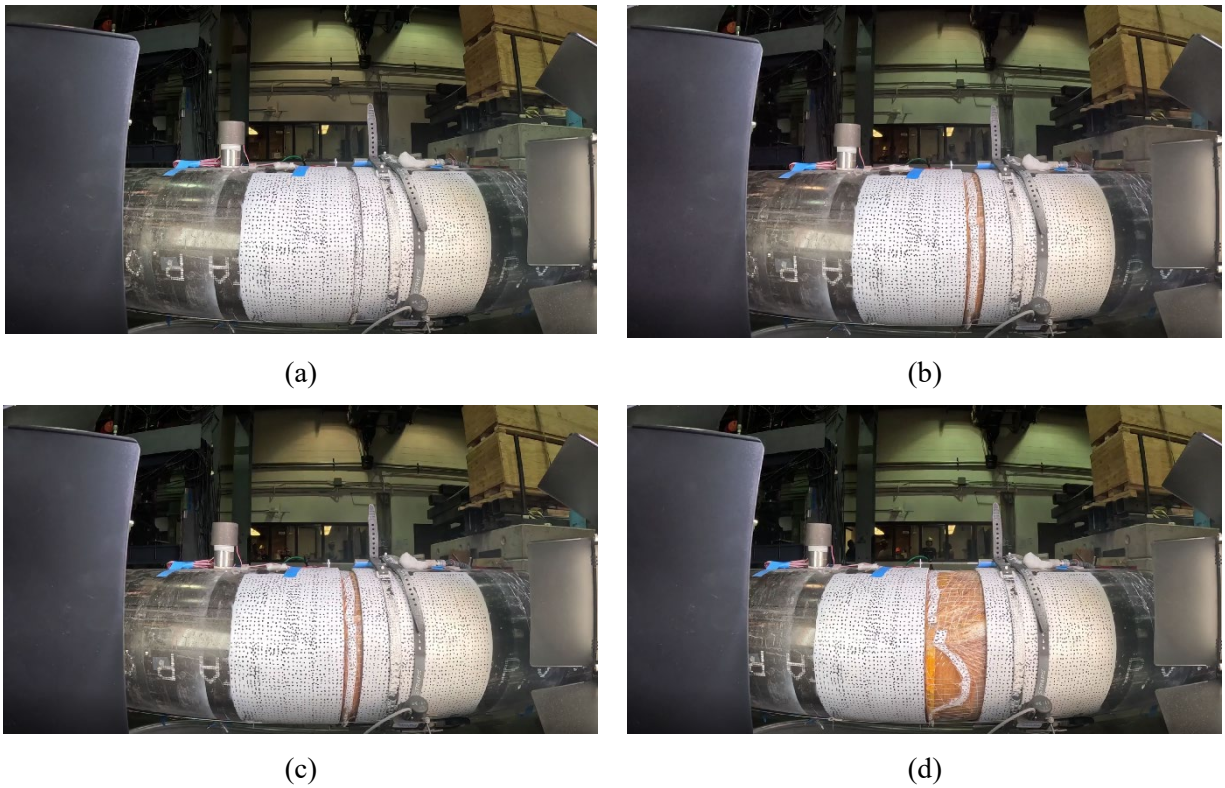

(a) (b)

(c) (d)

Figure 27. Sequence of ISES01 ultimate capacity test showing: (a) pretest, (b), before first loss of axial force capacity (c) after first loss of axial force capacity, and (d) end of first test sequence

5.2 ISES02 Results

The specimen for ISES02 is composed of a steel host pipe with nominal initial gap opening of 6.0 in. (152 mm) and rehabilitated with I-Main CIPP installed with a pre-liner. An overview of the operations performed on ISES02 is provided in Table 15.

Table 15. Major mechanical procedures on ISES02

General Operation	Num. of Cycles	Target Deformations	Test Configuration
Traffic Cycles	500,000	0.036° Rotation	30 in. - 40 in. - 30 in.
Small Adjacent Excavation	1	0.4° Rotation	30 in. - 40 in. - 30 in.
Large Adjacent Excavation	1	0.8° Rotation	30 in. - 40 in. - 30 in.
Traffic Cycles	100,000	0.05° Rotation	30 in. - 40 in. - 30 in.
Thermal Expansion Cycles	50	0.25” COD	Weight supported axial testing
Ultimate Capacity Test	1	Maximum Force	Weight supported axial testing

5.2.1 ISES02 Bending Results

During the first phase of testing, the specimen was subjected to 500,000 traffic cycles at varying pressure levels, as outlined in Table 16. A sinusoidal displacement wave was applied transversely to achieve several different target rotations over the duration of testing. Tests were conducted at a frequency of 1 to 2 Hz throughout. Figure 28 illustrates the moment-rotation response for selected traffic cycles, representative of the overall performance across the testing duration.

Transverse displacements were applied to achieve rotations ranging from 0.034° to 0.038°. The moment required to reach these rotations ranged from 8.0 kip-in (0.9 kN-m) to 9 kip-in. (1.0 kN-m). In the initial cycles, the apparent stiffness was approximately 250 kip-in./deg. (28.3 kN-m/deg.), while in the later cycles, the apparent stiffness decreased to about 225 kip-in./deg. (25.4 kN-m/deg.), indicating a 10% reduction in stiffness.

At around the 460k cycle, the specimen was accidentally lifted from its starting position, imposing a negative moment and rotation. Figure 29 shows the moment relative to rotation for this incident. During this incident, a maximum negative rotation of about 0.72° was applied with a corresponding negative moment of about 70 kip-in. (7.9 kN-m). A few traffic cycles were applied at the peak of this incident before returning the specimen to its neutral position. Once the incident was resolved, traffic cycles were resumed to complete 500,000. While not intentional, these cycles, performed at nearly the maximum rotation applied

during the AE cycles discussed next, demonstrates the IRP's capacity to accommodate unanticipated loading.

Table 16. Testing details for traffic cycles

Test ID	Approx. Cycle	Internal Pressure [psi]	Loading Rate [Hz.]	Stiffness [kip-in./deg. (kN-m/deg.)]
BC01	1,000	10	1	250 (28.2)
BC04	100,000	10	2	250 (28.2)
BC07	200,000	30	2	245 (27.7)
BC10	300,000	30	2	240 (27.1)
BC13	400,000	30	2	225 (25.4)
BC15	500,000	65	2	150 (16.9)
BC17	600,000	65	1	135 (15.3)

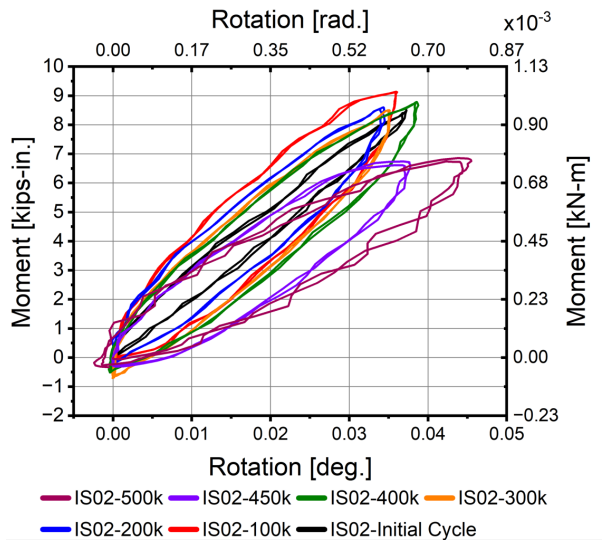

Figure 28. ISES02 moment vs. rotation for selected traffic cycles

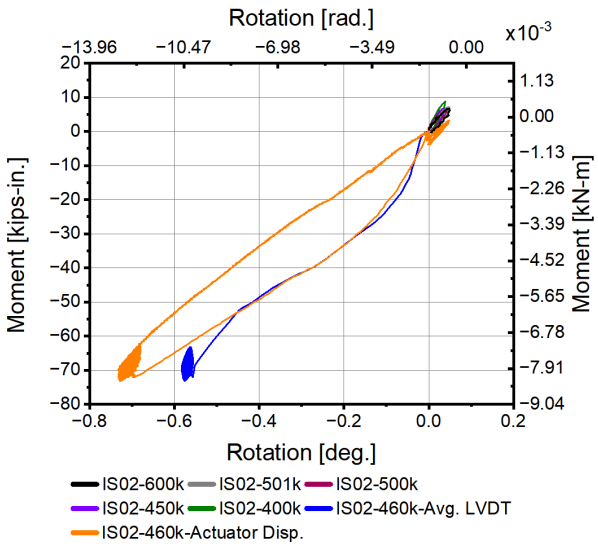

Figure 29. ISES02 moment vs. rotation for accidental large displacement

Following the application of 500,000 traffic cycles, two larger transverse deformations were applied to the specimen to simulate ground movement caused by adjacent excavation events. Figure 30 presents the actuator displacement and force over time for each lateral deformation applied. Additionally, this figure includes average measurements of the LVDTs positioned 1.5 in. (38 mm) on either side of the crack opening. Based on these measurements, the resultant rotation was calculated and plotted against the corresponding moment applied to the specimen, shown in Figure 31.

The first transverse displacement applied to the specimen simulated a smaller adjacent excavation (AE) event, while the second represented a larger, more significant excavation. During the first test, a

maximum rotation of 0.4° was achieved at an applied moment of 35 kip-in. (4.0 kN-m), while the second test reached a maximum rotation of 0.8° at an applied moment of 69 kip-in. (7.8 kN-m). The apparent stiffness for both AE events was approximately 87 kip-in./deg. (9.8 kN-m/deg).

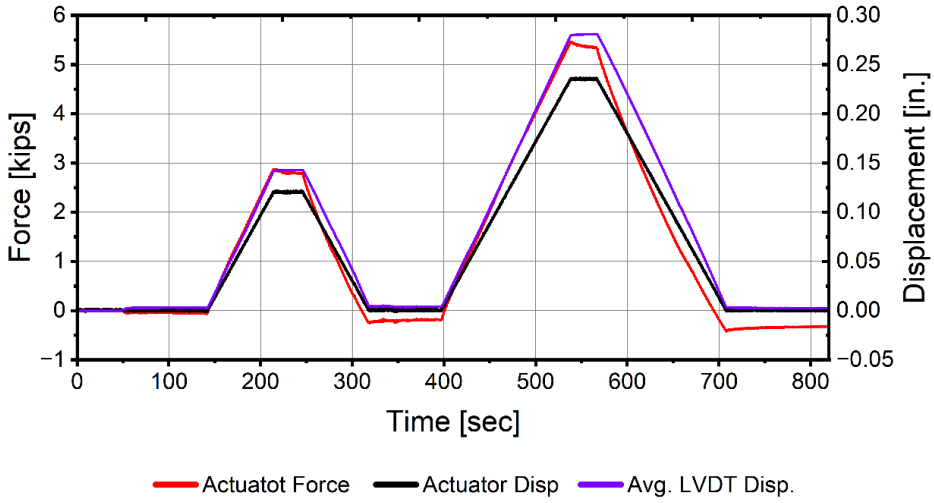

Figure 30. ISES02 actuator displacement, actuator force, average LVDT displacement vs. time for adjacent excavation events

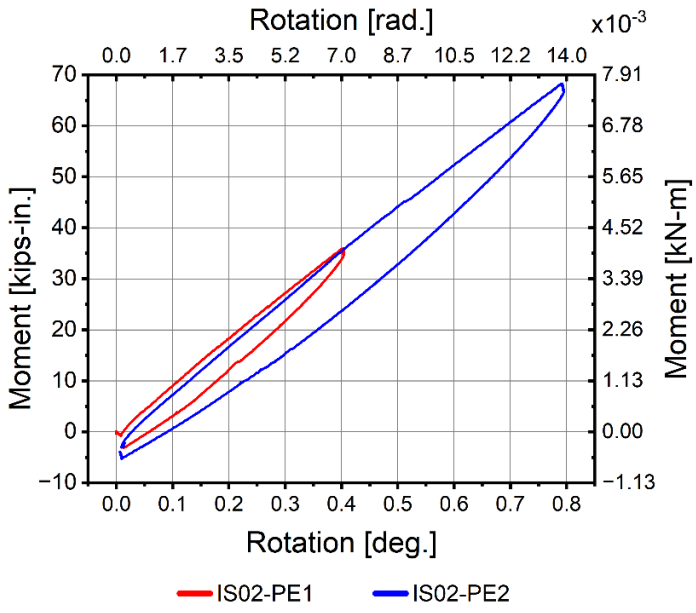

Figure 31. ISES02 moment vs. rotation for adjacent excavation events

To complete transverse testing for this specimen, an additional 100,000 traffic cycles were applied following the larger AE deformations. Figure 32 shows the moment-rotation response of selected cycles. After the AE tests, the traffic cycles were updated to achieve a target rotation of about 0.05°, 40% greater than the target rotation of 0.036° observed during the cycles prior. The applied moment required to reach this target rotation was approximately 7 kip-in. (0.8 kN-m), which was similar to the applied moment for the cycles prior. Despite these increases, the apparent stiffness for the cycles following the AE events was about 140 kip-in./deg. (15.8 kN-m/deg.), representing a 38% decrease relative to traffic cycles prior to the lifting incident, and a 7% decrease relative to traffic cycles after the lifting incident and before the AE events.

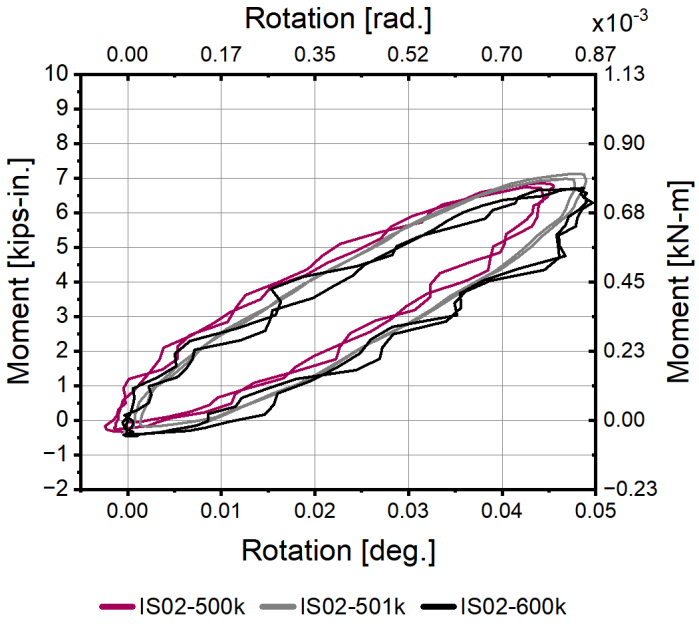

Figure 32. ISES02 moment vs. rotation for traffic cycles pre- and post-AE tests

In summary, the apparent stiffness of the specimen for traffic cycles at the start of testing was approximately 250 kip-in./deg. (28.3 kN-m/deg.) and decreased to 135 kip-in./deg. (15.3 kN-m/deg.) by the end of transverse testing, indicating an overall reduction of 46% after all traffic cycles and AE events were completed.

5.2.2 ISES02 Axial Results

Once transverse testing was completed, the specimen was then moved to the axial testing frame to perform 50 thermal expansion cycles simulating deformations caused by temperature changes over a 50-year design life. To simulate thermal expansion, axial displacements were applied to the specimen at a quasi-static strain rate. Figure 33 presents the applied actuator displacement, actuator force and average LVDT measurements relative to time for each cycle applied. Unfortunately, some data was lost for a few of the cycles, so data recorded from our Digital Imaging Correlation (DIC) was used to fill the gap. More information on the DIC can be found in Appendix A.1 of this report. Figure 34 shows the load relative to the applied gap/crack opening displacement (COD) for the selected axial cycles. The COD is the average of the LVDTs located at the crown and invert.

A preliminary cycle with a relatively small target displacement was conducted to measure the specimen's initial stiffness. During this cycle, the actuator applied a displacement that generated approximately 6 kips (27 kN) of tensile force, resulting in a measured COD of 0.06 in. (1.5 mm). From these measurements, an initial stiffness of around 170 kip/in. (30.0 kN/mm) was calculated. This stiffness was then used to calculate the target COD for the subsequent cycles. The average stiffness for all cycles performed was approximately 160 kip-in. (18.1 kN-m).

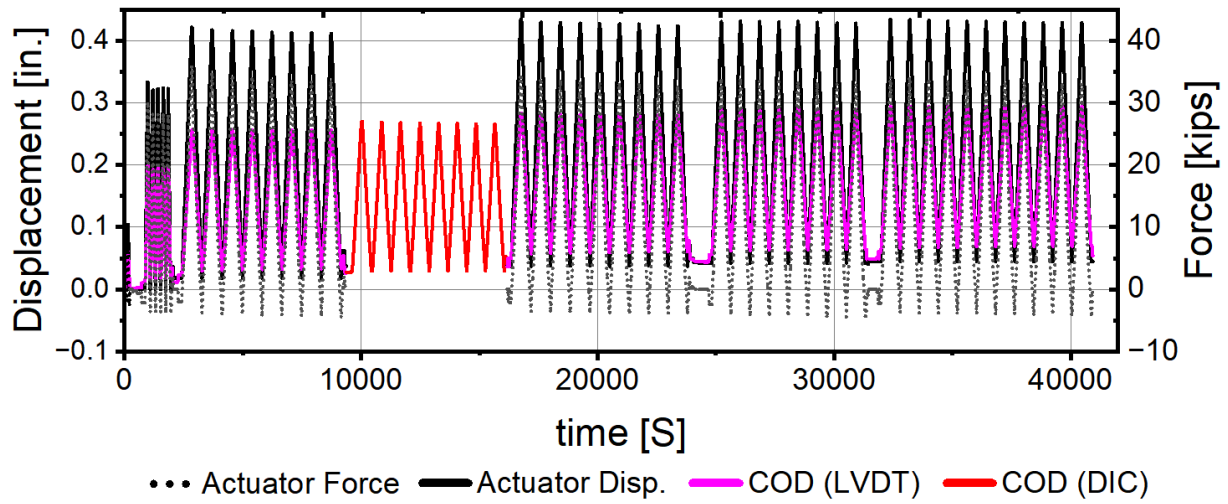

Figure 33. ISES02 actuator displacement, actuator force, and average LVDT measurements vs. time for thermal expansion cycles

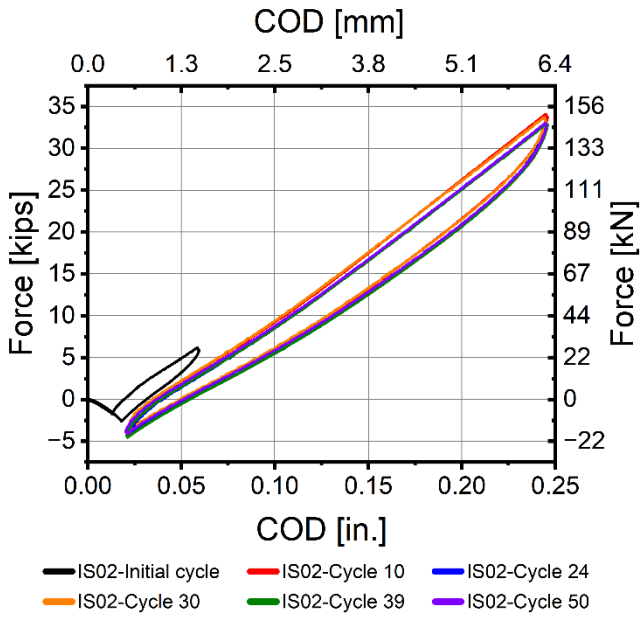

Figure 34. ISES02 actuator load vs. crack opening displacement (COD) for thermal expansion cycles

Once thermal expansion cycles were completed, the specimen was axially loaded to its ultimate capacity. Figure 35 shows the axial force relative to the COD over the duration of this test. The specimen reached a peak ultimate force capacity of about 51 kips (227 kN) at a COD of about 0.65 in. Following this peak, a sudden drop in force occurred, reducing the applied axial tension to around 45 kips (200 kN). As axial displacement continued to be applied, the force built up again, reaching a softer local maximum of about 49 kips (218 kN) before gradually reducing in force as the COD increased. The first load drop was associated with full detachment of the IRP from the host pipe. Because pressurization plugs were used at either end of the specimen, leakage at the center of the specimen did not correspond with detachment, however, it is assumed the specimen would have leaked to some extent at this point. The accumulated force and subsequent drops after the first event are associated with frictional resistance that develops between the IRP and host pipe interface. As the IRP is pulled out of the host pipe, the contact area between the two is reduced, corresponding to a gradual reduction in applied load.

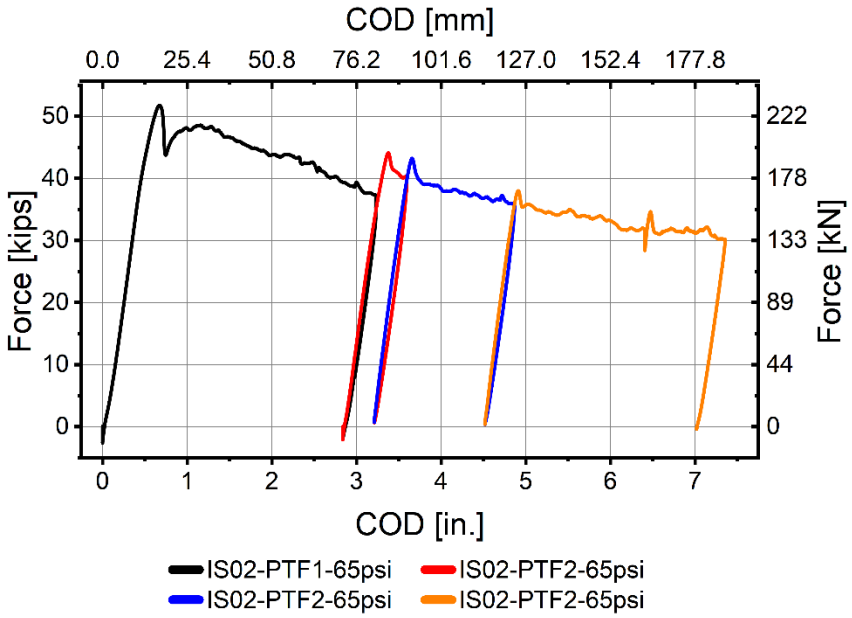

Figure 35. ISES02 axial force vs. crack opening displacement

Following the initial ultimate capacity sequence (shown in black), several additional sequences were performed at varying displacement rates. Further details about the influence of displacement rates on the specimen's axial force capacity are discussed in subsequent sections of this report. Overall, the trend showed a gradual decline in force capacity as COD increased. The final maximum tensile force recorded was approximately 30 kips at a COD of 7.25 in. (184 mm). Figure 36 shows the specimen (a) before loading, (b) during loading, and (c) after rupture occurred.

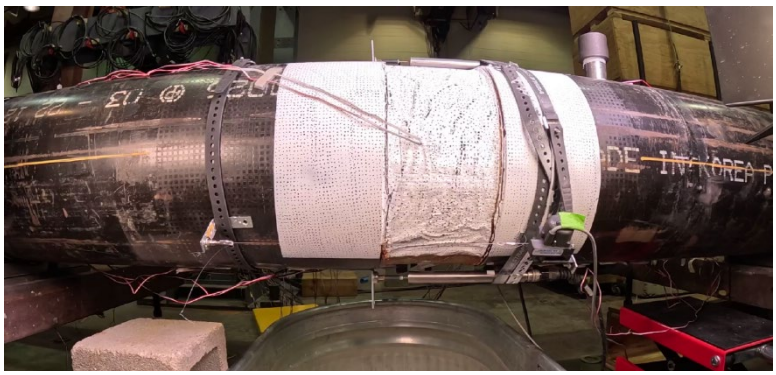

(a) Pretest

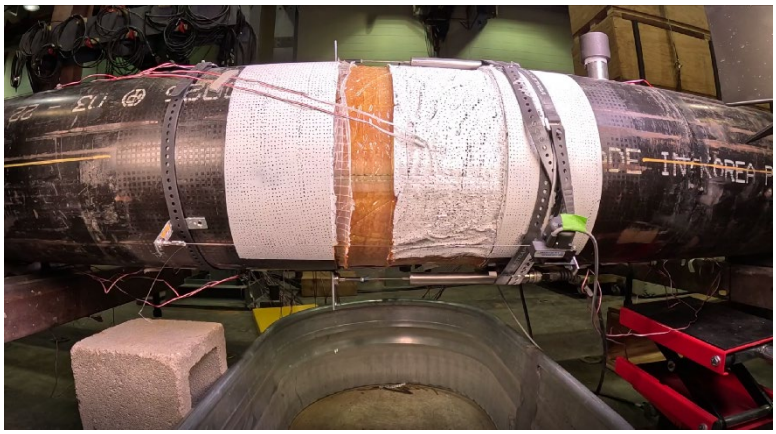

(b) First Leak

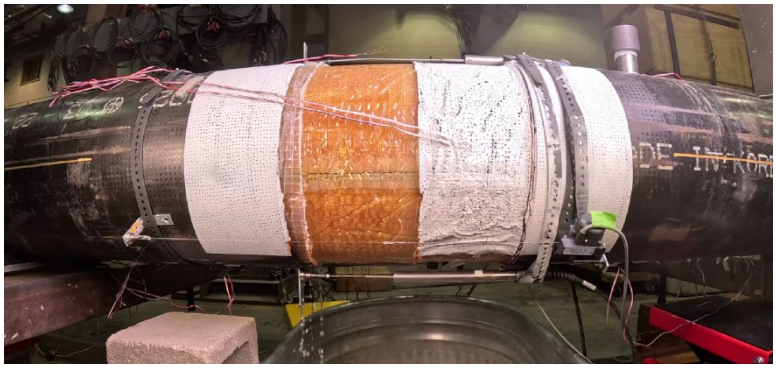

(c) End of first test sequence

Figure 36. Sequence of images showing ISES02 ultimate capacity test

5.3 ISES03 Results

The specimen for ISES03 is composed of a steel host pipe with nominal initial gap opening of 0.5 in. (12.2 mm) and rehabilitated with I-Main CIPP installed without a pre-liner. An overview of the operations performed on ISES03 is provided in Table 17.

Table 17. Major mechanical procedures on ISES03

General Operation	Num. of Cycles	Target Deformations	Test Configuration
Traffic Cycles	500,000	0.044° Rotation	30 in. - 40 in. - 30 in.
Small Adjacent Excavation	1	0.45° Rotation	30 in. - 40 in. - 30 in.
Large Adjacent Excavation	1	0.9° Rotation	30 in. - 40 in. - 30 in.
Traffic Cycles	100,000	0.05° Rotation	30 in. - 40 in. - 30 in.
Thermal Expansion Cycles	50	0.035" – 0.055" COD	Weight supported axial testing
Ultimate Capacity Test	1	Maximum Force	Weight supported axial testing

5.3.1 ISES03 Bending Results

During the first phase of testing, the specimen was subjected to 500,000 traffic cycles at varying pressure levels, as outlined in Table 18. A sinusoidal displacement wave was applied transversely to achieve several different target rotations over the duration of testing. Tests were conducted at a frequency of 1 to 2 Hz throughout. Figure 37 illustrates the moment-rotation response for selected traffic cycles, representative of the overall performance across the testing duration.

Transverse displacements were applied to achieve rotations ranging from 0.043° to 0.048°. The moment required to reach these rotations ranged from 28 kip-in (3.2 kN-m) to 32 kip-in (3.6 kN-m). In the initial cycles, the apparent stiffness was approximately 745 kip-in./deg. (85 kN-m/deg.), while in the later cycles, the apparent stiffness decreased to about 650 kip-in./deg. (75 kN-m/deg.), indicating a 13% reduction in stiffness. The variations in the width of the cyclic loops are attributed to the rate of loading effects, which are discussed in greater detail later in this report.

Table 18. Testing details for traffic cycles for IS03

Test ID	Approx. Cycle	Internal Pressure [psi]	Loading Rate [Hz.]	Stiffness [kip-in./deg. (kN-m/deg.)]
BC01	1,000	10	1	330 (37.3)
BC05	100,000	13	2	745 (84.2)
BC08	200,000	30	2	695 (78.5)
BC10	300,000	30	2	680 (76.8)
BC14	400,000	60	2	635 (71.7)
BC16	500,000	65	2	650 (73.4)
BC19	600,000	65	2	520 (58.8)

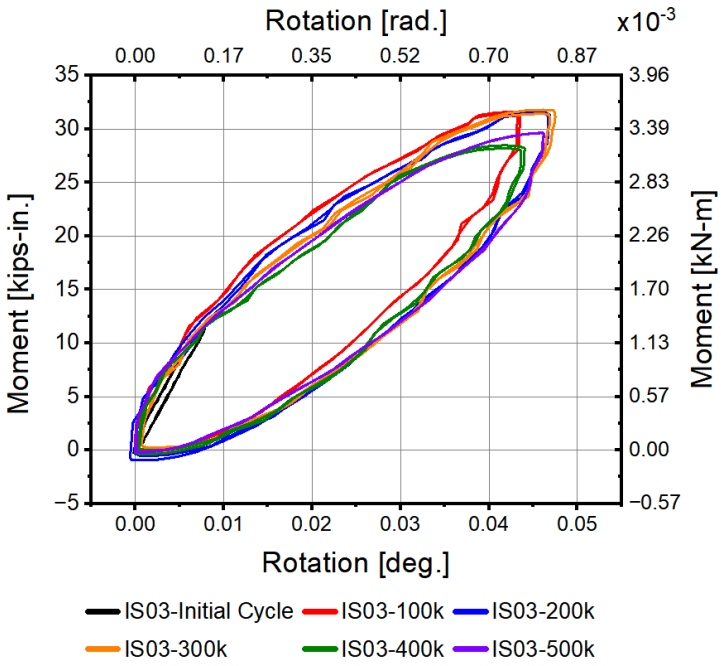

Figure 37. ISES03 moment vs. rotation for selected traffic cycles

Following the application of 500,000 traffic cycles, two larger transverse deformations were applied to the specimen to simulate ground movement caused by adjacent excavation events. Figure 38 presents the actuator displacement and force over time for each lateral deformation applied. Additionally, this figure includes average measurements of the LVDTs positioned 1.5 in. (38 mm) on either side of the crack opening. Based on these measurements, the resultant rotation was calculated and plotted against the corresponding moment applied to the specimen, shown in Figure 39.

The first transverse displacement applied to the specimen simulated a smaller adjacent excavation (AE) event, while the second represented a larger, more significant excavation. During the first test, a maximum rotation of 0.5° was achieved at an applied moment of 160 kip-in. (18.1 kN-m), while the second test reached a maximum rotation of 0.9° at an applied moment of about 205 kip-in. (23.2 kN-m) The apparent stiffness for both AE events was approximately 350 kip-in./deg. (40 kN-m/deg.), which is 45% lower than the stiffness measured during the previous traffic cycle (650 kip-in./deg.).

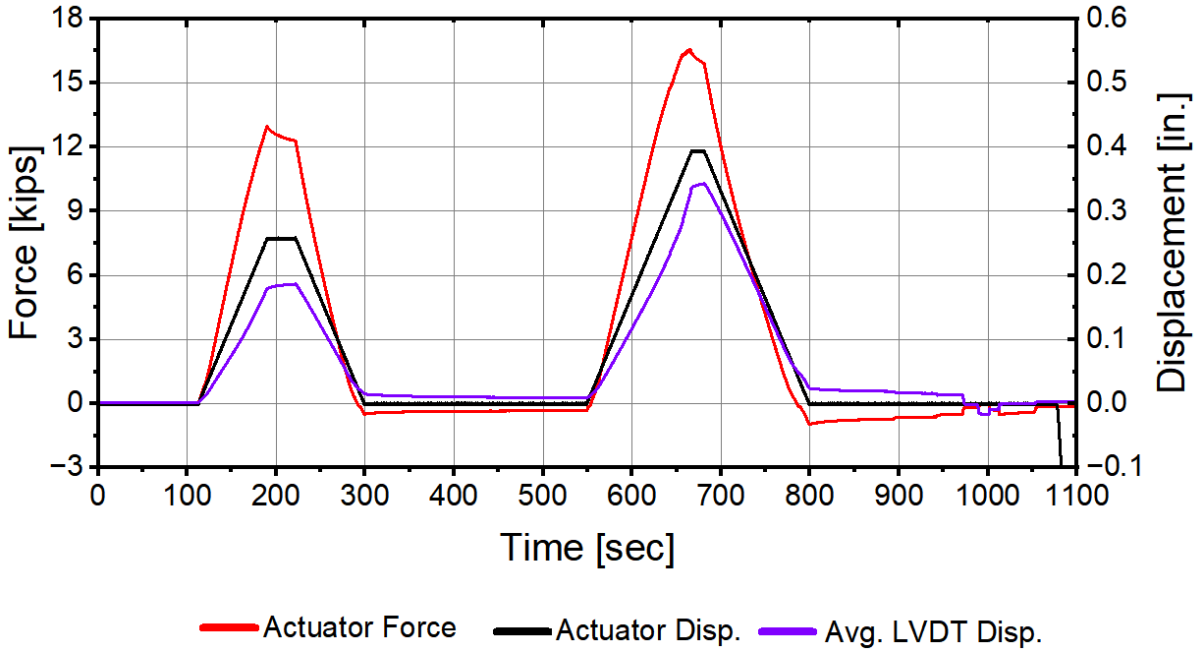

Figure 38. ISES03 actuator displacement, actuator force, average LVDT displacement vs. time for adjacent excavation events

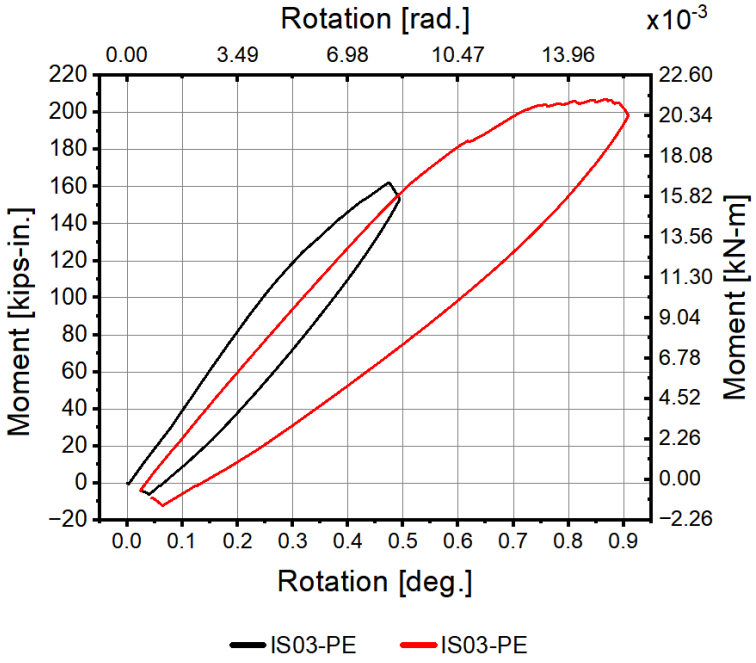

Figure 39. ISES03 moment vs. rotation for adjacent excavation events

To complete transverse testing for this specimen, an additional 100,000 traffic cycles were applied following the larger AE deformations. Figure 40 shows the moment-rotation response of selected cycles. After the AE tests, the traffic cycles were updated to achieve a target rotation of about 0.05°. The applied moment required to reach this target rotation was approximately 25 kip-in. (2.8 kN). The apparent stiffness for the cycles following the AE events was about 520 kip-in./deg. (60 kN-m/deg.), representing a 20% decrease relative to earlier traffic cycles.

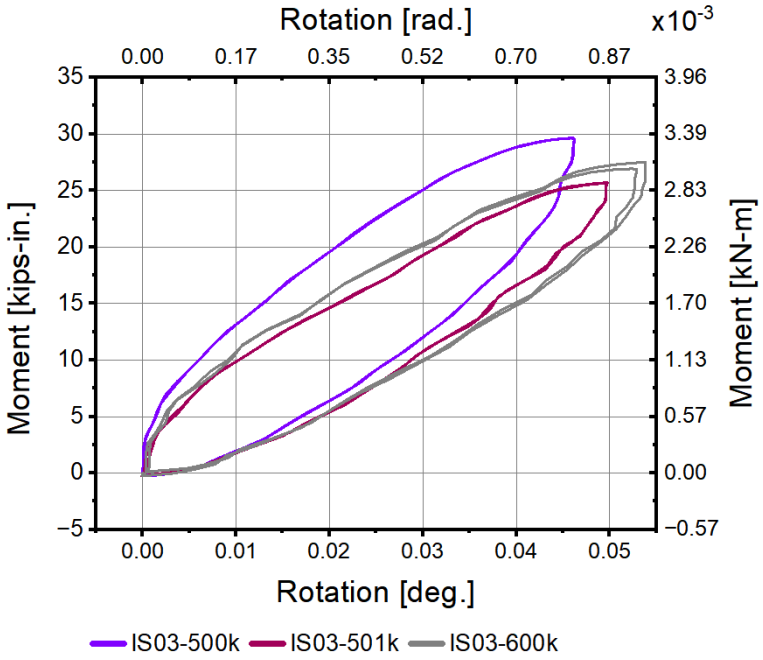

Figure 40. ISES03 moment vs. rotation for traffic cycles pre- and post-AE tests

In summary, the apparent stiffness of the specimen for traffic cycles at the start of testing was approximately 745 kip-in./deg. (85 kN-m/deg.) and decreased to 520 kip-in./deg (60 kN-m/deg.). by the end of transverse testing, indicating an overall reduction of 30% after all traffic cycles and AE events were completed.

5.3.2 ISES03 Axial Results

Once transverse testing was completed, the specimen was then moved to the axial testing frame to perform 50 thermal expansion cycles simulating deformations caused by temperature changes over a 50-year design life. To simulate thermal expansion, axial displacements were applied to the specimen at a quasi-static strain rate. Figure 41 presents the applied actuator displacement, actuator force and average LVDT measurements relative to time for each cycle applied. Figure 42 shows the load relative to the applied gap/crack opening displacement (COD) for the selected axial cycles. The COD is the average of the LVDTs located at the crown and invert.

Several preliminary cycles with relatively small target displacements were conducted to measure the specimen's initial stiffness. During these cycles, the actuator applied a displacement that generated approximately 16 kips (71 kN) of tensile force, resulting in a measured COD of 0.015 in. (0.38 mm). From these measurements, an initial stiffness of approximately 1600 kip/in. (280 kN/mm) was calculated. This stiffness was then used to calculate the target COD for the subsequent cycles. As the testing progressed, the target COD increased because the apparent stiffness from each set of cycles was used to adjust the target displacement for the following set. In the early cycles, the average stiffness of the specimen was about 1600 kip/in. (280 kN/mm), while during the later cycles, the average stiffness dropped to around 1000 kip/in. (175 kN/mm), indicating a reduction of about 27%.

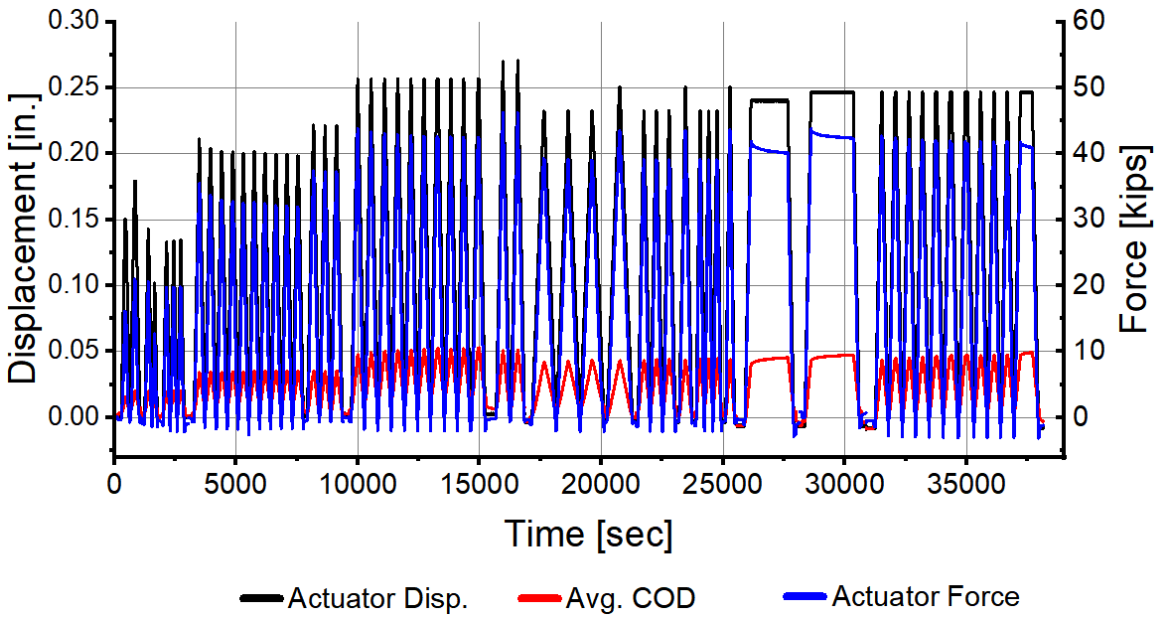

Figure 41. ISES03 actuator displacement, actuator force, and average LVDT measurements vs. time for thermal expansion cycles

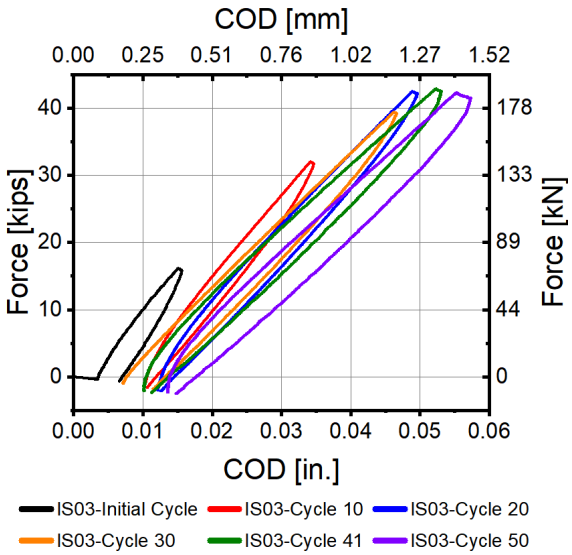

Figure 42. ISES03 actuator load vs. crack opening displacement (COD) for thermal expansion cycles

Once thermal expansion cycles were completed, the specimen was axially loaded to its ultimate capacity. Figure 43 shows the axial force relative to the COD over the duration of this test. The specimen reached a peak ultimate force capacity of about 65 kips (290 kN) at a COD of about 0.39 in. (9.9 mm). At this point, a rupture in the IRP occurred, ending the test. The apparent stiffness was approximately 170 kips/in. (30 kN/mm). Figure 44 shows the specimen (a) before loading, (b) during loading, and (c) after rupture occurred.

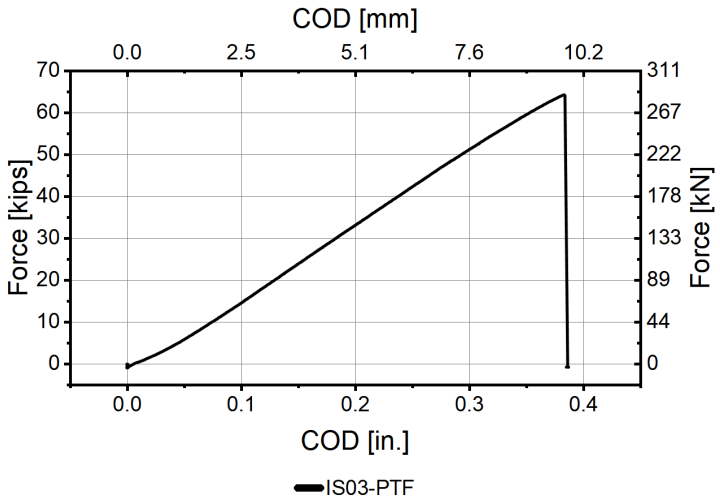

Figure 43. ISES03 axial force vs. crack opening displacement

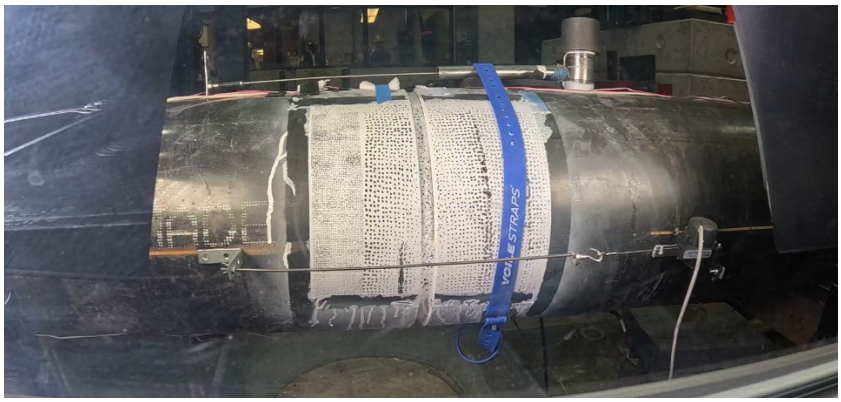

(a)

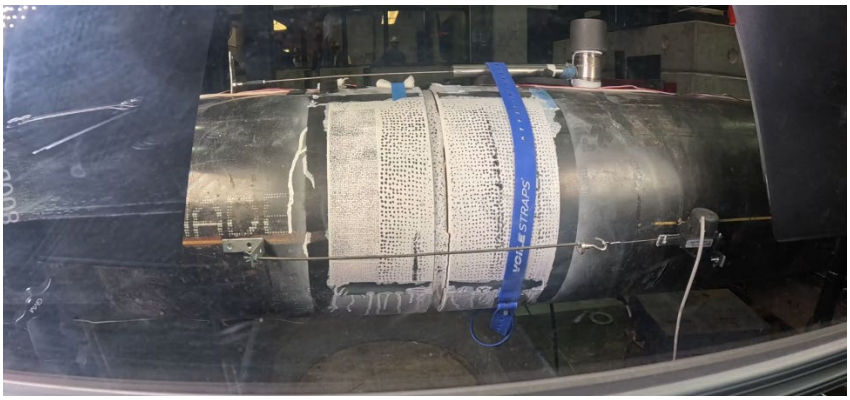

(b)

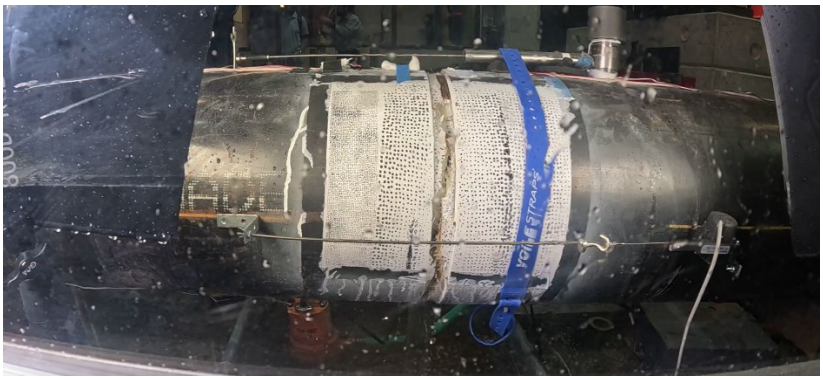

(c)

Figure 44. Sequence of images showing ISES03 ultimate capacity test including (a) start of test, (b) during loading, and (c) post failure

5.4 ISES04 Results (Cornell Specimen)

A coarse overview of the operations performed on ISES04 is provided in Table 19. This table lists the main loading procedures applied to the specimen. Information in this section is summarized with respect to general operation, number of tests and test cycles, test deformation, and configuration. The tests involved: 1) initial bending to verify operation of the equipment, 2) 500,000 cycles of repetitive traffic loads, 3) deformation imposed by parallel trench excavation, involving rotation about the center of the specimen of approximately 0.42° and 0.79°when leakage was observed. The rotational stiffness associated with traffic loading was $k_\theta \approx 330$ in.-kips (36630 mm-kN) per degree.

Table 19. Major mechanical procedures on ISES04

General Operation	Number of Tests or Cycles	Nominal Deformation Level	Test Configuration
Initial Preliminary Bends	24	0.036° Rotation	25 in. - 40 in. - 25 in.
Traffic Loading Bending Cycles	500,037	0.042° Rotation	25 in. - 40 in. - 25 in.
Adjacent Excavation	2	0.42° Rotation, 0.84° Rotation	25 in. - 40 in. - 25 in.
Traffic Loading Bending Cycles	Not performed due to failure	NA	25 in. - 40 in. - 25 in.
Axial Cycles	Not performed due to failure	NA	Weight supported axial testing
Axial Tension	Not performed due to failure	NA	Pull to failure

5.4.1 ISES04 Bending Results

Six sets of four practice cycles (twenty-four total cycles) were performed on ISES04 to check that the instrumentation was functioning and assess specimen stiffness. All traffic load cycles were applied ed at a cyclic frequency of 2 Hz, with a data sampling rate of 32 Hz.

The traffic load testing involved over 500,000 cycles of load principally at cyclic frequencies of 1 Hz and 2 Hz. The targeted rotation was 0.036° for the first 100,000 cycles and 0.042° for an additional 400,000 cycles, set in consultation with University of Colorado at Boulder (CUB). Applied global rotations ranged from about 0.024° to 0.042°. The actuator displacement associated with achieving these rotations was about 0.03 in. (0.76 mm).

A methodology for selecting the appropriate vertical displacements and global rotations from traffic loads for the rotational stiffness of the pipeline specimen was developed at Cornell University (e.g., O'Rourke et al., 1996; Stewart et al., 2015). The methodology was adapted to more precise numerical modeling by CUB. During the tests on Specimen SNES04, global rotation, as well as vertical and horizontal displacements, were provided by CUB. One of the purposes of testing Specimen SNES04 was to compare

the results with those of similar specimens at CUB. To meet this goal, it was necessary to test for the same deformations from repetitive traffic, parallel excavation, undermining, and thermal expansion/contraction at both Cornell and CUB. That way, one can compare the test results from two different institutions for the same deformations.

Traffic load testing at Cornell was performed on a daily basis. The cyclic loading was started and stopped on the same day to guard against unintended deformation of the specimen during night time or weekend loading. The tests were always run when personnel were able to observe and control the testing. A total of 41 groups, or episodes, of testing were performed to achieve a total slightly larger than 500,000 cycles. The number of cycles per each testing period varied from about 14,000 to 16,500.

Of fundamental importance for pipelines subjected to bending from rolling surface loads is the rotational stiffness at the lined gap or crack between two adjacent pipes. Figure 45 shows the moment vs global rotation of the specimen. The moment vs rotation traces a hysteresis loop, where the rotational stiffness can be defined as the slope of the line connecting the two apices of the hysteresis loop. The slope of that line is the stiffness $k_\theta = (\Delta M)/\Delta\theta$, as illustrated in the figure. The data in the figure were taken close to the third cycle with $k_\theta \approx 320$ in.-kips (35520 mm-kN) per degree, and from near the 41st cycle with $k_\theta \approx$ 340 in.-kips (37740 mm-kN) per degree.

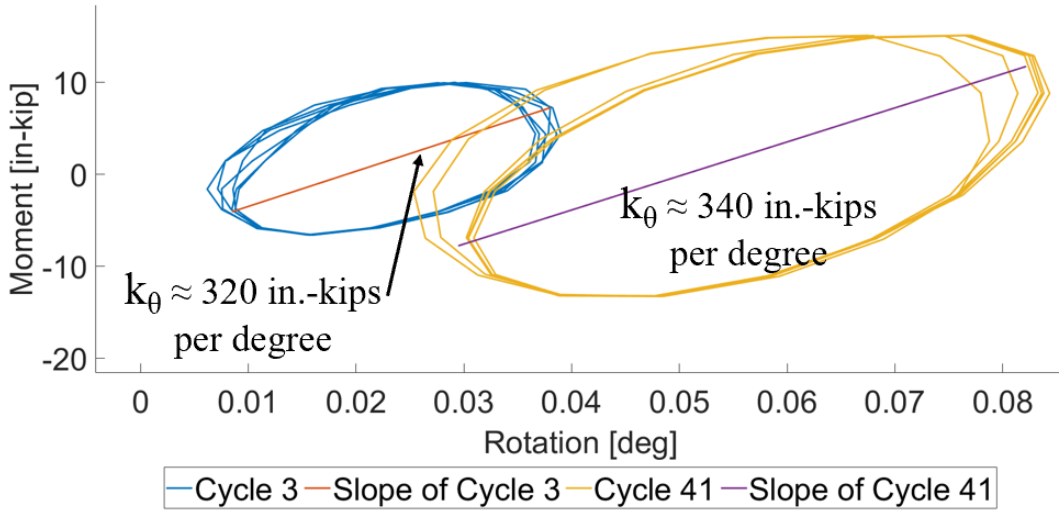

Figure 45. Typical moment vs rotation and rotational stiffness, k_θ

Figure 46 shows the hysteresis loops associated with 1,000, 10,000, 100,000, and 500,000 cycles of traffic load. The maximum difference in the rotational stiffness is between $k_\theta \approx 300$ in.-kips (33.3 m-kN) per degree at 100,000 cycles and $k_\theta \approx 400$ in.-kips (44.4 m-kN) per degree at 500,000 cycles.

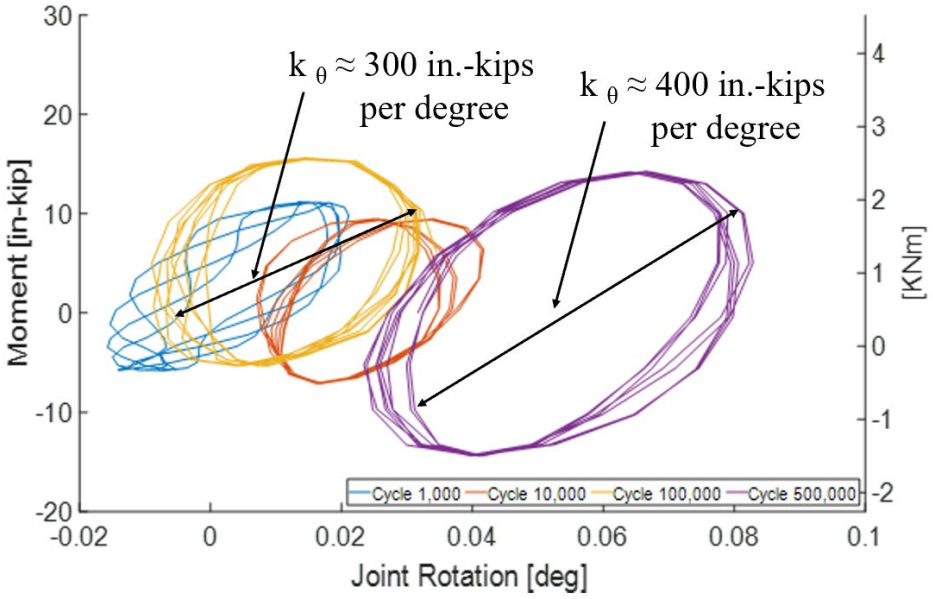

Figure 46. Moment vs. rotation for various cycles of traffic load

Stewart et al. (2015) evaluated the rotational stiffness at the mechanical joints of 12-in. (300-mm) diameter CI pipelines that were reinforced with a flexible polymer lining. They measured rotational stiffness $k_\theta = 200$ in.-kips (22,600 mm-kN) per degree for traffic loading. This value is about 60% of the rotational stiffness for similar conditions measured for this report.

After being subjected to 500,000 cycles of equivalent traffic load, no reduction in internal pressure nor leakage was observed in the test specimen.

To simulate parallel excavation effects, the loading saddles were loosened so that there was no rebound, nor restoration of the pipeline to its initial position. Parallel excavation effects were first modeled as a one-way loading to a rotation of approximately 0.42°. The actuator was then returned to its initial test position, and it was planned to load the specimen to a rotation of 0.84°. These rotations were provided by CUB. They correspond to a parallel excavation with maximum soil displacements of 2.5 in. and 5 in. (63.5 mm and 127 mm).

Figure 47 presents the load path plotted in moment vs rotation space. Representative hysteresis loops for traffic loading are shown, followed by rotation to 0.42° and unloading. As shown in the figure, leakage was first observed at 0.79° when the internal pipe pressure dropped 3 psi (21 kPa). There was a

steep drop in moment after about 0.92°, which was accompanied by a pressure drop to approximately 55 psi (380 kPa).

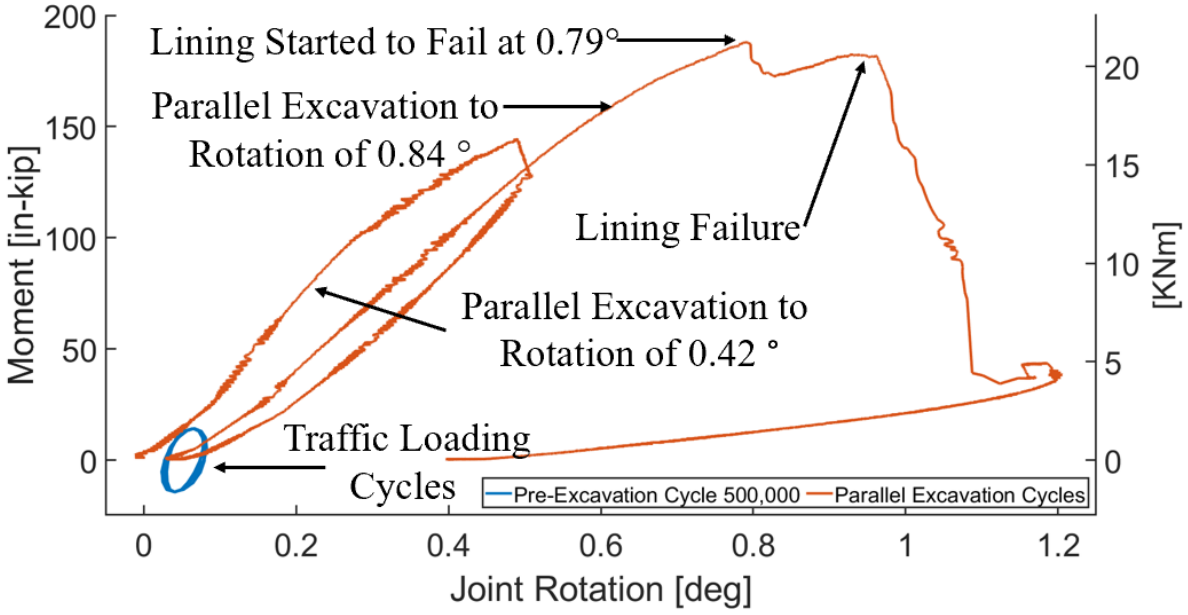

Figure 47. Moment vs. rotation of traffic cycles (~500,000) and two cycles of adjacent excavation

During the first parallel excavation simulation, cracking noises could be heard coming from the pipe when the rotation was about 0.15°. These cracking noises occurred during the remainder of the test. They intensified at 0.79°.

The specimen was unloaded and drained. It was then reloaded to the rotation at first leakage, and inspected with a camera, light, and measuring scale that could be moved along the interior of the pipeline. A crack in the lining was observed at the bottom of the invert near the center of the lined gap between the two pipes. The crack was approximately 13 in. (650 mm) long from about the 8 o'clock to 4 o'clock positions while looking north along the longitudinal axis of the specimen. The maximum crack width was approximately 0.10 in. (2.5 mm) wide, with its widest portions between the bottom of the invert and the 4 o'clock location.

Figure 48 is a photograph of the crack in the Insituform lining from inside the specimen looking at the invert, with south to the top of the photo. The pipeline was loaded so that the joint flexed about 1°, approximating the deflection that occurred when leakage was first observed. The scale at the left was at the 6 o'clock position. The top black rectangle is 0.28 in. (7 mm) wide.

The crack in the lining occurred at the location of maximum strain from bending. It coincided with the maximum theoretical distortion from a parallel excavation.

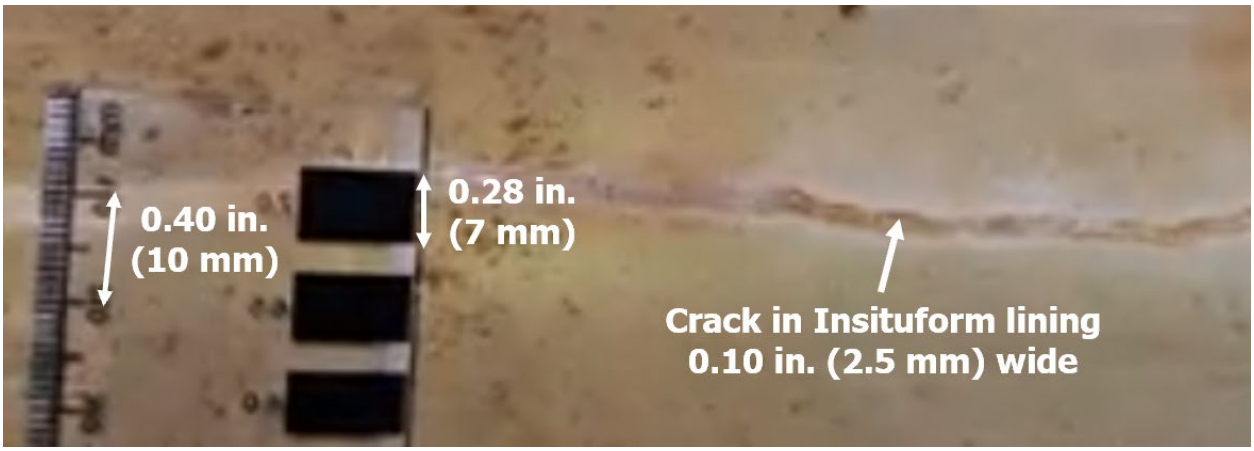

Figure 48. Photo of crack in I-Main lining at invert of pipeline specimen

6 Discussion of Results

Four specimens were composed of a steel host pipe with nominal initial gap openings of either 0.5 in. (ISES01, ISES03, and ISES04) or 6.0 in. (ISES02) and rehabilitated with I-MAIN CIPP. ISES01 and ISES02 were also installed with a pre-liner, while ISES03 and ISES04 were not. Each specimen underwent the same testing program, including the application of 600,000 traffic cycles, 2 larger adjacent excavation (AE) events, 50 thermal expansion cycles, and a final ultimate axial capacity test. ISES04 was the only exception to this due to a rupture that occurred during the second AE cycle, ending testing on the specimen prior to axial testing.

6.1 Traffic Cycles

The following section summarizes and compares key test results for each test performed. Table **20** summarizes the results for traffic cycles performed on each specimen, including the loading geometry, the cycle count, the target rotation, the average moment applied, and the approximate effective stiffness. Although some differences can be observed between the specimens tested, primarily due to the presence of a pre-liner, it is important to note that there were no significant degradations in performance observed for the duration of traffic loading prior to adjacent excavation tests for each specimen tested. Cycles performed after AE events generally had a reduced stiffness for each specimen. The stiffness for ISES01 reduced by 6%, while the stiffness for ISES02 and ISES03 reduced by about 30% and 20%, respectively. However, at the 460k cycle count, ISES02 experienced a relatively significant negative rotation and moment, which may contribute to the reduction in stiffness observed. Since ISES04 ruptured during AE testing, there were no cycles recorded after.

6.2 Adjacent Excavation

After approximately 500,000 traffic cycles were applied, several larger bending moments were applied to the specimen to simulate the effects of AE events. Table 21 summarizes the results for AE events performed on each specimen, including the loading geometry, the test ID, the target rotation, the maximum moment applied, and the approximate effective stiffness. **Error! Reference source not found.** shows a comparison of the moment vs. rotation for each specimen for both a small adjacent excavation event and a larger adjacent excavation event. Figure 50 and Figure 51 show comparisons of each specimen for the smaller AE event and the larger AE event, respectively.

Table 20. Summary of traffic cycles

ID (Gap/Crack Width)	Geometry	Approx. Cycle Count	Rotation (deg.)	Moment [kip-in (kN-m)]	Approx. Stiffness [kip-in/deg (kN-m/deg.)]
ISES01* (0.5 in.)	30”- 40”- 30”	1 - 500,000	0.030° - 0.038°	8.0 – 11.0 (0.9 – 1.2)	330 – 250 (37 – 28)
		500,001 – 600,000	0.046° - 0.048°	11.5 – 11.8 (1.30 – 1.33)	235 (26.5)
ISES02* (6.0 in)	30”- 40”- 30”	1 - 460,000	0.034° - 0.038°	7.0 – 9.0 (0.8 – 1.0)	250 – 225 (28 – 25)
		465,000 – 500,000	*0.045°*	*7.0 (0.80)*	*150 (17)*
		500,001 – 600,000	0.045° - 0.050°	6.5 – 7.0 (0.73 – 0.80)	145 – 135 (16.5 – 15)
ISES03 (0.5 in)	30”- 40”- 30”	1 - 500,000	0.043° - 0.048°	27.0 – 33.0 (3.1 – 3.7)	745 – 650 (84 – 73)
		500,001 – 600,000	0.050° - 0.054°	25.5 – 27.5 (2.9 – 3.1)	520 (59)
ISES04 (0.5 in)	25”- 40”- 25”	1 - 500,000	0.03° - 0.05°	20 – 30 (2.2 – 3.4)	670 – 600 (76 – 68)

* Indicates that a pre-liner was installed.

During the smaller AE event, ISES01 had an approximate stiffness of about 120 kip-in. (13.5 kN-m), while ISES02 had a smaller approximate stiffness of about 87 kip-in./deg. (9.8 kN-m/deg.), approximately 27% less stiff. This reduction in stiffness can largely be attributed to the larger initial crack width for ISES02 (6.0 in.). A larger initial crack width increases the effective crack width for the specimen, which allows for more strain development along the softer repair material before interacting with the much stiffer host pipe material. ISES03 had an approximate stiffness of about 330 kip-in./deg. (37.3 kN-m/deg.), which was 175% more stiff than ISES01. Unlike ISES01, the repair material for ISES03 was not installed with a pre-liner, which allowed the repair material to bond with the host pipe during installation. The significant increase in stiffness between these two specimens is primarily due to this bonding between the repair material and the host pipe. ISES04 had an approximate stiffness of about 300 kip-in./deg. (33.9 kN-m/deg.), a 9% reduction between ISES03. ISES03 and ISES04 were the only matching specimens, both having an initial crack width of 0.5 in. and no pre-liner. However, ISES04 was tested in a different testing laboratory, which may introduce greater likely hood for systematic errors, contributing to the 9% reduction in stiffness observed.

For the larger excavation event, ISES01 and ISES02 were displaced to maximum rotations of about 1.1° and 0.8° and loaded with a maximum moment of about 110 kip-in. (12.4 kN-m) and 86 kip-in. (33.3 kN-m), respectively. Approximate stiffnesses of 110 kip-in./deg. and 86 kip-in./deg. were recorded for these

two specimens, respectively, resulting in only a 22% reduction in stiffness, compared to the 27% reduction observed during the smaller AE event. ISES03 and ISES04 were displaced to maximum rotations of about 0.9° and 0.79° and loaded with a maximum moment of about 205 kip-in. (12.4 kN-m) and 190 kip-in. (33.3 kN-m), respectively. ISES03 and ISES04 both achieved non-linear behaviors during the larger AE events. ISES04 fractured during this test, halting further testing on this specimen.

The stiffness of each specimen decreased slightly between the smaller AE event and the larger AE event. There was an 8.5% reduction in stiffness for ISES01, 1.0% reduction for ISES02, 18% reduction for ISES03, and a 20% reduction for ISES04. Specimens ISES01 and ISES02 were constructed using a pre-liner between the I-MAIN CIPP and the steel host pipe. There was a larger reduction in stiffness observed between each AE event for the specimens constructed without the pre-liner. Non-linear responses occurred for these two specimens, contributing to the larger reduction in stiffness observed between the larger AE event and the smaller AE event.

Table 21. Summary of adjacent excavation loading

ID (Gap/Crack Width)	Geometry (in.)	Test ID	Rotation (deg.)	Moment [kip-in.(kN-m)]	Approx. Stiffness [kip-in./deg (kN-m/deg.)]
ISES01* (0.5 in.)	30 – 40 – 30	AE 1	0.58°	70 (7.9)	120 (13.6)
		AE 2	1.10°	120 (13.6)	110 (12.4)
ISES02* (6.0 in)	30 – 40 – 30	AE 1	0.40°	35 (4.0)	87 (9.8)
		AE 2	0.80°	69 (7.8)	86 (9.7)
ISES03 (0.5 in)	30 – 40 – 30	AE 1	0.48°	160 (18.0)	330 (37.3)
		AE 2	0.90°	205 (23.2)	270 (30.5)
ISES04 (0.5 in)	25 – 40 – 25	AE 1	0.48°	145 (16.4)	300 (33.9)
		AE 2	0.79°	190 (21.5)	240 (27.1)

* Indicates that a pre-liner was installed.

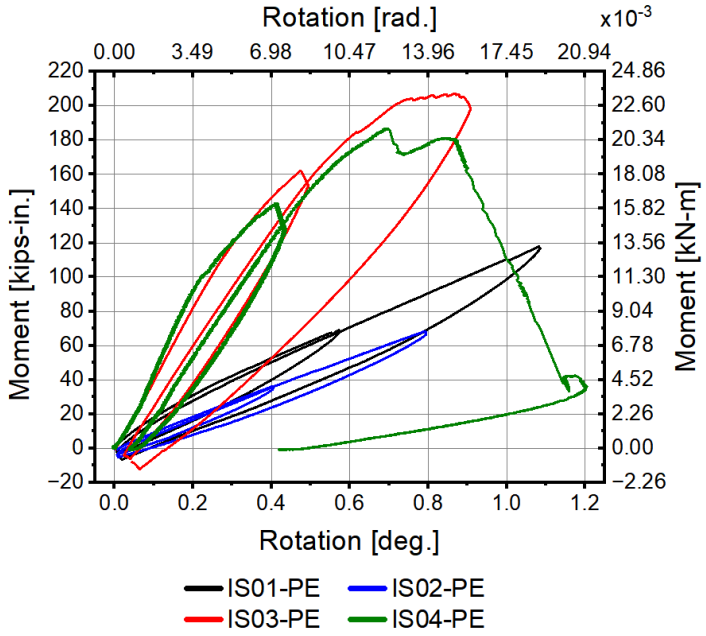

Figure 49. Moment vs. rotation for adjacent excavation events for each specimen

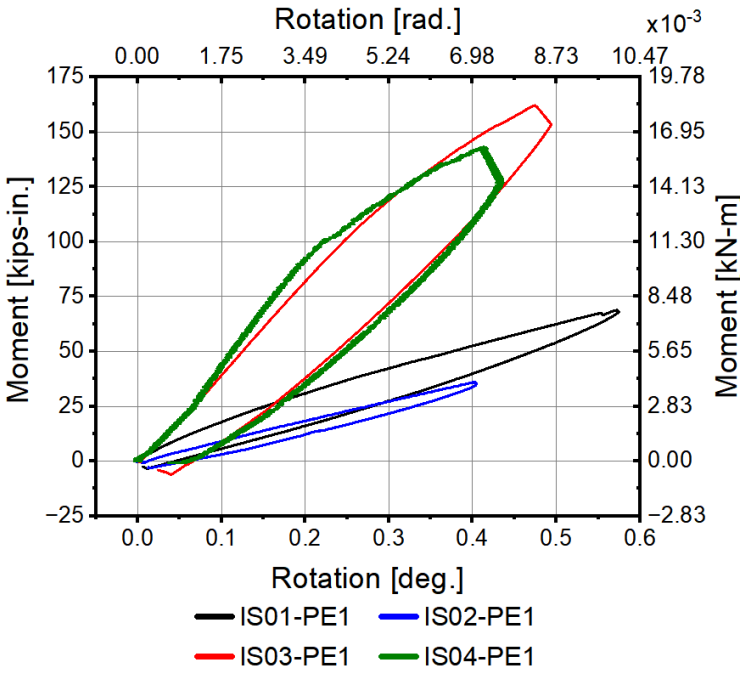

Figure 50. Moment vs. rotation for small adjacent excavation events for each specimen

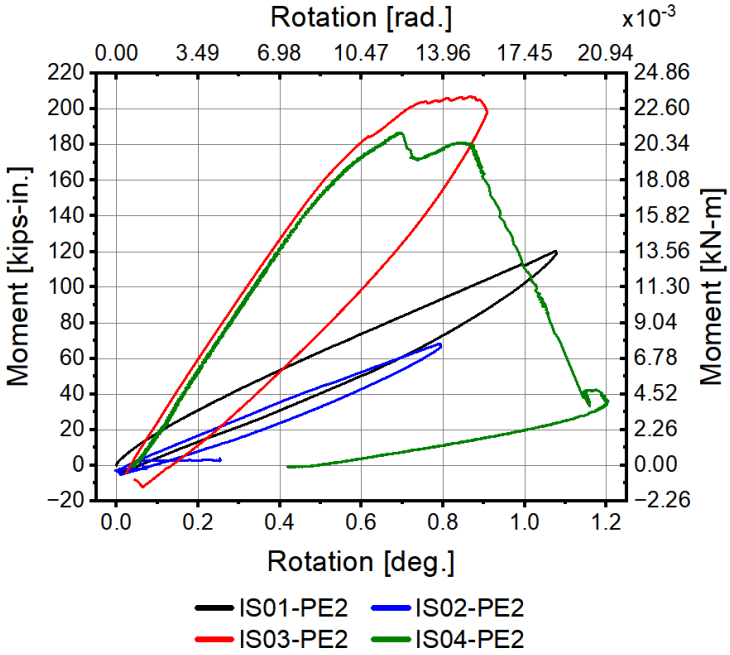

Figure 51. Moment vs. rotation for large adjacent excavation events for each specimen

6.3 Thermal Expansion Cycles

After adjacent excavation tests and approximately 100,000 additional traffic cycles, specimens were then subjected to axial thermal expansion cycles. Table 22 summarizes the results for axial thermal expansion cycles performed on each specimen, including the cycle count, the target COD, the approximate maximum force applied, and the approximate effective stiffness for each specimen.

Table 22. Summary of thermal expansion cycles

ID (Gap/Crack Width)	Approx. Cycle Count	Average COD [in. (mm)]	Approx. Max Force [kips (kN)]	Approx. Stiffness [kip/in (kN/mm)]
ISES01* (0.5 in.)	1 - 50	0.18 – 0.26 (4.6 – 6.6)	28.0 – 40.0 (124.5 – 177.9)	156 – 154 (27.3 – 27.0)
ISES02* (6.0 in)	1 - 50	0.25 (6.35)	32.5 – 34.0 (144.6 – 151.2)	136 – 130 (23.8 – 22.8)
ISES03 (0.5 in)	1 - 50	0.034 – 0.055 (0.86 – 1.40)	32.0 – 43.0 (142.3 – 191.3)	940 – 780 (165 – 135)
ISES04 (0.5 in)	NA	NA	NA	NA

* Indicates that a pre-liner was installed.

6.4 Ultimate Axial Capacity

After more than 50 thermal expansion cycles were applied, each specimen was then loaded to its ultimate force capacity. Table 23 summarizes the results for each specimen during ultimate capacity testing, including the COD at the instance of initial debonding, the maximum COD prior to loss in force capacity, the ultimate force capacity, and the approximate effective specimen stiffness. Figure 52 shows the applied axial force relative to COD for each specimen. Figure 53 provides a magnified view of the initial loading relative to COD before initial debonding.

ISES01 and ISES02 reached ultimate force capacities of about 61 kips (271 kN) and 50 kips (222 kN) at CODs of about 0.81 in. (20.6 mm) and 0.67 in. (17.0 mm), respectively. Each of these specimens had an approximate stiffness of 75 kips/in. (13 kN/mm). ISES03 reaches an ultimate force capacity of 65 kips (290 kN) at a COD of about 0.39 in. (9.9 mm), resulting in an approximate stiffness of 170 kips/in. (30 kN/mm). The apparent stiffness for ISES03 was about 127% greater than the apparent stiffness for the two prior specimens. However, at the point of ultimate force capacity, ISES03 ruptured, losing all force capacity and pressure capacity in an instance. Rupture never occurred for ISES01 and ISES02, and instead had a gradual reduction in force capacity as COD increased due to frictional effects between the repair material and the host pipe. Despite ISES01 and ISES02 showing almost identical initial stiffnesses, differences in response did occur after ultimate force capacity was achieved. ISES01 experienced sudden drops in force, starting at around 30 kips (130 kN) in magnitude. As COD increased, these drops in force reduced in magnitude, reaching a smaller local maximum force capacity each time. However, ISES02 only experienced an initial drop in force by about 10 kips (45 kN) before stabilizing to a steady loss in force capacity as the COD increased. ISES01 reached a maximum COD of about 8.8 in. (225 mm) with a force capacity of about 30 kips (135 kN) before concluding the test. ISES02 reached a maximum COD of about 7.4 in. (188 mm) with a force capacity of about 30 kips (135 kN) before concluding the test.

At the end of ISES01, one compressive cycle was applied to compare frictional resistance in the other direction. The axial compressive force reached about 40 kips after 0.5 in. of applied COD before beginning to plateau. This resulted in a slightly stiffer loading response (80 kips/in [14 kN/mm]) compared to the stiffness during initial tensile loading. The maximum COD change for this compressive test was around 1.0 in. (25 mm), with the highest recorded compressive force being approximately 48 kips.

Table 23. Summary of ultimate capacity tests

ID (Gap/Crack Width)	COD @ Ultimate Force Capacity [in. (mm)]	Ultimate Force Capacity [kip (kN)]	Approx. Stiffness [kip/in (kN/mm)]
ISES01* (0.5 in.)	0.81 (20.6)	61 (271)	75 (13)
ISES02* (6.0 in)	0.67 (17.0)	50 (222)	75 (13)
ISES03 (0.5 in)	0.39 (9.9)	65 (289)	170 (30)
ISES04 (0.5 in)	NA	NA	NA

* Indicates that a pre-liner was installed.

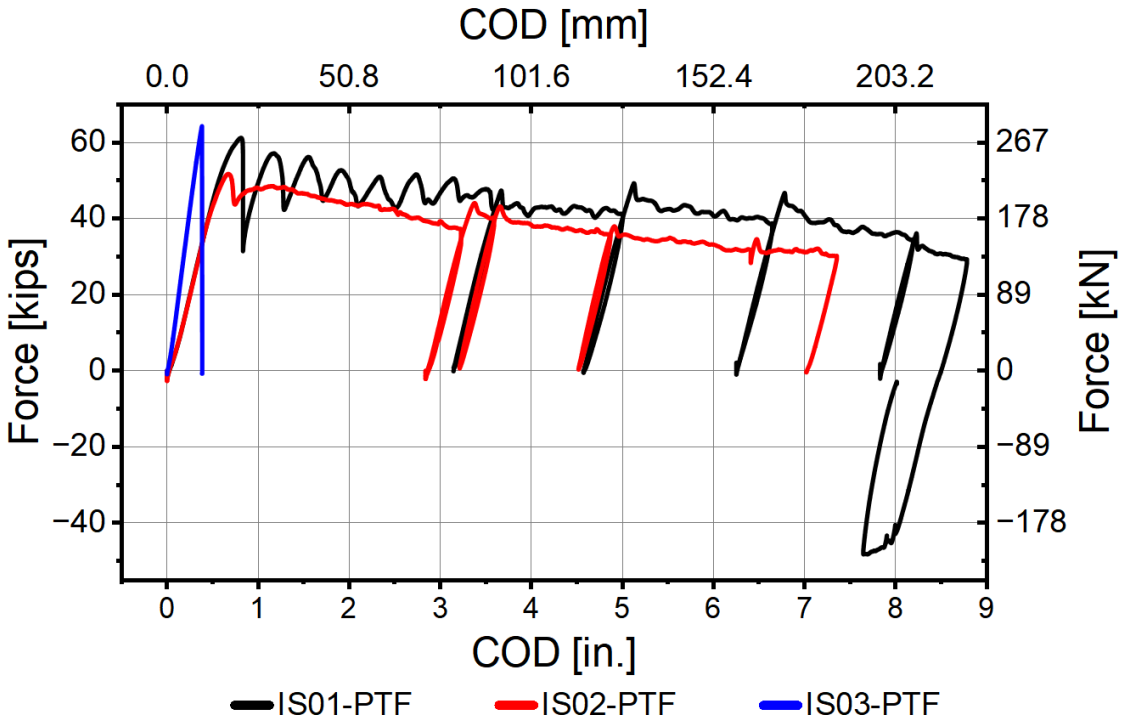

Figure 52. Axial force vs. COD for ultimate capacity tests for all specimens

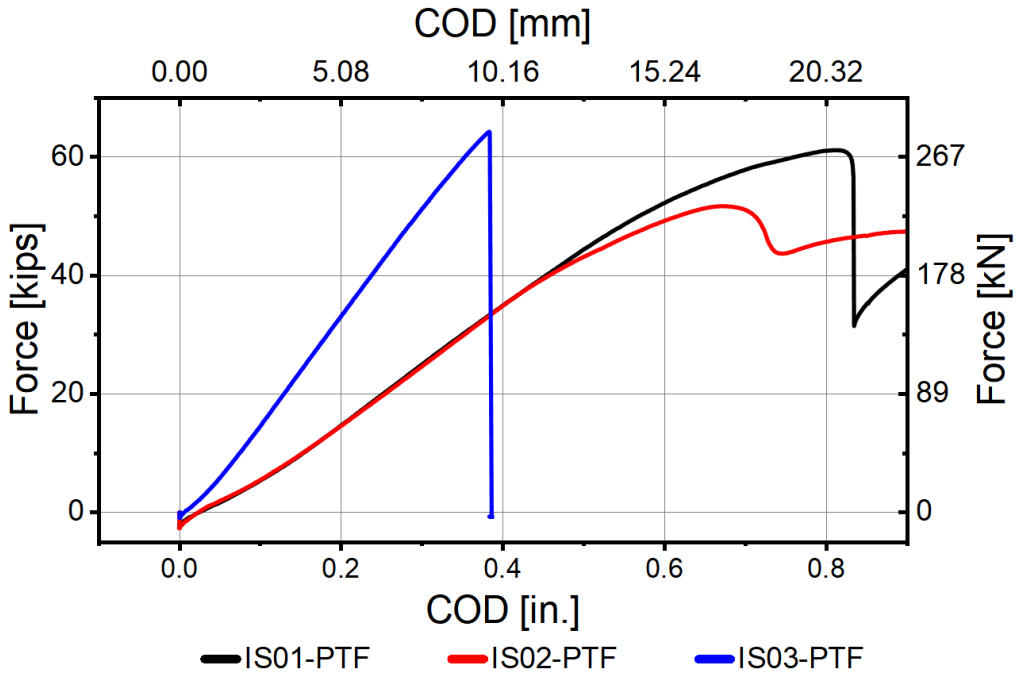

Figure 53. Axial force vs. COD at initial loading for ultimate capacity tests for all specimens

6.5 Water backtracking

For the duration of testing performed on each specimen, no significant leakage was observed due to material degradation. However, slow drips of water were observed at different times, possibly due to water backtracking from end seals between the IRP and the host pipe. For specimen IS01, a series of pressure tests were conducted to assess leakage and water backtracking under various conditions. Initially, during the sample preparation phase, a few drips were observed at the crack opening when pressure was first applied. Before testing, Weko seals were installed by manufacturer service techs. This early indication of potential backtracking influenced careful monitoring and adjustments during some tests. Prior to starting the axial cycles, inflatable pipe plugs (IPPs) were installed near each end of the specimen to improve the seal between the host pipe and liner at the termination points (ends of the specimen) and reduce water backtracking. The intention of this adjustment was to isolate internal pressure to the center of the specimen so that the region with the circumferential crack and other host pipe defects could be assessed for leakage. During the first pull-to-failure test (IS01-PTF1), leakage was noted at the west end IPP. No leakage was observed in other areas.

In the second pull-to-failure test (IS01- PTF2), IPP pressure was set to approximately 45 psi, with the internal specimen pressure at 20 psi. During this test a maximum tensile force of 48.9 kip (217.5 kN) was reached. A leak was detected at the center of the pipe, indicating further challenges in fully containing

water during high-pressure scenarios. The third pull-to-failure test (PTF3) was temporarily halted when the East IPP began to slide out of the specimen. Testing resumed by compressing the pipe at 0 psi. During this compression phase, cracking and popping sounds were heard, and a maximum compression force of 45.2 kip was recorded. Table 24 shows the summary of water back tracking for IS01.

Table 24. Summary of water backtracking observations for specimen IS01

Test ID	Description related to pressure
Sample preparation	Weko seals were installed by manufacturer service techs prior to testing. There were a few drips at the beginning of the pressure test at crack opening.
First axial cyclic test	IPPs replaced end caps to overcome water backtracking between the liner and host pipe.
PTF1	The west IPP was not entirely effective in sealing the liner. The average force applied during the test was 42 kip. Leakage was observed at the west end. A question remains as to whether the pipe leaked at the center crack during or after the PTF test. No leakage was noted at the other locations.
PTF 2	Approximately 45 psi of pressure was applied to the IPP, with an internal specimen pressure of 20 psi. The maximum tensile force reached during testing was 48.91 kip. A leak was detected at the center of the pipe.
PTF 3	The test was halted due to the East IPP sliding out. Compression of the pipe then began at 0 psi. During compression, cracking and popping sounds were audible. A maximum compression force of 45.2 kip was recorded during testing.

IS02 specimen preparation was conducted with a focus on detecting any leakage or water backtracking between the host pipe and liner. The sequence of tests highlighted different aspects and issues unique to this specimen, particularly related to pressure adjustments and the use of sealing techniques. Before testing, Weko seals were installed by manufacturer service techs. IPPs were not used on IS02 during the bending tests but were used for the axial test. Throughout the bending cycles, observations were made to determine if any leakage occurred. During the AC06 (axial cyclic) test, initial pressurization faced difficulties due to significant air within the system. The first pull-to-failure test (PTF1) revealed notable events as cracking sounds began around 38 kips and continued around 42 kips. The west side of the liner was observed slowly pulling out, indicating a shift in liner position under stress. Adjustments to the load rate were made to stabilize the internal pressure, which was dropping over time. Loading rates were then gradually increased. Testing was paused and unloaded when a leak was detected. The internal specimen pressure was constant during this stage. In the second pull-to-failure test (PTF2), the starting load rate was increased, and dripping at the center had slowed. For this part of the test, unloading and loading were conducted to record stiffness data for different loading rates. Pauses continued throughout the test to

monitor leaks, with a final adjustment to decrease the loading rate. During this phase, the system consistently held a pressure of 60-62 psi. Table 25 shows the summary of water back tracking for IS02.

Table 25. Summary of water backtracking observations for specimen IS02

Test ID	Description related to pressure
Sample preparation	Weko seals were installed by manufacturer service techs prior to testing. There were a few drips at the beginning of the pressure test at crack opening.
First axial cyclic test	IPPs replaced end caps to overcome water backtracking.
PTF1	Cracking sounds noted at 38 and 42 kips, with the liner's west side gradually pulling out. Load rate decreased as internal pressure was dropping. Increased load rate. Paused and unloaded upon detecting a leak. Pressure likely constant during test.
PTF2	Dripping decreased at center. Increased load rate and quickly unloaded and reloaded to capture stiffness curve. Paused at middle of test for leak inspection, decreased load rate, and continued testing while maintaining 60-62 psi.

IS03 specimen testing began with traffic loading applied to the pipe to observe potential leakage and water backtracking. Early in the test, with an internal pressure of 10 psi, the pipe appeared to be "sweating" as water beaded up along the crack edge and dripped at a rate of approximately 1-2 drops per second. As the test continued to the 30,000-cycle mark, no significant leak was observed during pressurization, suggesting a stable seal under the current load and pressure. However, when the internal pressure was raised to 65 psi, leakage resumed with a noticeable increase to around 2-3 drops per second. Over time, this rate gradually slowed to about 1 drop per second as testing progressed, indicating a possible settling of the seal or minor adjustment in the water flow. Table 26 shows the summary of water back tracking for IS02.

Table 26. Summary of water backtracking observations for specimen IS03

Test ID	Description related to pressure
Sample preparation	Weko seals were installed by manufacturer service techs prior to testing. There were a few drips at the beginning of the pressure test at crack opening.
Traffic loading	Specimen showed water beading at crack edge and dripping at 1.4 drops per second at 10 psi. At around 30,000 cycles, no leak observed during pressurization. When internal pressure reached 65 psi, leak rate increased to 2-3 drops per second, slowing to about 1 drop per second as testing progressed.
First axial cyclic test	IPPs replaced end caps to overcome water backtracking by providing a better seal between the pipe and liner.

7 Summary & Conclusions

This section summarizes the findings of the testing program performed on 12 in. (300-mm) diameter specimens repaired with the I-Main™. Four steel host pipe specimens were tested and prepared with a nominal 0.5 in. (12.7 mm) or 6 in. (150 mm) gap of exposed I-Main™ lining, with approximately 5 ft (1.52 m) of host pipe on either side of the gap. They were subjected to cyclic flexural and axial loading using specialized testing equipment at the Center for Infrastructure, Energy, and Space Testing (CIEST) at the University of Colorado Boulder and the Bovay Laboratory Complex at Cornell University.

The general methodology consisted of applying bending deformation to a pipe specimen, followed by axial loading, predominantly in tension. Bending involved 500,000 short duration (1 to 2 Hz) cycles representing cyclic deformation caused by overhead traffic. This fatigue testing was followed by larger bending deformations reflective of the system responses to adjacent excavation activity, which in turn were followed by roughly 100,000 additional "traffic" cycles. An ultimate parallel excavation deformation was then performed prior to the start of axial testing. In axial testing, 50 or more axial cycles were applied, representing the thermal deformation over 50 years associated with annual temperature change (ΔT) of 50°F (27.8°C). Final axial tension tests were performed to assess the ultimate pullout capacity of the host pipe and I-Main™ lining. Most testing was performed at about 65 psi (450 kPa) of internal water pressure.

The levels of excavation movement assumed for the adjacent excavation cycles were associated 2.5 in. (63.5 mm) and 5 in. (127 mm) for the small and large events, respectively. The 5 in. (127 mm) level of soil displacement is expected to be used to set maximum parallel excavation deformation levels in future studies. The targeted rotational deformations depend on the stiffness of the repair pipe and the nature of the bonding between the repair and host pipe. If another IRP technology had a similar stiffness to I-Main™, similar deformation levels would be anticipated. Initial stiffness tests of specimens and comparison with analytical and/or numerical models will inform the degree of bonding and, thus, deformation levels (for example see Klingaman et al., 2024).

The stiffness of the specimens in bending ranged from roughly 100 to 300 kip-in./deg (11 -33 kN-m/deg), using a global rotation calculated by LVDTs positioned on either side of the crack opening. While the initial crack width did influence changes in stiffness between specimens, the primary contributing factor to changes in stiffness was the presence of a pre-liner installed with the IRP. Specimens constructed with a pre-liner were significantly less stiff than those constructed without. The stiffness for each type of specimen varied around ± 20% relative to its respective average. Maximum moments achieved in the lateral loading of all specimens ranged from 70 kip-in. to 200 kip-in. (8 kN-m to 23 kN-m).

For ISES04, adjacent excavation cycles imposed rotations of approximately 0.42° and 0.79°, with leakage observed during the latter. A crack in the lining was observed at the bottom of the invert near the center of the lined gap between the two pipes. The crack was approximately 13 in. (650 mm) long from about the 8 o'clock to four o'clock positions while looking north along the longitudinal axis of the specimen. The maximum crack width was approximately 0.2 in (5 mm) wide and was measured when the specimen was reloaded to the rotation at first leakage, or approximately 0.79°. It occurred at the location of maximum strain from bending.

For the other three specimens, the axial load stiffness associated with thermal load application generally ranged between 130 kip/in. (23 kN/mm) and 940 kip/in. (165 kN/mm). Again, the presence of a pre-liner between the host pipe and IRP significantly reduced the stiffness relative to the specimen tested without a pre-liner. The principal reduction in stiffness was observed immediately after the first thermally-driven displacement cycle. All three specimens experienced upwards of 50 such cycles.

As intended by the test program, the ultimate capacity in axial tension of three specimens was achieved. Specimen with pre-liner experienced IRP detachment from the host pipe. This occurred at loads around 50 to 60 kips (220 - 265 kN) with CODs at failure from roughly 0.7 in. to 0.8 in. (18 - 20 mm). Additional cycles were applied to these specimens to characterize the friction between the IRP and host pipe post-detachment under various internal pressures, demonstrating considerable resistance to further pullout.

The specimen without pre-liner (ISES03), experienced fracture at the gap opening, which occurred at an applied load of 65 kips (290 kN) and a COD of 0.39 in. (9.9 mm).

The I-Main^{TM} repair system performed well under applied external loads representative of 50 years of service. No cracks or significant structural damage to the IRP were observed during service life testing for three of the specimens. Specimens with a pre-liner were allowed to debond locally from the host pipe to accommodate strain concentrations while achieving containment and continuity. While this testing program and the applied cycles were limited to a 50-year service life due to project time constraints, the performance observed suggests that longer durations of testing could demonstrate the ability of the system to accommodate a service life exceeding 50 years. This research demonstrates that the proposed service life testing procedures can be accommodated by an existing trenchless technology and supports further applications of the proposed methods.

References

Ahmadi, H., Manalo, A., Dixon, P.G., Salah, A., Karunasena, W., Tien, C.M.T., … Wham, B.P. (2024). "Temperature change-induced linear and nonlinear axial responses of internal replacement pipe (IRP) systems for pipeline rehabilitation incorporating the effects of soil friction". *Structures*, *62*(March), 106247. doi.org/10.1016/j.istruc.2024.106247

Allouche, E.N., Alam, S., Simicevic, J., Sterling, R., Condit, W., Matthews, J., & Selvakumar, A. (2014). "A pilot study for retrospective evaluation of cured-in-place pipe (CIPP) rehabilitation of municipal gravity sewers". *Tunnelling and Underground Space Technology*, *39*, 82–93. doi.org/10.1016/j.tust.2012.02.002

ASME. (2018). *Article 403 Nonmetallic Internal Line for Pipe: Sprayed Form for Buried Pipe*. *ASME PCC-2-2018 Repair of Pressure Equipment and Piping*. New York: ASME.

ASTM. (2014). "D638-14 Standard Test Method for Tensile Properties of Plastics". West Conshohocken, PA: ASTM International. doi.org/10.1520/D0638-14.1

ASTM. (2016a). "F3182 - 16 Standard practice for the application of spray-applied polymeric liners inside pipelines for potable water". *ASTM International*. West Conshohocken, PA. doi.org/10.1520/F3182

ASTM. (2016b, August 1). "F1216: Practice for Rehabilitation of Existing Pipelines and Conduits by the Inversion and Curing of a Resin-Impregnated Tube". West Conshohocken, PA: ASTM International. doi.org/10.1520/F1216-16

ASTM. (2017a). "D3030/D3039M: Test Method for Tensile Properties of Polymer Matrix Composite Materials". *Annual Book of ASTM Standards*. West Conshohocken, PA: ASTM International. doi.org/10.1520/D3039_D3039M-17

ASTM. (2017b, February). "F1743: Practice for Rehabilitation of Existing Pipelines and Conduits by Pulled-in-Place Installation of Cured-in-Place Thermosetting Resin Pipe (CIPP)". West Conshohocken, PA: ASTM International. doi.org/10.1520/F1743-17

ASTM. (2018). "D5813 - 04 Standard Specification for Cured-In-Place Thermosetting Resin Sewer Piping Systems". doi.org/10.1520/D5813-04R18

ASTM. (2019). "F2207-06: Standard Specification for Cured-in-Place Pipe Lining System for Rehabilitation of Metallic Gas Pipe". West Conshohocken, PA. doi.org/10.1520/F2207-06R19

AWWA. (2019). "Committee Report: Structural Classifications of Pressure Pipe Linings". American Water Works Association (AWWA).

Dixon, P.G., Salah, A., Ahmadi, H., Ulrich, M.E., Hubler, M.H., Dashti, S., … Wham, B.P. (2023a). "An Analytical Approach for Thermally Induced Axial Deformation in Rehabilitated Pipelines". *Proceedings: Pipelines 2023* (pp. 260–269). Reston, VA: American Society of Civil Engineers. doi.org/10.1061/9780784485026.028

Dixon, P.G., Tafsirojjaman, T., Klingaman, J., Hubler, M.H., Dashti, S., O'Rourke, T.D., … Wham, B.P. (2023b). "State-of-the-Art Review of Performance Objectives for Legacy Gas Pipelines with Pipe-in-Pipe Rehabilitation Technologies". *Journal of Pipeline Systems Engineering and Practice*, *14*(2), 1–13. doi.org/10.1061/JPSEA2.PSENG-1371

Fu, G., Shannon, B., Rathnayaka, S., Deo, R., & Kodikara, J. (2020). *State of The Art Literature Review on CIPP liners*. *CRC Project: Smart Linings for Pipe and Infrastructure*.

Jeon, S.-S., O'Rourke, T.D., Neravali, A.N., O'Rourke, T.D., & Neravali, A.N. (2004). "Repetitive Loading Effects on Cast Iron Pipelines with Cast-in-Place Pipe Lining Systems". *Journal of Transportation Engineering*, *130*(6), 692–705. doi.org/10.1061/(ASCE)0733-947X(2004)130:6(692)

Klingaman, J., Dixon, P.G., Wham, B.P., Dashti, S., & Hubler, M.H. (2022). "Traffic Loading Effects on Rehabilitated Cast Iron Distribution Pipelines". *Proceedings: Pipelines 2022* (pp. 313–323). Reston, VA: American Society of Civil Engineers. doi.org/10.1061/9780784484296.037

Klingaman, J., Wham, B.P., Dixon, P.G., & Dashti, S. (2025). "External loading-induced deformations of deteriorated pipelines rehabilitated with internal replacement technologies". *Tunnelling and*

Underground Space Technology, *157*(March), 106272. doi.org/10.1016/j.tust.2024.106272

Lu, H., Behbahani, S., Azimi, M., Matthews, J.C., Han, S., & Iseley, T. (2020). "Trenchless Construction Technologies for Oil and Gas Pipelines: State-of-the-Art Review". *Journal of Construction Engineering and Management*, *146*(6), 03120001. doi.org/10.1061/(asce)co.1943-7862.0001819

Najafi, M. (2005). *Trenchless Technology: Pipeline and Utility Design, Construction, and Renewal (Design considerations for trenchless renewal methods)* (1st ed.). New York: McGraw-Hill Education. Retrieved from https://www.accessengineeringlibrary.com/content/book/9780071422666

O'Rourke, T.D., Netravali, A.N.A.N., Pendharkar, S.M., Tonkinson, A., Chaudhuri, D., & Toprak, S. (1996). *Evaluating Service Life of Anaerobic Joint Sealing Products and Techniques*. Cornell University, Ithaca, NY, USA.

Roboski, J., & Finno, R.J. (2006). "Distributions of ground movements parallel to deep excavations in clay". *Canadian Geotechnical Journal*, *43*(1), 43–58. doi.org/10.1139/t05-091

Stewart, H.E., O'Rourke, T.D., Wham, B.P., Netravali, A.N., Argyrou, C., Zeng, X., & Bond, T.K. (2015). "Performance Testing of Field-Aged Cured-in-Place Liners (CIPL) for Cast Iron Piping". Cornell University, Ithaca, NY.

Vladeanu, G., & Matthews, J.C. (2018). "Analysis of risk management methods used in trenchless renewal decision making". *Tunnelling and Underground Space Technology*, *72*(November 2017), 272–280. doi.org/10.1016/j.tust.2017.11.025

8 Appendices

Appendix A.1 Digital Image Correlation (DIC) measurement

CUB employed digital image correlation (DIC) to capture the strain field of pipeline specimens by tracking pixel movements through image correlation algorithms. To improve contrast, the central repair area was painted white, followed by black speckle dots after drying. As shown in Figure 54, a tripod was positioned to mount two 2.4-megapixel digital cameras with low-distortion lenses for 3D deformation measurement. These cameras, connected to a desktop computer, captured images every 125 ms, stored on an external hard drive via Vic-Snap software. High intensity lighting enhanced contrast for reliable deformation analysis, aligning with the strain measurement system.

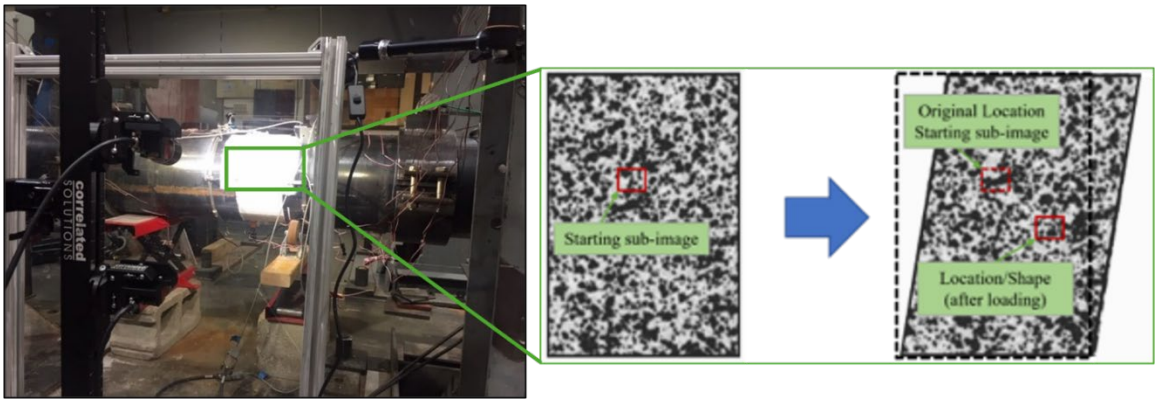

Figure 54. DIC setup for in-frame specimen associated with measurement mechanisms

Calibration is a crucial pre-testing step that involves inputting the ruler into the software for deformation calculations. A target pad is selected based on the area of interest; for this test, a pad with evenly spaced speckles at 14 mm intervals was used. As shown in Figure 55, the calibration pad should be positioned as close to the target sample as possible and adjusted at various in-plane and out-of-plane angles to capture 15–20 images. Eventually, it is crucial to keep the projection error below 0.1 to achieve reliable measurement accuracy.

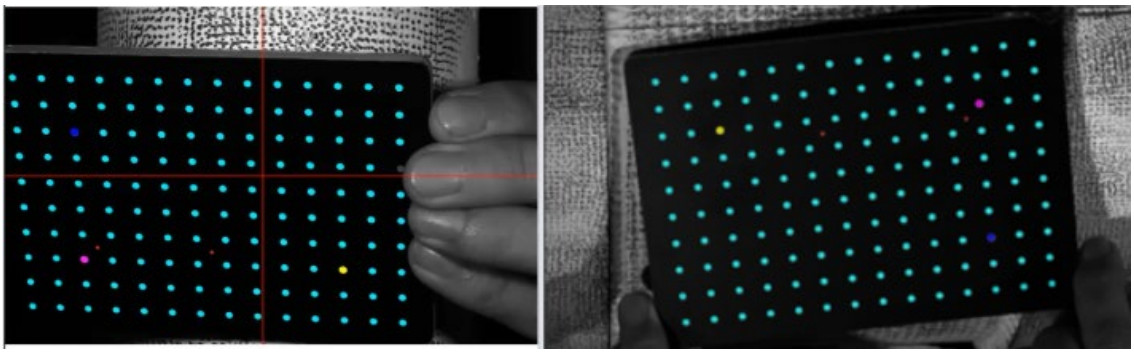

Figure 55. Calibration process before testing steps

Table 27 summarizes the DIC measurement records for specimens ISES01, ISES02, and ISES03. CUB conducted DIC measurements during the first parallel excavation test for these specimens to comprehensively assess their mechanical properties, which could provide valuable insights for designing testing parameters for upcoming bending and axial cycle tests. As previously described, calibration steps are essential for processing DIC images and extracting deformation data, and the calibration score is directly influenced by camera aperture and other hardware settings such as light intensity and oblique angle. To enhance experimental efficiency and reduce setup time, the CUB teams protected the DIC system from external mechanical disturbances that it is allowable for consistent calibration image sets to be used in conjunction tests. Additionally, a projection error check was conducted before each test to ensure the score remained below 0.1.

Table 27. Overview of DIC measuring on specimen tests

Specimen ID	Test Type	Test Date (Y/M/D)	DIC	Calibration (Y/M/D)
ISES01	Parallel Excavation	2024/03/18	Yes	2024/03/18
	Axial Loading	2024/06/04	Yes	2024/06/04
	Axial Loading	2024/06/06	Yes	
	Axial Loading	2024/06/07	Yes	2024/06/07
	Axial Loading	2024/06/10	Yes	
	Axial Loading	2024/06/11	Yes	2024/06/11
	Axial Loading	2024/06/12	Yes	2024/06/12
	Axial Loading	2024/06/13	Yes	
	Pull to Failure	2024/06/18	Yes	
ISES02	Parallel Excavation	2024/06/17	Yes	2024/06/17
	Axial Loading	2024/07/29	Yes	2024/07/29
	Axial Loading	2024/07/30	Yes	2024/07/30
	Axial Loading	2024/07/31	Yes	2024/07/31
	Axial Loading	2024/08/01	Yes	

	Axial Loading	2024/08/08	Yes	2024/08/08
	Axial Loading	2024/08/13	Yes	2024/08/13
	Pull to Failure	2024/08/15	Yes	2024/08/15
	Pull to Failure	2024/08/22	Yes	2024/08/22
ISES03	Parallel Excavation	2024/08/09	Yes	2024/08/09
	Axial Loading	2024/09/24	Yes	2024/09/24
	Axial Loading	2024/10/07	Yes	2024/10/07

Figure 56 compares DIC measurements with conventional sensor readings taken at the same time. A high R^2 value demonstrates the reliability of DIC technology in capturing sample deformation. Using field-scale measurements instead of local point measurements from LVDT provides advantages for developing predictive models to assess pipeline degradation mechanisms, which we are currently investigating.

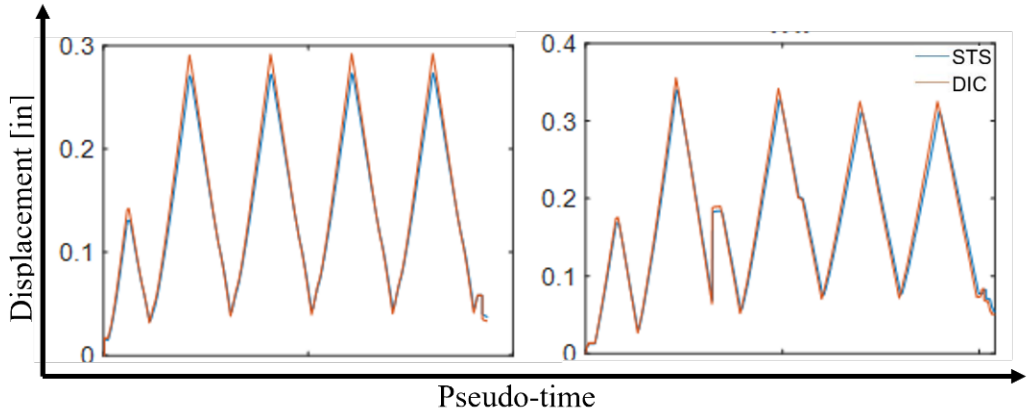

Figure 56. Comparisons between DIC and conventional measurements with R^2 equal to 99%

Figure 57 displays the DIC measurements of axial deformation (e_{xx}) from the pull-to-failure test on ISES02 specimen that features a 6-inch width crack. The x-axis in Figure 60(B) represents the image index which is linearly proportional to the test duration at a ratio of 125 ms. Overall, DIC system successfully captured the experimental pattern of loading, unloading, and reloading to failure. Unlike conventional strain gauges, DIC provided full-field strain measurements with a high resolution of 1E-4 microstrain. Figure 60(A) illustrates the region of interest (ROI) alongside two rectangular boxes (R0 and R1) designated for strain gradient analysis, with R0 located at the center of the crack area and R1 closer to the host pipe. During the pull-to-failure test, R0 consistently exhibited the highest axial deformation, with the final strain approaching nearly 0.02 microstrain. In contrast, specimens nearer to the host pipe displayed smaller deformations due to the constraints imposed by boundary conditions. These strain gradients will serve as

valuable references for calibrating the predictive model currently being developed by the CUB team to assess the debonding degree of PIP rehabilitation under thermal variations.

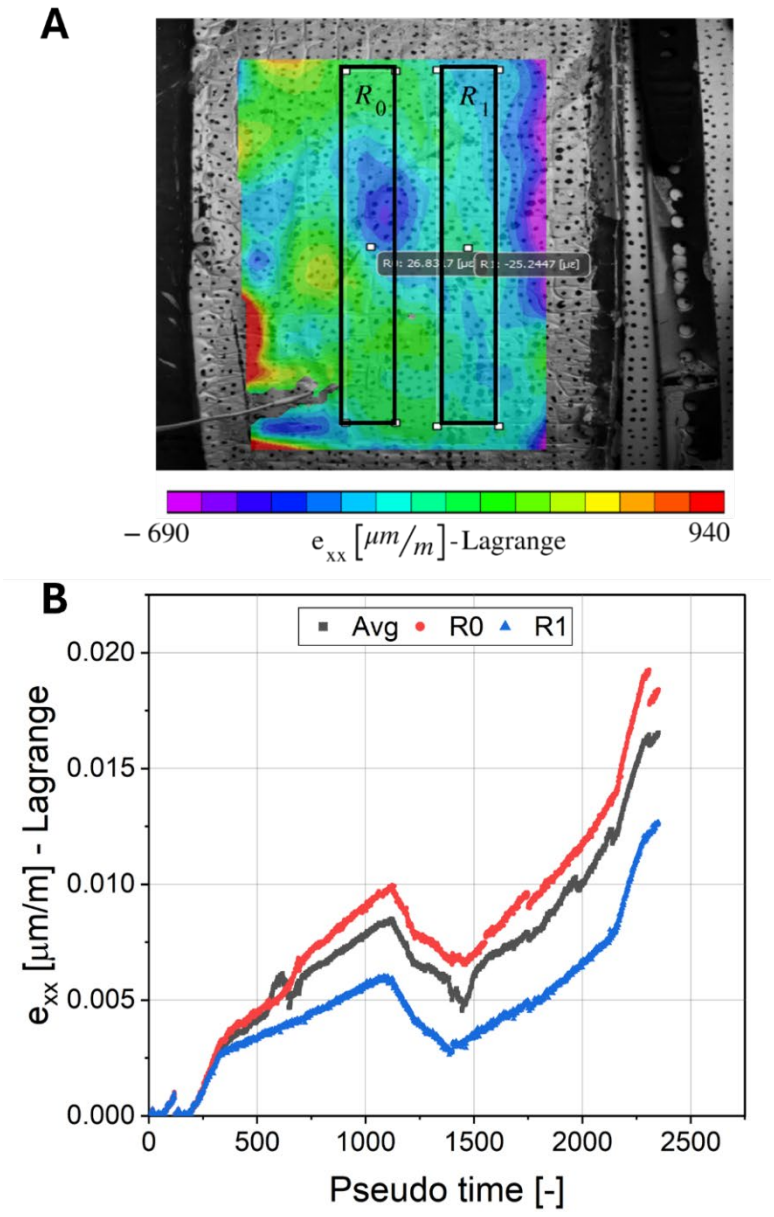

Figure 57. DIC measurements from the pull-to-failure test on ISES02: (A) Color contour of axial deformation (e_{xx}) in the crack area; (B) Comparison of plot curves for the average of the ROI, R0, and R1.

Appendix B.1 Burnout test

A portion from each tested tensile coupon (previously discussed in Section 3.1) was utilized to determine the fiber mass fraction through a burnout test at the University of Southern Queensland. Initially, the weights of the crucibles with and without samples were recorded. Subsequently, the crucibles with samples were placed inside an electric furnace (Figure 58) and heated to 580°C until all resins were completely burnt. After cooling, the weights of the samples with the crucibles were recorded, and the fiber mass fractions were calculated and documented in Table 28. The samples before and after the burnout test are shown in Figure 59 a and b, respectively.

After recording the weights of the samples, the plies of the samples were segregated to examine the ply orientations of each layer, as illustrated in Figure 60 and Figure 61.

Figure 58. Samples in an electric furnace

(a)

(b)

Figure 59. Samples (a) before and (b) after burnout test

Table 28. Fiber mass fraction

Crucible no.	Specimen no.	Mass of crucible (g)	Initial total mass of crucible and specimen (g)	Total mass of crucible and specimen after burnout (g)	Fibre content (%)
1	1-1	24.1372	29.2201	25.7843	32.405
3	1-2	24.0890	29.2091	25.7552	32.542
4	2-1	24.8913	31.0935	26.7425	29.847
6	2-2	23.9456	29.6224	25.6277	29.631
8	3-1	22.0080	26.7188	23.5238	32.177
9	3-2	24.2993	29.6885	26.1222	33.825
				Average:	31.738
				SD:	1.652

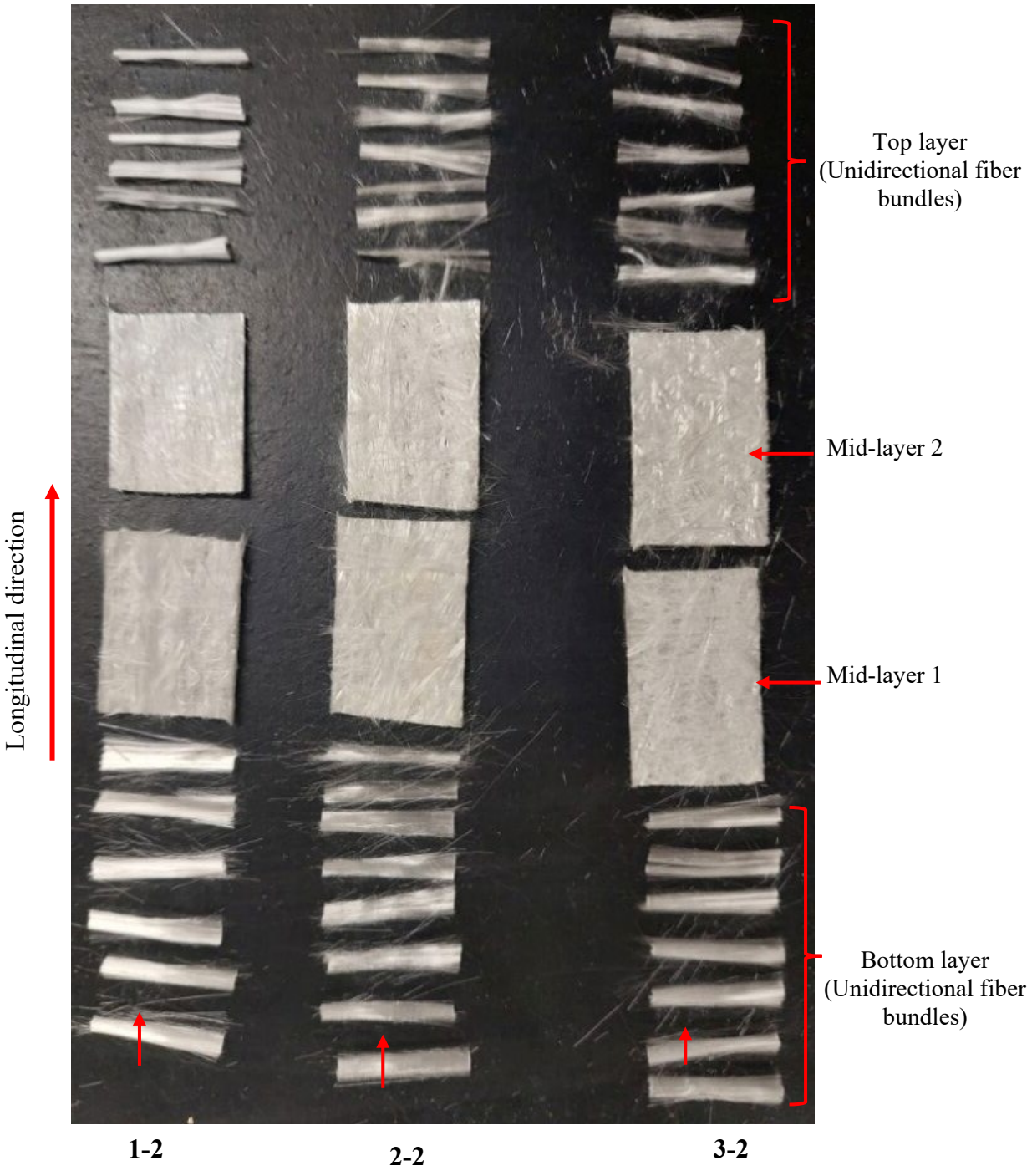

Figure 60. Ply orientation of the Insituform material

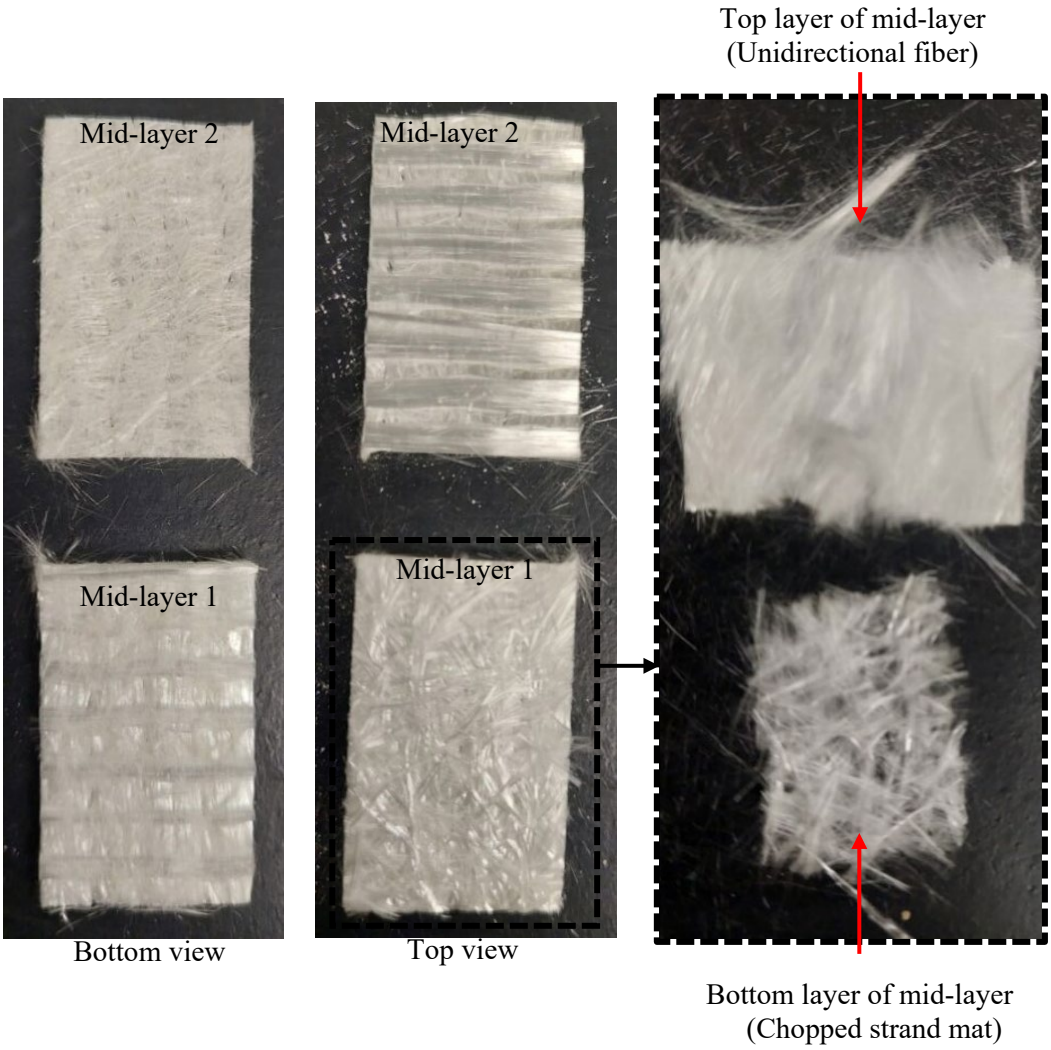

Figure 61. Mid-layers of Insituform material